EFFECTS OF IMPURITIES ON CRYSTAL GROWTH PROCESSES

SENDHIL KUMAR POORNACHARY

(*M. Tech., Indian Institute of Technology Delhi*)

A THESIS SUBMITTED

FOR THE DEGREE OF DOCTOR OF PHILOSOPHY

DEPARTMENT OF CHEMICAL AND BIOMOLECULAR ENGINEERING

NATIONAL UNIVERSITY OF SINGAPORE

2007

Acknowledgments

The present work has been carried out at the Institute of Chemical and Engineering Sciences (ICES), one of the national research labs under the Agency for Science, Technology and Research (A*STAR), in Singapore. The financial support provided by the National University of Singapore (NUS), and partially by the pharmaceutical company Merck, Sharp and Dohme (Singapore), is gratefully acknowledged.

Through the 4 years of training as a doctoral student at NUS–ICES, and working in the fascinating area of crystallization, I have begun to appreciate the excitement that S*cience* can provide on pursuing research as a career. I gratefully acknowledge all those people who have been instrumental to instill this curiosity upon me.

I would like to express my sincere gratitude to my advisor, Prof. Reginald Tan, for his invaluable guidance and support throughout this work. I would like to specially thank Prof. Tan for giving me the opportunity to interact with many of the leading researchers in the area of crystallization and process chemistry – Prof. Roger Davey (The University of Manchester, UK), Prof. Brian Cox and Dr. Simon Black (AstraZeneca, UK), and Dr. Keith Carpenter (ICES) during the course of this work. I gratefully thank all of them for helpful discussions and their constant encouragement. My visit to the University of Manchester as a researcher in the School of Chemical Engineering and Analytical Sciences for one month period, and working with Prof. Davey has indeed been a rewarding experience!

I am very grateful to my co-advisor, Dr. Pui Shan Chow of ICES, for her invaluable guidance and moral support throughout this work. She has always been

available for technical discussions and has given her time for proof reading my reports. With the good associations of Prof. Tan and Dr. Chow, I have certainly improved my scientific writing and presentation skills to a great extent.

My gratefulness is extended to all the colleagues in Crystallization and Particle Sciences group at ICES for technical assistance and useful advices during the research stage. I would like to specially thank Mr. Jin Wang for helping in performing the AFM experiments, Dr. Zaiqun and Ms. Jiawei for helping with the ATR-FTIR experiments, Dr. Venkat for helping in programming the data acquisition software, and Mr. Chin Lee for training in optical microscope. I gratefully appreciate the discussions with Ms. Sivashankari of NUS on molecular simulation. Special thanks goes to Dr. Murthy for his enthusiastic training on Hysys (a process simulation package) during tutorial sessions for NUS chemical engineering undergraduates.

Many thanks are due to all my friends who have made the stay in Singapore a pleasant and a memorable one. Finally, I am deeply indebted to my parents for their continuous support and love no matter the distance.

Sendhil Poornachary

December, 2007

Table of Contents

Summary

A key issue in crystallization process is the reproducibility of solid-state attributes of the crystalline product. Whenever there is a batch-to-batch variation in the crystal habit or polymorphs, a crucial issue may well be the presence or absence of key "impurities" in the material used to obtain the crystalline products, besides possible changes in the operating conditions. Given such a situation, it is not only important to identify the sources of the impurities, but also understand the mechanisms underlying their role on the crystal growth process. Only then a robust process can be developed to isolate the crystal products with the desired "physical" and "chemical" purity. Having said this, the objective of this work is to determine the effect of impurities on the growth of glycine crystals in aqueous solutions. Subsequently, we aim to develop a systematic approach to predict impurity effects on the crystal habit and polymorphism.

In this work, glycine, a simple amino acid, was used as the primary solute. The higher homologous amino acids were added in trace amounts to glycine solutions in order to simulate the presence of impurities. These chosen impurities have many of the structural and chemical characteristics of the host (glycine) molecule but differ in some specific way.

In the first part, batch crystallization experiments were performed to investigate the effect of impurities on the α-glycine crystal habit. With many of the impurities, habit modification was observed along the *b*-axis of α-glycine crystals, consistent with previously reported studies. However, in the presence of amino acids with excess carboxylic side chains, viz. aspartic and glutamic acids, additional habit modification was observed along the fastest growing *c*-axis. On the basis of the fact that these two amino

acids exist in two charged states (zwitterions and anions) and building on the "stereoselectivity" mechanism, it is surmised that the zwitterions interact with the (010) faces and the anions with the (011) faces. Consequently, the adsorbed impurity molecules inhibit crystal growth by disrupting the incorporation of solute molecules normal on the surface. Towards rationalizing these observations, molecular modeling techniques are used to visualize the interaction of impurity species at the crystal surfaces (in *Materials Studio modeling*, Accelrys Software Inc.). Subsequently, the interactions are quantified using atom-atom potential energy calculations.

In the second part, a systematic approach is proposed to select amino acid impurities (viz. aspartic and glutamic acids) that can operate as stereospecific nucleation inhibitors, and in doing so affect the polymorph formation of glycine crystals. To this end, the habit modification in α-glycine crystals by the two impurities is linked with suppression of nucleation of the metastable α-form. The principles of "stereochemical nucleation control" and "self-poisoning" mechanisms are invoked in order to rationalize the nucleation of γ-glycine.

In the final part, *in situ* observations of the α-glycine crystal surface using Atomic Force Microscopy provided a molecular scale picture of the physical processes taking place during crystal growth. From the morphological changes observed on the growth surface at various impurity concentrations, it is suggested that the impurity molecules selectively adsorb at kink sites on the (010) step face of α-glycine. Furthermore, the observed relationships between the step velocity and impurity concentration is corroborated with the Cabrera-Vermilyea model by applying the Langmuir isotherm model to describe the impurity adsorption dynamics.

Nomenclature

ABBREVIATION

AFM	Atomic Force Microscopy
ATR	Attenuated Total Reflectance
AE	Attachment Energy
BFDH	Bravais-Friedel-Donnay-Harker
BCF	Burton-Cabrera-Frank
CSD	Cambridge Structural Database
CCD	Charge-Coupled Device
C–V	Cabrera–Vermilyea
COMPASS	Condensed-phase Optimized Molecular Potentials for Atomistic Simulation
CVFF	Consistent Valence Force Field
DFT	Density Functional Theory
ESP	Electrostatic Potentials
FTIR	Fourier Transform Infrared
FBRM	Focused Beam Reflectance Measurement
HT	High-throughput
HPLC	High Pressure Liquid Chromatography
IR	Infrared
MZW	Metastable Zone Width
NMR	Nuclear Magnetic Resonance
PXRD	Powder X-ray Diffraction
PBC	Periodic Bond Chain
SAXS	Small Angle X-ray Scattering
SANS	Small Angle Neutron Scattering
WAXS	Wide Angle X-ray Scattering
XRD	X-ray Diffraction

SYMBOLS

C_{ss}	Solute concentration at the supersaturated state
C_{eq}	Solute concentration at the equilibrium temperature
C_i	Impurity concentration in solution
d_{hkl}	Interplanar spacing along [*hkl*] direction
E_{sl}	Slice energy
E_{att}	Attachment energy
ΔE_{sl}	Difference of slice energies between pure and impurity incorporated crystal growth layer
E_{cr}, E_{latt}	Crystal energy or lattice energy
ΔG	Gibbs free energy change
ΔH_{sub}	Enthalpy of sublimation
(*hkl*)	Miller index of a crystal face
J	Crystal nucleation rate
k, k_B	Boltzmann constant
L_i	Distance between impurity adsorption sites on the crystal surface
T	Temperature
v	Linear growth rate of crystal face
v_o, V_o	Step velocity in pure solution
V_I	Step velocity in impure solution
α	Surface entropy factor
σ	Supersaturation
γ	Interfacial tension
ρ_c	Critical diameter of a 2-D nucleus
θ	Surface coverage of impurity

List of Tables

List of Figures

CHAPTER 1

Introduction

1.1. Crystallization and Particle Engineering

Solution crystallization is widely used as a purification technique and as a separation process in the production of fine chemicals and pharmaceuticals. Over 90% of all pharmaceutical products contain drug substances in particulate, generally crystalline, form (Shekunov and York, 2000). Nevertheless, traditionally, crystallization has often been regarded as a "low-tech" area of chemical production. Because of this, industrial crystallization as a large scale unit operation is still a technology with many poorly understood aspects.

Crystallization process defines both chemical purity and physical properties such as particle habit and size, crystal structure (also referred to as polymorph) and degree of crystal imperfection. The chemical purity is of utmost importance in pharmaceuticals because of its direct impact on therapeutic effects. In chiral drugs, for example, formation of solid solutions is a common problem resulting in variations in solid-state properties. Because of this, the dissolution rates of some pharmaceutical solids dramatically change as a function of chiral impurity concentration. On the other hand, the impact of physical properties on bulk drug manufacturing could be two-fold. First, the operational characteristics of downstream processing are strongly influenced by the solid-state properties of crystals. For example, filtration behavior of the product from its mother liquor can profoundly be affected by particle habit and size distribution. Second, formulation of the solid dosage form can be greatly influenced by the crystal attributes as

in the case of tabletting by direct compression. This procedure requires good powder flow properties, uniform mixing between drug and excipients, and the ability to consolidate and bond under pressure (Shekunov and York, 2000).

Other physical (crystal) attributes that have drawn greater attention in pharmaceutical manufacturing in recent years is that of solid forms – polymorphs and solvates. Polymorphic forms can have remarkably different physical properties including solubility and melting point resulting in different stability and bioavailability of drug products. Accordingly, crystalline variations are responsible for a wide range of formulation problems, such as bio-equivalence, as well as chemical and physical instability of the solid drugs in their final dosage forms. In addition, as polymorphism is associated with intellectual property rights, it is important to acquire complete knowledge of solid forms in a new drug entity. Otherwise, it may leave the opportunity for competitors to secure patent rights on alternative polymorphs and hence alternative formulations of the drug.

Recent studies have underscored that even minor changes in crystallization conditions, for examples, supersaturation, temperature, cooling rate, and impurities can produce significant changes in the crystal properties. These effects have been recognized as the major batch-to-batch and source variation problems leading to inconsistency of the product properties. One well known example is the case of *Ritonavir*, an anti-retroviral drug manufactured by Abbot Laboratories (Chemburkar et al., 2000). Only one crystal form was ever identified in the drug development process. Furthermore, it was assumed that polymorphism was immaterial to the product, since the drug was formulated as a semi-solid or liquid oral dosage form due to its lack of bioavailability in the solid state. However, two years into production, a new, more stable, solid form began to precipitate

in the original formulation, which was found to have significantly less favorable dissolution characteristics compared to the original polymorph. The unexpected production of a new, undesired polymorph led to prolonged investigation of the causes of and solutions to this problem, costing the company a significant amount of money. This example highlights the importance of characterizing a given active ingredient as thoroughly as possible in order to understand if and under which circumstances the drug substance exhibits polymorphism, so that the appearance of the 'wrong' polymorph can be avoided later during the production stage. Besides, during the production stage, monitoring and control of various process conditions is critical to ensure consistent crystal properties (Ulrich and Jones, 2004).

1.2. Understanding the Role of Impurities

Crystallization is essentially a supramolecular process by which an ensemble of randomly organized molecules (solute) in a solution come together to form an ordered three-dimensional molecular array. The attractiveness of this process lies in the fact that crystal growth is by and large specific to the product molecules, with impurities being usually rejected from the growing crystal surfaces. Consequently, relatively high-purity crystals could be obtained from solutions which may contain very many impurities (Davey and Garside, 2000).

Nevertheless, some impurities may interfere with the normal crystal growth process through what could be called "molecular trickery", and consequently impact the key crystal attributes. These impurities typically have a molecular structure similar to that of the primary solute, and can be reaction by-products or reactants or additives. Therefore, understanding the role of impurities on crystal growth process is essential for a robust

process development. In this direction, the development of the idea of “tailor made” additives has generated considerable insights. A stereochemical correlation between the solid state chemistry of the crystalline phase and the molecular structure of additives has been established by investigating into a number of host-guest molecular crystal systems (Weissbuch et al., 2003).

The shape of a crystal as grown from pure solution is determined by the relative growth rates of its crystallographic facets, with the slow growing faces preferentially expressed in the final habit. However, the presence of impurities in trace amounts in the crystallizing solution can significantly modify the crystal habit. Generally, this is a consequence of specific interactions of the impurity molecules with the crystal faces, subsequently causing growth inhibition normal to that face.

Impurity effects on crystal growth are dependent on both impurity concentration and solution supersaturation. An impurity molecule which is adsorbed onto the crystal surface causes a “pinning” effect on the advancement of step layers and impedes growth. The extent of this effect, in turn, is dependent on the concentration of impurity on the crystal surface. There exists a “dead zone” of supersaturation at which the step advancement is completely retarded. In order to recover crystal growth from “impurity poisoning” the supersaturation level which defines the thermodynamic driving force has to exceed a threshold limit (Land et al., 1999).

Interestingly, from the viewpoint of “crystal engineering”, additives present an option for product design, specifically by controlling and directing crystal habit and polymorphism. The proposed mechanism involves selective adsorption on crystal faces followed by inhibition of nucleation and growth of particular polymorphic forms. The

concept has been demonstrated in practice through a variety of processes – to achieve resolution of conglomerates (physical mixture of enantiomeric crystals) by inducing stereoselective habit modification using chirally resolved additives; to selectively inhibit nucleation of a racemic crystalline material during direct resolution of enantiomers by preferential (or entrainment) crystallization; to precipitate a polar crystal polymorph; and, to assign the absolute structure of chiral molecules and polar crystals. Furthermore, the approach has also been extended to explain the effect of a solvent or solvent mixture on the formation of stable and unstable polymorphs (Weissbuch et al., 1991).

1.3. Research Objectives and Approach

The objective of this work is to understand the mechanisms by which impurities affect solid-state attributes of the crystalline product, and consequently, to develop a systematic approach to predict impurity effects on crystal habit and polymorphism of glycine, the simplest amino acid. Trace amounts of higher homologous amino acids were chosen as impurities to meaningfully understand the interactions with glycine crystal at the molecular level. The thesis work will comprise the following milestones:

- Determine the effect of impurities on glycine crystal habit and polymorphs by performing batch cooling crystallization experiments in the presence and absence of impurities.
- Explain the effect of impurities on crystal habit modification by modeling the interactions between impurity molecules and glycine molecules at the host crystal surfaces. Subsequently, characterize impurity–crystal intermolecular interactions using atom-atom potential energy calculations.

- Measure metastable zone widths for pure glycine solution and for solutions doped with impurities at different concentration levels.
- Monitor the impurity effects on glycine crystal growth *in situ* using Atomic Force Microscopy (AFM). Correlate the surface morphology changes observed in the presence of impurities with the experimental crystal habit modification and molecular modeling results.

1.3. Dissertation Outline

Chapter 2 introduces the theoretical aspects of crystal nucleation and growth in pure solution as well as in the presence of impurities. The effects of impurities on crystal habit modification and nucleation of crystal polymorphs are reviewed. The concepts involved in molecular modeling and simulation of impurity effects on crystal growth are briefly discussed.

Chapter 3 outlines the model system, experimental procedures and characterization techniques.

Chapter 4 reports the results on habit modification in α-glycine crystals in the presence of impurities. Some new experimental observations are presented and compared with the previous work. It is proposed that solution speciation of the impurities controlled by pH influence the stereoselective interactions with the α-glycine crystal. The arguments are corroborated with molecular modeling, conformational analysis of impurity molecules, and supporting data derived from IR spectroscopy.

Chapter 5 reports habit modeling of α-glycine crystal from its molecular crystal structure. The simulated crystal habit is compared with the shape of as grown α-glycine crystals from solution. Subsequently, the experimental habit modification reported in

chapter 4 is rationalized using atomistic simulation of impurity interactions at the crystal surfaces.

Chapter 6 reports the effect of impurities on the nucleation of glycine crystal polymorphs. A strategy for selecting (or screening) impurities which can effect structural modification in glycine crystallization is proposed. Accordingly, the thermodynamically stable γ-glycine is crystallized from solutions containing "certain" impurities, in contrast to the nucleation of the kinetically favored α-glycine from pure aqueous solution. The arguments presented are supported with nucleation kinetics data derived from metastable zone width measurements and morphological changes observed in the crystal polymorphs obtained in the presence of the impurities.

Chapter 7 reports *in situ* monitoring of crystal growth using AFM. The advancement molecular steps on the (010) face of an α-glycine crystal in aqueous glycine solution, in the presence and absence of an impurity, is imaged. The mechanism by which impurities inhibit the advancement of molecular steps and the influence of supersaturation on recovering crystal growth from impurity poisoning are investigated.

Chapter 8 gives a summary of the significant outcomes of this study together with the scope for future work.

CHAPTER 2

Crystallization Kinetics and Impurity Effects

Crystallization is essentially a molecular recognition process occurring on a "grand scale" that allows separation and purification of the desired compound to produce high purity products. However, the attributes of the product crystals depend on various operating conditions. For example, the crystal shape could be affected by a number of factors such as the supersaturation (vis-à-vis solute concentration), solvent medium, presence of impurities and/ or additives, crystallization temperature, hydrodynamics, etc., A holistic understanding of the mechanisms of crystal growth, and the influence of the various operating conditions is, therefore, a prerequisite for the design and development of a robust crystallization process. In this chapter, the fundamental aspects of solution crystal growth are discussed. Furthermore, the effect of impurities on crystal growth process in general, and more specifically of organic small molecules, is reviewed in the context of the current work.

2. 1. Role of Supersaturation

Supersaturation, the driving force for crystallization, can be achieved in several ways – for example by cooling a solution, or by solvent evaporation, or by the addition of an anti-solvent, or by changing the solution pH. A supersaturated solution, although in thermal equilibrium, is not at thermodynamic equilibrium. Concentration fluctuations in the solution can cause the solute molecules to come together as clusters. On a microscopic level a dynamic situation exists wherein clusters, in the form of dimers,

trimers, tetramers etc. are continuously formed and destroyed. Eventually, a critical cluster size is reached and a crystal is born (Ginde and Myerson, 1993).

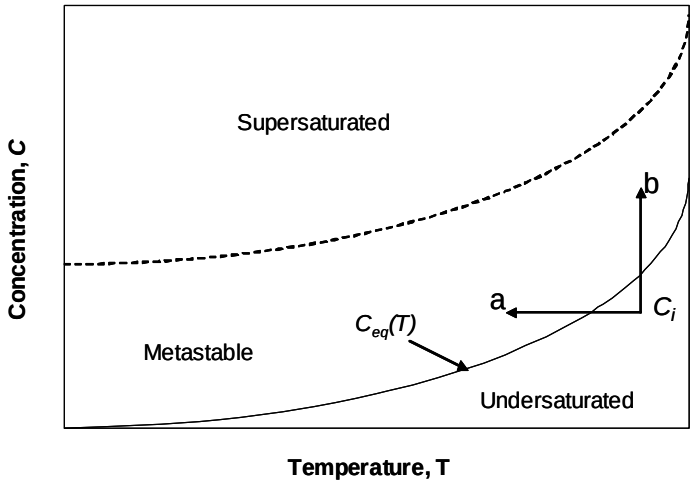

Figure 2- 1. The solubility/ supersolubility phase diagram (Davey and Garside, 2000)

In the phase diagram represented in Fig. 2-1 a solution lying above the solubility curve is *supersaturated* with respect to the equilibrium concentration corresponding to the temperature of the system. The generic definition of supersaturation (σ) in thermodynamic terms will be the difference in chemical potential of a molecule in its supersaturated state (μ_{ss}), and in its equilibrium state (μ_{eq}). In terms of measurable quantities supersaturation can be defined using solute activities or composition as (Davey and Garside, 2000):

$$\sigma = \left(\mu_{ss} - \mu_{eq}\right)/kT = \ln\left(a_{ss}/a_{eq}\right) = \ln\left(C_{ss}/C_{eq}\right) \qquad \textbf{2- 1}$$

In the above definition, solubility (C_{eq}) is defined as the mass of material that can be dissolved in a known volume or mass of liquid under given conditions of temperature and pressure. However, the solubility of a weak acid and weak base is more complicated to define since it will depend on the species of acid and base in solution under a given set

of conditions. The speciation depends on both solvent and pH and can be calculated from the measured pK_a values of the acid and base (Jones et al., 2005).

Of the many factors controlling crystal nucleation and growth kinetics, supersaturation is the primary, having a direct impact on the number, size, shape and structure of the product crystals.

2. 2. Nucleation Mechanisms and Kinetics

Crystallization is considered as a two-stage process. Nucleation is the first step in which the "birth" of crystal nuclei (a new solid phase) from the supersaturated solution occurs. Subsequently, the stable crystal nucleus grows in size. Nucleation can be either *primary*, which occurs in the absence of crystalline surfaces, or *secondary*, which requires the presence of a crystal surface for further generation of crystal nuclei. The *primary* nucleation from a homogeneous solution is central to the crystallization process and is best described by the classical nucleation theory developed by Gibbs, Volmer, and others (Mullin, 2001; Davey and Garside, 2001).

2.2.1. Classical nucleation theory

The classical nucleation theory proposes consecutive bimolecular addition of solute molecules to form the critical cluster, which would develop to form the stable crystal nucleus. The free energy for formation of a nucleus of critical size *n*, in a solution of supersaturation σ, is given by the balance between the energy gained by formation of bulk phase ($kT\ ln\ (\sigma)$ per molecule) and the energy required to form new surface area ($A = \beta n^{2/3}$). The equation is given by

$$\Delta G = -nkT\ln(\sigma) + \gamma\beta n^{2/3} \qquad \textbf{2- 2}$$

in which γ is the interfacial tension between the cluster and solution, and β is an area shape factor dependent on the nucleus shape. Accordingly, the free energy (ΔG) increases with the cluster size (*n*) until a maximum is reached at the critical size, and beyond which further growth leads to a decrease in free energy.

Nucleation is probabilistic event, with the chances for forming the critical nuclei depending on the height of the free energy barrier relative to *kT*. With increasing supersaturation, the barrier height and the critical size decrease resulting in spontaneous nucleation. Taking into consideration the activated nature of nucleation process, the rate at which critical sized nuclei can transform into mature crystals can be expressed in the form of an Arrhenius-type relationship:

$$J = K_J \exp(-B_J \gamma^3 / T^3 \sigma^2) \qquad \textbf{2- 3}$$

This equation highlights the effects of important variables – supersaturation, temperature and interfacial tension on the nucleation rate. At low supersaturations, the interfacial tension term dominates and there is insufficient free energy available via the supersaturation to create new surface. At some critical value of the supersaturation the nucleation rate increases exponentially, eventually reaching a maximum value. The nucleation theory predicts the transition from the metastable zone (of low nucleation rate) to the labile zone (of spontaneous nucleation) of a system in fair agreement with the experimental nucleation kinetics.

Nevertheless, the validity of the classical theory of nucleation is limited by the assumptions that it implicitly includes (Nývlt et al., 1985). Firstly, the classical theory is derived from the thermodynamics of a continuum, i.e. the size of the particles described is much greater than the intermolecular distances. This condition is not, however,

fulfilled for clusters and critical nuclei in the new phase (radius 5–10 Å) so that it cannot be a priori assumed that thermodynamics is applicable to the description of nucleation. Secondly, the change in Gibbs free energy on addition of a new species depends not only on the nucleus size but also on its configuration and site of attachment of the new species. Besides, assumption of equilibrium between the nucleus and the surrounding medium is nonrealistic because even at equilibrium, exchange of species between the two phases is accompanied by fluctuations (comparable with the nucleus size). Thus, a state can readily occur in which the nucleus attains the corresponding critical size without a change in the thermodynamic functions of the system. Thirdly, in the classical model, the macroscopic values of free surface energies may not represent the actual interfacial tensions of the critical sized nuclei.

2.2.2. Heterogeneous and Secondary Nucleation

In industrial crystallizers nucleation is mostly *primary heterogeneous*, with concomitant *secondary* nucleation. Heterogeneous nucleation is favored by the presence of dissolved or suspended foreign substance in the supersaturated solution, or the surfaces in contact with the crystallizing solution, which lower the free energy barrier for nucleation. The wetting properties of the foreign substance and their atomic packing arrangement (isomorphism with the crystal) are known to affect the heterogeneous nucleation. Secondary nuclei can either originate from the parent crystal or from the loosely ordered phase of the solute molecules near the crystal surface. In the previous case, tiny crystallites on the seed crystal can act as nucleation sites (initial breeding); or the dendrite crystals formed at higher levels of supersaturation can fragment in the solution and serve as nucleation sites (needle breeding or polycrystalline breeding); or

microabrasion of crystals at high stirring speeds can produce fragments that serve as nucleation sites (collision or attrition breeding). With a wide scope of generation of secondary nuclei, contact nucleation (vis-à-vis crystal-crystal, crystal-stirrer and crystal-crystallizer) forms an important source of secondary nuclei in the crystallizer (Myerson and Ginde, 2002).

Interestingly, recent works have exploited epitaxially induced crystallization on self assembled monolayers and multilayers (Kang et al., 2000; Lee et al. 2002, 2005; Dressler and Mastai, 2007), molecular single crystal substrates (Carter and Ward, 1993; Bonafede and Ward, 1995), and using surfactants in microemulsions (Allen et al., 2002) for the control of crystal size, morphology and polymorphism.

2.2.3. Kinetic measurements – metastable zone width and induction time

Under constant stirring and unseeded crystallization conditions, nucleation rates can be characterized either by measuring the metastable zone widths (i.e. the maximum allowable supersaturation before solid phase separation) at different cooling rates or by measuring the induction time (i.e., the time elapsed between the creation of supersaturation and the formation of the solid phase) as a function of supersaturation.

The determination of metastable zone is not only significant in determining the nucleation kinetics but also in defining a working zone for industrial crystallization processes. From the operational viewpoint, an optimal cooling profile designed to be just within the MZW prevents excessive crystal nucleation and growth, and therefore ensures narrow crystal size distribution (Mersmann and Bartosch, 1998; Moscosa-santillán et al., 2000; Fujiwara et al., 2002; Ulrich and Strege, 2002). Nevertheless, because of the fact that the MZW is a kinetic parameter, it is influenced by several factors such as the

cooling rate (Ginde and Myerson, 1993), solution thermal history (Harano et al., 1982), agitation intensity and the presence of impurities (Beckmann et al., 1990; Ginde and Myerson, 1993; Myerson and Jang 1995; Sangwal and Mielniczek-Brzóska, 2004).

In isothermal systems, induction times measured as a function of supersaturation can be used to estimate the crystal–liquid interfacial tension (γ), which is an important fundamental parameter in the classical nucleation theory. However, the existence of an induction period in a supersaturated system is contrary to expectations from the classical nucleation theory, which assumes ideal steady-state conditions and predicts immediate nucleation once supersaturation is achieved. Therefore, the induction period is generally considered as being made up of three parts: a relaxation time (t_r) for the system to achieve a quasi-steady-state distribution of molecular clusters; time required for the formation of a stable nucleus (t_n); and time for the nucleus to grow to a detectable size (t_g) (Mullin, 2001).

Although the metastable zones are often employed to characterize homogeneous nucleation, it is important to note the underlying assumptions. In MZW measurements, it is assumed that at the moment when nuclei are first detected the rate of desupersaturation is equal to the rate of nucleation. But the true situation is that the created supersaturation is dissipated not only in the formation of new nuclei but also by growth on existing crystalline particles. Further, in the experimental determination of the metastable limit, nuclei are not detected at the moment of their creation but at some later time when they have grown to visible size (at say about 10 μm). However, with recent developments in laser diffraction and spectroscopic techniques it has been possible to probe into the early stages of crystal nucleation (refer to section 2.2.5).

2.2.4. Effect of impurities

The effect of impurities on crystal nucleation is more often reflected by changes in the measured values of metastable zone widths and induction periods. However, it has not been possible to attempt a general explanation for the impurity effects on the nucleation step. Many of the proposed hypotheses are based on an adsorption-based mechanism. If the impurities adsorbed on the surface of developing crystal nuclei can block the active growth sites, it leads to an increase in the supersaturation barrier for homogeneous nucleation (Sangwal and Mielniczek- Brzóska, 2004). On the other hand, the impurity molecules adsorbed on the nucleus surface can increase the interfacial tension, which is, however, limited by the small size of the near-critical nuclei clusters. In both these cases, the metastable zone widths (or the induction periods) increase in solutions doped with the impurities. Other suggestions propose that certain ionic impurities may act as structure-breakers in the solution phase. However, the latter argument has not been substantiated with sufficient experimental data (Mullin, 2001).

Interestingly, a few investigations have reported enhanced nucleation rates in the presence of impurities, as opposed to the above-mentioned nucleation suppression phenomenon. In this case, impurity molecules may adsorb on the nucleus surface and reduce the interfacial energy (limited by the small size of the near-critical nuclei clusters), or may themselves act as nucleation centers, enhance secondary nucleation by initiating crack propagation at the adsorbed defect sites on the crystal surface fostering the nucleation event in all the cases (Mullin, 2001; Kashchiev, 2000). In some cases, impurities may enhance the degree of cluster formation in a supersaturated solution, and

therefore, promote crystal nucleation (Ginde and Myerson, 1993; Myerson and Lo, 1991).

Of relevance to the current work, the effect of structurally-related impurities on the nucleation kinetics of organic small molecules will be reviewed here. Hendriksen and Grant (1995) determined the induction period before nucleation for paracetamol aqueous solutions in the presence of synthetic impurities using a laser attenuation technique. It was found that impurities such as p-acetoxyacetanilide, p-acetamidobenzoic acid, methylparaben, orthocetamol and metacetamol caused significant inhibition of nucleation. The induction time measurements, as a function of supersaturation and absolute temperature, were used to estimate the interfacial tension between the solution and the critical nucleus in the presence and absence of the impurities. The calculations revealed that those impurities for which the nucleation inhibition effect was more pronounced had resulted in higher interfacial energies. The mechanism of nucleation inhibition was explained based on a structural approach: the ease with which the impurity can be incorporated into the developing nucleus of paracetamol depended upon the similarity of the size, shape and intermolecular interactions of the guest molecule with the host molecule. Subsequently, a host molecule would encounter a guest template of energy, shape and steric configuration quite unlike a paracetamol lattice, and its incorporation would then be inhibited (cf. section. 2.4.2). Hendriksen et al. (1998) further rationalized this mechanistic interpretation of impurity–host interactions by studying the impurity effects on the paracetamol crystal habit and quantitatively determining the impurity concentration incorporated into the crystals. It was proposed that the impurities

which on incorporation into the crystal lattice “disrupted” the H-bonding network reduced the stability of the emerging nucleus.

Myerson and Jang (1995) correlated the propensity of alkanoic acids (additives) in inhibiting nucleation of adipic acid by a comparison of their binding energies on the adipic acid crystal surfaces. The effect of alkanoic acids on the metastable zone width of adipic acid in ethanol solution were measured employing a differential scanning calorimeter. The measured values were found to increase with increasing carbon number to C_{14}, decrease from C_{14} to C_{16} and then increase again thus correlating well with the results obtained from the binding energy calculations.

Pino-García and Rasmuson (2004) demonstrated a structural correlation between the conformation of the additive molecules and their effect on the nucleation of vanillin (4-hydroxy-3-methoxybenzaldehyde). Induction periods for the nucleation of vanillin in the presence of additives were determined experimentally and compared with the interaction energies of the additives with the dominant facets of vanillin crystals. It was concluded that the additive molecules having the same molecular configuration (viz. three functional groups bonded to the benzene ring) as the host molecule experienced more favorable interaction energies with the crystal faces and had a greater impact on the crystal–solution interfacial tension. On the other hand, the additive molecules with a modified configuration (viz. two functional groups bonded to benzene ring) had a lesser impact on the nucleation kinetics, as dictated by the adsorption energies and the extent of hydrogen bonding with the host crystal.

Ginde and Myerson (1993) studied the effect of an impurity (valine) on the metastable zone width of glycine solutions and correlated the results obtained with cluster

formation. The presence of valine had caused enhanced concentration gradients (vis-à-vis cluster formation) in supersaturated glycine solutions and a decrease in metastable zone width compared to the pure system, indicating that the impurity acted as a nucleating agent.

Hennessy et al. (2004) examined the mediating role played by chemical inhibitors that are commonly used to prevent or delay wax crystallization in crude oil. Metastable zone width measurements of a solution of homologous mixtures of n-alkanes in the presence of polymeric additives showed inhibitive effect on the wax crystallization. Furthermore, a direct correlation between the molecular structure of the polymeric additives used and the resultant crystallization behavior was revealed from combined in-situ small and wide angle X-ray scattering (SAXS/WAXS) techniques. The additives, comprising of polar macromolecules with nonpolar alkyl chains protruding from the backbone, bound within the basal plane of the wax crystal structure through intermolecular interactions of an epitaxial nature. The results also suggested that inhibitor/wax ordering has taken place in solution prior to crystallization.

2.2.5. Polymorphism – structural origin

Many of the chemical compounds crystallize in more than one phase, which have different molecular packing arrangements in the solid state. This phenomenon, known as polymorphism, is better understood by explaining the kinetics of crystal nucleation from a structural viewpoint. In this context, the Ostwald's *Rule of stages* postulates that a crystallizing system progresses from the supersaturated state to equilibrium in stages, each stage representing the smallest possible change in free energy. Thus, a polymorphic system would move through each possible polymorphic structure before crystals of the

most stable phase appear. For a dimorphic system, this means the initial appearance of the metastable form (phase I), followed by their transformation to the stable form (phase II). This phenomenon may be explained by a surface crystallization mechanism. For example, the least stable form has the highest volume free energy and the lowest specific step free energy and, correspondingly, the highest average step velocity and crystal growth rate. In addition, the radius of critical nuclei should be smaller and the nucleation rate higher for the least stable form. As a result, the crystallization of the least stable form should dominate at high supersaturations (Shekunov and York, 2000).

Nevertheless, the Ostwald's rule is empirical and proposed based on observations of many systems. Cardew and Davey (1982) analyzed theoretically the effect of crystallization of a simple dimorphic system at a constant temperature. By consideration of the supersaturation of the initial solution with respect to the two forms they were able to derive relative nucleation rates. Three types of behavior were recognized, dependent on the total variation of nucleation and growth rate: (a) the more stable form would crystallize preferentially at all concentrations, (b) the stable form would crystallize preferentially only at high concentrations, (c) the less stable form would crystallize preferentially only at intermediate concentrations. Hence, there is the whole range of possible behaviors with supersaturation in respect of the polymorphic expectations.

Recent studies have been aimed towards a structural understanding of crystal nucleation from supersaturated solutions so that the kinetics involved in the process is fully understood. Nevertheless, the molecular self-assembly processes prior the nucleation event occur on the timescale of 10^{-6} s and are difficult to investigate experimentally (Davey, 2003). Therefore, small angle scattering techniques using SAXS

(Small Angle X-ray Scattering), SANS (Small Angle Neutron Scattering) and WAXD (Wide Angle X-ray Diffraction), and spectroscopic techniques using NMR, Raman and IR (Infra red) are used to probe into the mechanisms underpinning the structural (polymorphic) changes under different solvent environments and crystallization conditions. Case studies exemplifying this are briefly reviewed here.

(a) Chattopadhyay et al. (2005) have used SAXS to study the nucleation of the amino acid glycine from its aqueous supersaturated solution. Their results indicated that glycine molecules exist as dimers in the supersaturated solution. A transformation from mass fractal structure to surface fractal structure was observed during the crystallization process, which could be the signature of a two-step nucleation process.

(b) Parveen et al. (2005) have demonstrated a direct relationship between molecular self-association in solution and H-bonded motifs in the subsequently crystallized solid phases by applying IR spectroscopy to concentrated solutions of tetrolic acid.

(c) Davey et al. (2002) observed the appearance of short-lived metastable crystalline and liquid crystalline states during cooling crystallization of sunflower seed oil, benzamide and para-azoxyanisole melts that were consistent with precrystalline molecular assembly. However, supersaturated solutions showed no evidence of long-range ordering prior to the appearance of crystals.

(d) Endo et al. (2003) used time-resolved SANS experiments to investigate the effect of a polymer additive on the crystallization of $CaCO_3$. The results indicated morphogenesis occurring at the nano- to mesoscales. The consequent crystal morphologies obtained in the presence and absence of the additive were in agreement with that of the prenucleation studies.

(e) Profir et al. (2002) observed the formation of metastable conglomerates during the crystallization of mandelic acid in water using an ATR-FTIR (Attenuated Total Reflectance – Infrared) spectrometer. The metastable conglomerates transformed to a stable racemic compound after a time lag depending on the operating conditions during crystallization.

In addition to the above experimental studies, molecular modeling and simulation have provided insights into understanding of crystal nucleation from solutions from a structural viewpoint (Anwar and Boateng, 1998; ter Horst et al. 2002; Hammond et al., 2005). Furthermore, another school of thought assumes that the supersaturated solution contains clusters corresponding to all the possible polymorphs. Exploiting this concept, monolayers or auxiliary molecules are utilized to stabilize or inhibit the development of clusters corresponding to desired crystal structures (Weissbuch et al. 2003). This aspect would be investigated further in the section 2.5.3.

2. 3. Crystal Growth

Just as crystal nucleation involves molecular self-assembling in 3-dimension from a supersaturated solution, subsequent growth of the crystal nucleus proceeds by a 2-D molecular self-assembling. Crystal growth proceeds by diffusion of solute molecules from the bulk solution to the interface, followed by surface reaction consisting of adsorption, surface diffusion and integration of the solute molecules into the crystal lattice. Under adequate mixing conditions, the resistance to diffusion of solute molecules from the bulk solution to the crystal–solution interface is negligible, and surface integration is the rate-limiting step of crystal growth. Under these conditions, crystal

growth is conceived to take place in a layer-by-layer fashion with the linear growth velocity of the face defined in a direction normal to that face.

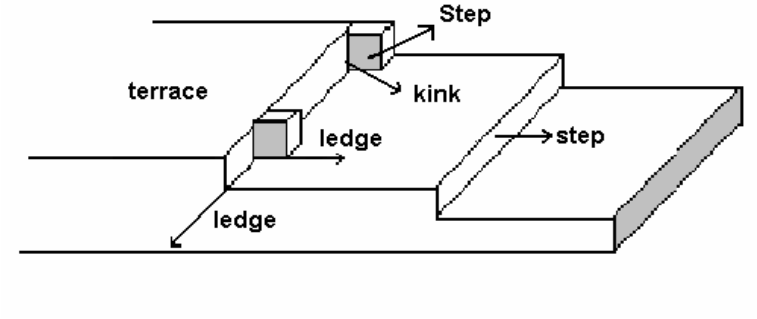

Figure 2- 2. Schematic representation of topographic features on a growing crystal surface – the Kossel model.

2.3.1. Theories and growth models

As proposed by the *Kossel model* an apparently flat crystal surface is in fact made up of moving layers (steps) of monoatomic height, which may contain one or more kinks (Fig. 2-2). In addition, there can be loosely adsorbed growth units (atoms, molecules or ions) and vacancies in the surfaces and steps. Growth units are most easily incorporated into the crystal at a kink; the kink moves along the step and the face is eventually completed. Hence the linear growth rate (v) of a face can be expressed can be expressed in terms of the step velocity (v_0), the step height (h) and the interstep (y_0) spacing (Myerson and Ginde, 2002):

$$v = v_0 h_0 / y_0 \qquad \textbf{2- 4}$$

If it is assumed that the linear growth rate is proportional to the total binding energy of a growth unit to that surface, it could be expected that v (kink face) > v (step face) > v (flat face) (Davey and Garside, 2000).

A surface entropy factor α is defined to reflect on the ease with which a surface can form sites with multiple binding interactions and hence an indication of the ease with

which a surface can grow. For crystal growth from solution the α-factor can be calculated from measurable quantities by the equation

$$\alpha = \xi\left[\left(\Delta H_f \big/ RT\right) - \ln x_{eq}\right] \qquad \textbf{2- 5}$$

with ΔH_f being the heat of fusion and x_{eq} the solubility. $\xi = E_{sl} / E_{cr}$ is a crystallographic (anisotropic factor) factor that describes the intermolecular interactions in the crystal surface of interest, in which E_{sl} is the total interaction energy per molecule in the layer of the growth face and E_{cr} is the total crystallization or lattice energy. On the basis of the definition of the α-factor and the possible pathways by which a solute molecule become integrated into a lattice position on a growth face the following growth mechanisms were proposed (Davey and Garside, 2000).

(a) Continuous or Rough Interface Growth

If the energy required to form a step is low (α<3) the crystal surface will contain many kink and step sites, which subsequently allows easy integration of growth units. By this mechanism, the growth rate normal to the surface is linearly proportional to the solution supersaturation.

(b) Surface or 2-D nucleation

As α increases (3<α< 5) the inherent roughness of the interface decreases. Under such conditions the growth units form clusters of 2-D nuclei on the surface. The circumference of such islands becomes the source of new step and kink sites at which additional growth units can join the surface. For example, growth of the (111) and (001) faces of L-glutamic acid in aqueous solution proceeds through formation of wavy growth steps one over the other that is characteristic of the surface nucleation model (Fig. 2-3).

The height of the step (0.47 ± 0.02 nm) originating on each island corresponded to the minimum lattice spacing (0.485 nm) for the growth direction (Kitamura and Onuma, 2000). In this model, also known as the "birth and spread" mechanism, it is assumed that the spread of nuclei proceeds at a finite constant rate that is independent of size. Growth rate normal to a face depends on the supersaturation by the relation

$$v = k_{SN}\sigma^{5/6}\exp\left(\frac{-B}{\sigma}\right) \qquad \textbf{2- 6}$$

The exponential term in equation 2-5 arises due to the activation energy required to create a critical sized 2-D nuclei with an edge tension γ_e. This model, however, fails to account for crystal growth at lower supersaturations where the driving force required for surface nucleation is not met.

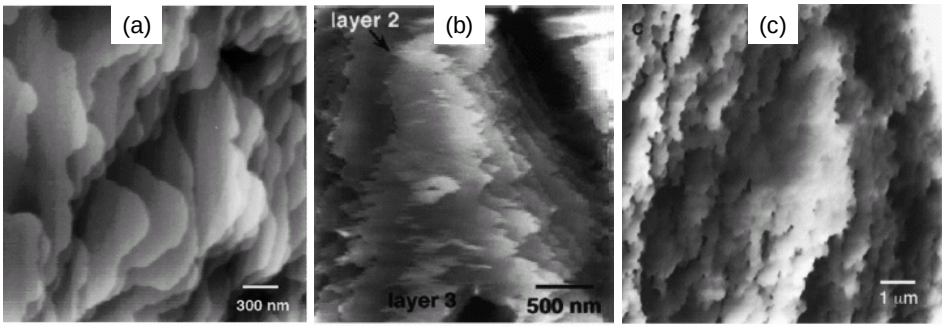

Figure 2- 3 Atomic force microscopic images (AFM) showing surface morphologies of L-glutamic acid: (a) the (111) face and (b) the (001) face in pure solution; (c) the (111) face in the presence of L-Phe as the impurity (Kitamura and Onuma, 2000).

(c) Spiral or Screw Dislocation growth

As α rises above 5, the enhanced intermolecular interactions in the plane of the interface result in a molecular surface that is flat. In this case surface nucleation is unlikely because of increasing value of γ_e, especially at low supersaturation. An alternative mechanism is the creation of steps by dislocations due to built-in lattice defects. Subsequent growth of crystal face is perpetual along the spiral staircase once the

screw dislocation has been formed. In situ AFM observations of macromolecular crystal growth has provided excellent evidences for this mechanism (Fig. 2-4).

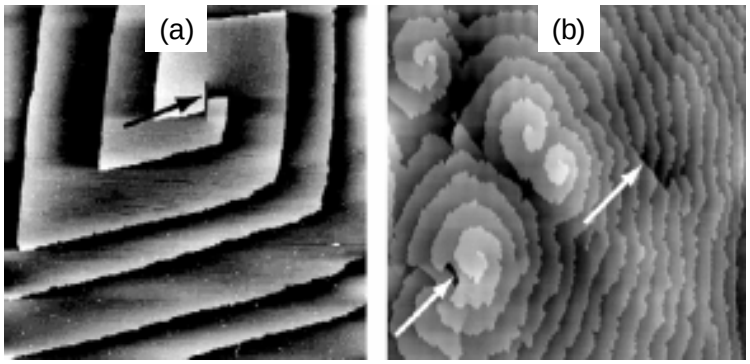

Figure 2- 4 In situ AFM images showing the formation of screw dislocations with vicinal hillocks on the surfaces of (a) glucose isomerase and (b) canavalin protein crystals (Malkin and Thorne, 2004).

By assuming a regular distribution of monoatamic steps, the maximum theoretical growth rate for the given level of supersaturation is given by the Burton-Cabrera-Frank (BCF) relationship of the form:

$$v = k_{SG} \frac{\sigma^2}{\sigma_1} \tanh\left(\frac{\sigma_1}{\sigma}\right) \qquad \textbf{2- 7}$$

in which $k_{SG} \propto \exp(-\Delta G_{desolv} / kT)$ and $\sigma_1 \propto \gamma_e / s$ (s is the strength of the dislocation source). In accordance with the BCF equation, crystal growth rates vary from a parabolic dependence on supersaturation to a linear dependence as the supersaturation increases (Davey and Garside, 2000). Growth rate measurements as a function of supersaturation indicated the BCF mechanism operative on the {010} and {011} faces of an α-glycine crystal grown from aqueous solution (Li and Rodríguez-Hornedo, 1992). It was furthermore supported by in-situ AFM observations of the surface growth morphologies of these crystal faces (Carter et al., 1994).

2.3.2. Effect of impurities

Impurities adsorb selectively on to different crystal faces and retard their growth rates. However, to effect growth inhibition it is not necessary for the impurity to achieve total face coverage. Utilizing the *Kossel model* for crystal growth, three sites may be considered at which impurity species may become adsorbed and disrupt the flow of growth layers across the faces, viz. at a kink, at a step or on a ledge (face) between steps. A theoretical investigation into the implications of adsorption of impurities at each of these sites can help to understand the mechanism of impurity action in reducing step velocities (Davey and Mullin, 1976). In the first case, adsorption at a kink site would effectively reduce their number and cause an increase in the inter-kink distance. As a result the advancement of step will be rate-limited by the formation (density) of kinks resulting in polygonized growth steps with a reduced velocity. If this mechanism were to be active, growth inhibition may be affected at very low impurity levels in the solution.

On the other hand, adsorption of impurities giving monolayer coverage at a step would reduce the number of sites available for growth at the step and hence reduce its velocity. However, for adsorption of impurities corresponding to less than monostep coverage, the advancing step could squeeze between the impurity species relatively unimpeded. According to this mechanism, below a critical concentration of impurity in solution the layer velocity would be unaffected and it would rapidly decrease above the critical concentration.

Finally, adsorption of impurity on a ledge would result in decrease in the surface area as well as in the surface flux of growth units to the step, and thus reduce the step

velocity. In accordance with this mechanism, the step velocities in pure (v_0) and impure solution (v_I) and the concentration of impurity (c_I) can be related by the expression,

$$\left(v_0 - v_I\right) \Big/ v_0 = Kc_I \Big/ \left(1 + Kc_I\right) \qquad \textbf{2- 8}$$

where $K = \left(k_{ads} / k_{des}\right) = \exp(-\Delta G / RT)$, and ΔG is the free energy of adsorption of the impurity species. Consequently, if step site or ledge site adsorption is the preferred mode, much higher levels of impurity concentration may be required for effective reduction of step velocity.

In support of the above arguments, in situ observations using AFM have shed light on impurity effects on crystal growth. In the presence of L-Phenylalanine (an impurity), the advancing steps on the (111) face were corrugated and the surface morphology became irregular (see Fig. 2-3c). This could be clearly distinguished from the surface morphology observed under a pure growth solution (cf. Fig. 2-3a). The kinetic effect of L-Phe on the growth rate was explained based on the step "pinning" mechanism (Kitamura and Onnuma, 2000). The theoretical basis of this mechanism as proposed by Cabrera and Vermilyea (1958) is discussed later in section 2.3.3.

Paracetamol crystals grown in the presence of structurally-related additives (acetanilide and metacetamol) showed corrugated steps on the (001) face as compared to the surface topography obtained from pure solution. The branched appearance of the steps indicated adsorption of impurity molecules onto step or terrace regions that caused pinning of the growth steps. In situ images of the (001) face obtained during incubation in paracetamol solution doped with 4 mol% acetanilide showed holes emerging on the surface. These holes deepened towards the crystal core and also spread out laterally as a consequence of dissolution of the face indicating that the impurity caused an increase in

the solubility of paracetamol. Conversely, in the presence of metacetamol, the growth steps on the (001) face acquired a pointed appearance due to pinning and resulted in decreased step velocity (Thompson et al. 2004).

AFM imaging of an adipic acid (an excipient material) crystal in the presence of a structurally-related habit modifier, octanoic acid, revealed changes in step morphology and growth mode on the (100) face. Crystal growth from an un-doped solution could proceed only after a critical supersaturation, presumably, to disrupt the bound water molecules at the surface. Thereafter, growth proceeded through formation of large macrosteps that moved rapidly across the surface. At low levels of impurity concentration, single molecular steps dominated the crystal surface, with the macrosteps becoming less. Although the step edges moved noticeably slowly, the impurity concentration was not sufficient to completely stop tangential growth, presumably, because the strongly adsorbed water layer may reject the majority of the more hydrophobic octanoic acid molecules. However, on increasing the additive concentration (corresponding to a molar ratio of approximately 1:175 octanoic acid:adipic acid), growth on the (100) face was inhibited, as a direct consequence of the impurity binding to the surface and pinning the monomolecular growth steps (Keel et al., 2004).

Several other studies have demonstrated the impurity action on the growth of macromolecular crystals (McPherson et al., 1996; Land et al., 1997; Kuznetsov et al., 1999; Malkin et al., 2004). Detailed investigations revealed that such impurity effects on the growth kinetics yielded deviation from facet planarity, morphological changes, composition variation and structural defects. For example, AFM observations on a lysozyme crystal in commercial and purified solutions revealed impurity effects on the

(101) surface as against the (110) surface. Among the typical residual impurities contained in commercial lyzozyme, only covalently bound lysozyme dimer affected the (101) step morphology. From the measurements of separation distances of adsorbed impurities on the surface, and an estimate of the critical nucleation size, it was inferred that the impurities reduced the step velocity according to the mechanism described by Cabrera and Vermilyea (Nakada et al., 1999).

Investigations on the impurity effects on the growth of inorganic crystals have shed light on a number of natural phenomena such as mineralization in geochemical and biological environments (Davies et al., 2000), control of biomineralization within tissues and extra-cellular fluids (Qiu et al., 2005; Weaver et al., 2006), and of biological antifreezes (Knight, 2000; Devarakonda et al. 2004).

2.3.3. The Cabrera–Vermilyea model

From the above discussions, it is clear that impurities that act as inhibiting agents induce a so-called 'dead zone', a regime of low supersaturation where crystal growth ceases. The classic theory of *Cabrera and Vermilyea* (1958) explained the behavior near the dead zone in terms of pinning of elementary step motion by impurities. A theoretical analysis of the effect of impurities on step velocity resulted in equation 2-6.

$$v = v_0 \sqrt{1 - 2\rho_c d^{1/2}} \qquad \textbf{2- 9}$$

where v_0 is the step velocity in the absence of impurities, ρ_c is the Gibbs-Thomson critical diameter for a 2-D nucleus (equation 2-7), and d is the average density of impurities just ahead of the step. A complete stoppage of growth would occur when the distance between the adsorbed impurities was less than $2\rho_c$. For spacings greater than

$2\rho_c$, the elementary growth layers could squeeze through the region between the adsorbed impurity species and crystal growth would continue, although at a lower rate when compared to the pure system.

The Gibbs-Thomson effect, on the basis of which the Cabrera–Vermilyea (C–V) model was derived, relates differences in free energy between step and solution to step curvature. In essence, greater curvature leads to smaller numbers of nearest neighbors along a step edge, reducing thermodynamic stability and increasing excess step free energy. This effect leads to a critical curvature, above which the excess free energy exceeds the chemical potential difference between crystal and solution. Consequently, steps can not exceed this curvature, which is set by the critical step radius ρ_c given by the relationship

$$\rho_c = \frac{\alpha\omega}{k_B T\sigma} \qquad \textbf{2- 10}$$

here α is the step-edge free energy per unit step height, ω is the molecular volume, k_B is Boltzmann constant, T is the absolute temperature, and σ is the supersaturation (Weaver et al., 2006). Furthermore, because $\rho_c \sim \sigma^{-1}$, impurity poisoning can be overcome by increasing supersaturation above a critical value. Then for some segments of the growth layers, $2\rho_c$ becomes smaller than impurity spacing and the steps begin to squeeze through the "fence" of impurities.

In order to compare the C-V model with measured data, it is necessary to relate d in equation 2-6 to the surface coverage θ of adsorption sites resulting in the equation

$$\left[1-\left(v/v_0\right)^2\right]^2 = \left(2\rho_c^{\,2}/L\right)\theta \qquad \textbf{2- 11}$$

in which *L* is the separation of lattice sites available to the adsorbed impurity (Black et al., 1986).

Despite general acceptance of the C–V model, recent studies have reported case studies which deviated from the behavior predicted by the model. For example, Land et al. (1999) proposed that resurrection of crystal growth out of the "dead supersaturation zone" in potassium dihydrogen phosphate (Fe^{3+} impurity) was accompanied by the propagation of macrosteps (bunches of monolayer steps), in contrast to the growth of elementary steps as proposed in the C–V model. Weaver et al. (2006) have proposed an improved model for describing impurity effects on crystal growth by synergizing the Langmuir model of adsorption dynamics along with the C–V model.

2. 4. Habit Modification

The overall shape of a crystal, often called its *habit* or *morphology* is bounded by the slow growing faces. The effect of impurities on the molecular scale growth kinetics (as discussed above) can lead to dramatic modification in the bulk crystal habit. The structural and kinetic aspects of habit modification by impurities are discussed in this section.

2.4.1. Molecular recognition at crystal interfaces

The surfaces of a growing crystal can be thought of as composed of 'active sites' that can have specific interactions with molecules in solution, in a manner similar to enzyme-substrate or antibody-antigen interactions. Using this concept of molecular recognition at crystal interfaces, a number of aspects of crystal nucleation and growth could be explained from the viewpoint of stereospecific interactions with the growth environment. Towards a systematic understanding of crystal growth in the presence of

impurities, "tailor-made" additives were used (Weissbuch et al., 1991). These additives are structurally similar to the solute molecules and are basically composed of two moieties: one, the 'binder', having a similar structure (and stereochemistry) to that of the substrate molecule on the crystal surface where it adsorbs. The second moiety, referred to as the 'perturber', is modified when compared to the substrate molecule, and thus hinders the attachment of the oncoming molecular layers of the solute molecules to the crystal surface. The mechanism of habit modification by tailor-made additives is schematically shown in Fig. 2-5.

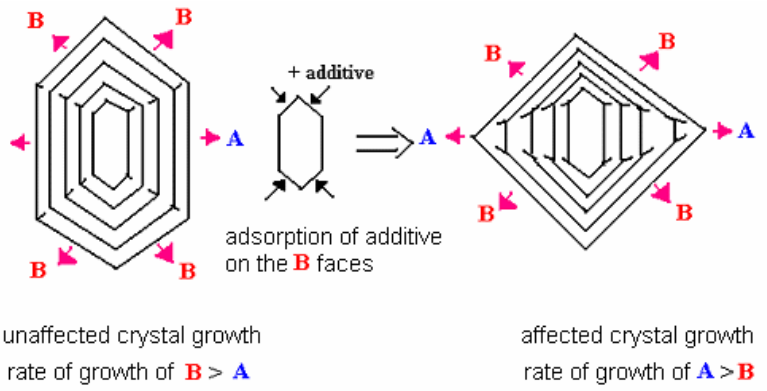

Figure 2- 5 Schematic representation of habit modification by tailor-made additives (Weissbuch et al., 1995).

2.4.2. Structural and kinetic effects

Previous studies have examined the influence of tailor-made additives on the crystal growth of organic materials by applying a structural approach. Some case studies are presented here.

(a) L-asparagine monohydrate crystals grown from supersaturated aqueous solutions have a prismatic morphology with preferred growth in the *x* direction. The habit is dominated by the slow growing {012} faces. In the presence of L-glutamic acid preferred growth occurs in the *y* direction and the {101} faces dominate the habit. The habit modification

can be rationalized through a stereoselective docking mechanism in which an imposter glutamic acid molecule occupies an adsorption site ahead of the step on the (101) face (Fig. 2-6). The replacement of $-CONH_2$ group of asparagine by $-CH_2COOH$ group of the glutamic acid molecule causes disruption of the (amino) N–H···O (amide) and (amine) N–H···O (carboxyl) hydrogen bonds which run along the *x* axis. The incoming carboxylic acid group of the next asparagine molecule has to interact with the carboxylic acid group of the glutamic acid rather than the amide and carbonyl groups of the asparagine molecule. The change in energetics at the crystal surface is consistent with the observed decrease in growth rate of the face (Black et al., 1986).

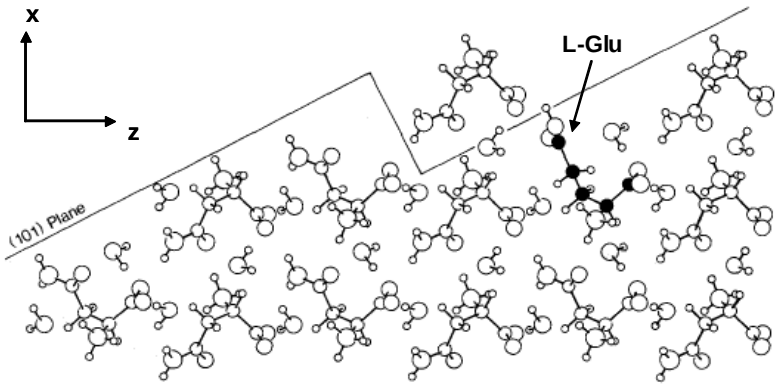

Figure 2- 6 Molecular modeling of the incorporation of L-glutamic acid molecule on the (101) face of L-asparagine monohydrate (Black et al., 1986).

(b) Adipic acid (an aliphatic dicarboxylic acid) crystallizes from aqueous solution with a plate-like morphology, with dominant (100) faces bounded by (001), (102) and (011) faces. In the presence of n-alkanoic monocarboxylic acids (viz. caproic acid, octanoic acid and decanoic acid) the growth rates of (011) and (001) faces are inhibited. The habit modification can be explained on the basis of incorporation of the additives into the adipic acid crystal lattice. Incoming adipic acid molecules will H-bond to a molecule in

the step on the (001) face and utilize the weak CH···O interaction to bind it to the layer below (Fig. 2-7). A monocarboxylic acid, much similar to an adipic acid molecule, can make use of its carboxylate functionality and its overall linear conformation to occupy a growth site and bind to the surface step. Consequently, this growth site will be effectively blocked with a methyl group exposed in place of the expected carboxylic acid. This will eventually slow crystal growth and give the (001) face increased morphological importance (Davey et al., 1992).

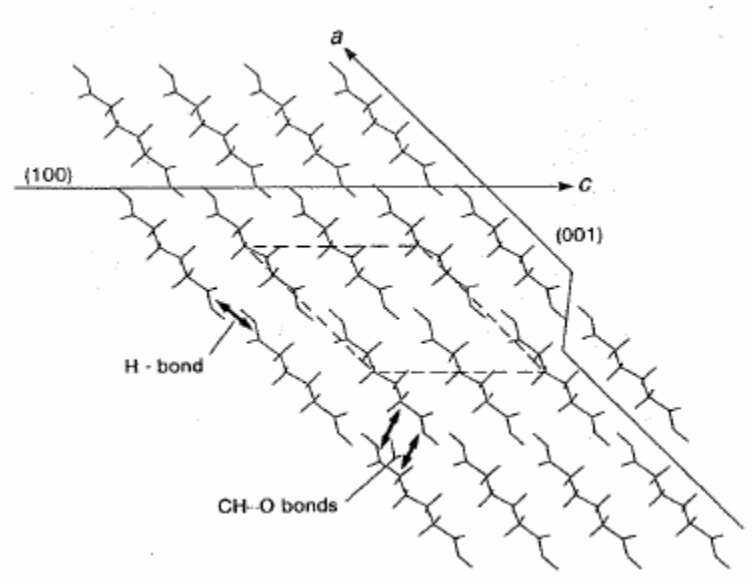

Figure 2- 7 Crystal structure of adipic acid viewed down the *b* axis (Davey et al., 1992)

(c) Urea crystallizes as needles elongated along the [001] direction from an aqueous solution. In the presence of biuret, the morphology is dramatically changed from needles to blocks with much smaller length: breadth ratios. The influence of impurity is explained by the replacement of two urea molecules in the crystal lattice by a biuret molecule. The impurity then disrupts the hydrogen bonding that is parallel to the *z*-axis (Davey et al., 1986).

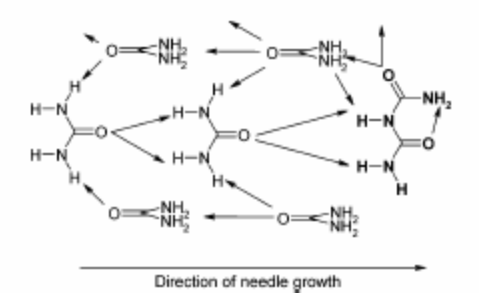

Figure 2- 8 Schematic representation of hydrogen bonding in urea and the disruption caused by the biuret molecule (Scott and Black, 2005)

(d) In the case of benzamide ($C_6H_5CONH_2$) crystallizing from ethanol, additions of benzoic acid, o- and p-toluamide retarded growth selectively in the *b*, *a* and *c* directions respectively (Berkovitch-Yellin et al., 1985). In benzamide crystals, the molecules form H-bonded cyclic dimers, further interlinked by H-bonds to yield ribbons parallel to the *b*-axis (Fig. 2-9). The ribbons are stacked along the axis to form stable (001) layers. These layers juxtapose along the *c*-direction, interacting via weak vdW interactions between phenyl groups, thus accounting for the {001} plate-like shape of the crystals. Benzoic acid additive (C_6H_5COOH), adopting a synplanar conformation (O=C–OH), can replace a molecule of benzamide at the end of a ribbon. However, at the site of the additive, an attractive N–H···O bond (–6.0 kcal/mol) is replaced by repulsion (1.0–2.0 kcal/mol) between adjacent oxygen lone-pair electrons of the bound additive molecule and of the oncoming benzamide molecule leading to an overall loss in energy of 7.0–8.0 kcal/mol. Hence, the presence of benzoic acid in solution inhibits the growth of the benzamide crystals along b-axis, transforming the pure plate-like crystals into needles elongated along the *a*-axis. On the other hand, the additive *o*-toluamide (*o*-$H_3CC_6H_4CONH_2$) can easily be adsorbed in the H-bonding chain without disrupting growth in the *b*-direction. The *o*-methyl group, emerges from the (10–4) side face, and thus interferes with growth in the *a*-direction along which the dimers are stacked. The additive p-toluamide (p-

$H_3CC_6H_4CONH_2$), whose p-methyl group perturbs the weak vdW interactions between the phenyl layers in the *c*-direction, produced thinner plates (Weissbuch et al., 1995).

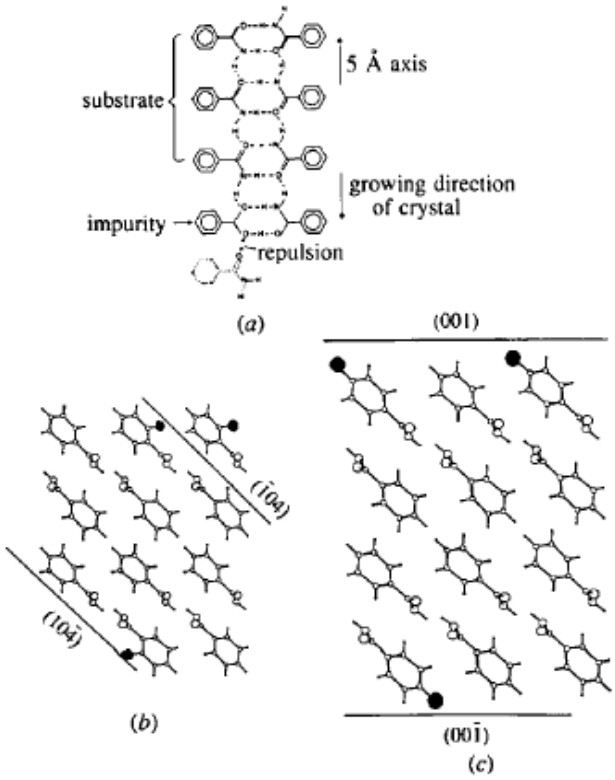

Figure 2- 9 (a) Packing arrangement of benzamide viewed along the *a*-axis, showing the effect of benzoic acid inhibiting growth along the *b*-direction; (b) packing arrangement of benzamide, viewed along the *b*-axis, showing the effect of *o*-toluamide inhibiting growth along the *a*-direction; (c) packing arrangement of benzamide, viewed along the *b*-axis, showing the effect of *p*-toluamide inhibiting growth along the *c*-direction (Weissbuch et al., 1995).

(h) In contrast to the above, the additive 2′-aminoacetophenone (AAP) shows two possible ways in which it might bind across the exposed surface of benzamide crystals (Fig. 2-10). In the former case, it acts as a conventional tailor-made additive similar to the action of benzoic acid. In the latter, the additive acts as a "motif capper" in which it binds across the carbonyl and amine groups exposed at the end of the H-bonded benzamide ribbon ("capping") and terminates its further extension. As a result, the motif-capper additive is able to induce self-replicating intergrowth of benzamide crystals giving rise to ordered crystal aggregates (Blagden et al., 2005).

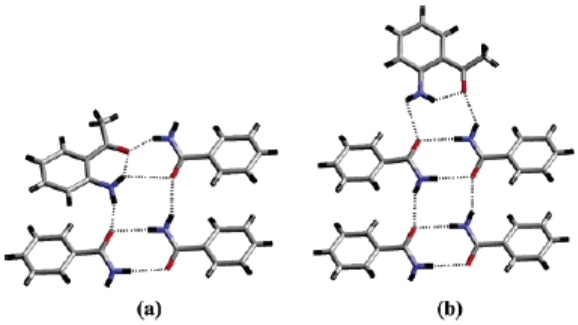

Figure 2- 10 Packing arrangement of benzamide chains showing (a) AAP as a tailor-made additive; (b) AAP as a motif-capper (Blagden et al., 2005).

(e) Morphological changes in paracetamol crystals by structurally related additives was explained based on the host-additive interactions (Hendriksen et al., 1998). The paracetamol crystal structure is predominantly H-bonded with molecular chains packed in a "herring bone" fashion (Fig. 2-11). The additive *p*-acetoxyanilide, whose ester group in the *p*-position is not only larger than the –OH group of the paracetamol molecule (which gives steric effect), but possesses no proton donor to contribute to the existing hydrogen bonding network in the host crystal structure, and hence results in a "blocking" effect. Acetanilide, on the other hand, has no group in the *p*-position and so there is no steric hindrance; however, because it has no proton donor it remains a strong blocker.

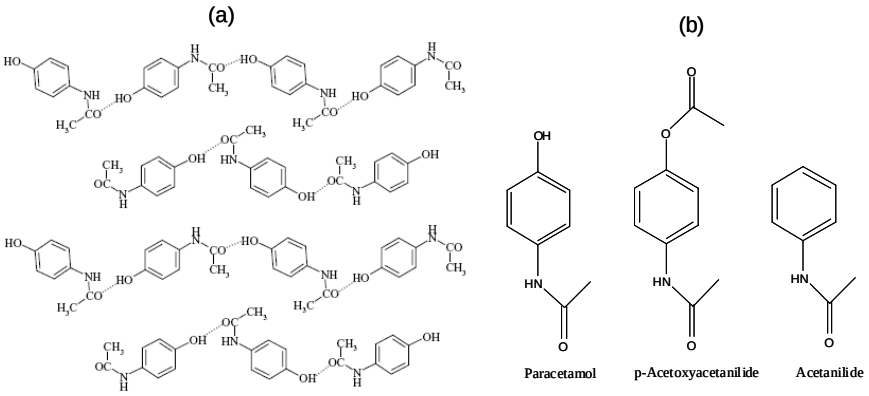

Figure 2- 11 (a) Molecular packing arrangement of paracetamol crystal structure (Thompson et al., 2004); (b) molecular structures of structurally related additives.

(f) With isomorphic impurities L-leucine and L-valine, the former modifies the habit of L-isoleucine from needlelike to hexagonal blade crystals by incorporating into the crystal lattice of the host. In contrast, L-valine is not incorporated within the bulk of the crystal and, consequently, has no effect on the crystal habit. It is concluded that similarities between the molecular and crystal structures of the solutes (primary species and impurities) can lead to the formation of a mixed crystal (Koolman and Rousseau, 1996).

The above discussed structural approach for impurity effects on crystal morphology is often corroborated by kinetic measurements. For example, the influence of L-glutamic acid on the growth rates of (101) and (012) faces of L-asparagine monohydrate was investigated in terms of the Cabrera–Vermilyea model. In the case of the (101) faces the relative growth rate decreased linearly with increasing concentration of additive in solution until growth is completely inhibited, which is consistent with the C–V model. In contrast growth rate of the (012) faces decreased to an asymptotic non-zero value at higher additive concentrations. This suggested that some additional factor is limiting the adsorption of glutamic acid in the surface layer, possibly due to changes in either solid state, surface or solution characteristics (Black et al., 1986).

The growth inhibition of adipic acid crystals in the presence of n-alkanoic acids, of which the structural aspects was discussed earlier, has been further validated from kinetic data. Desupersaturation profiles for pure adipic acid and in the presence of n-alkanoic acids yielded estimates on the influence of the additives on the induction time for crystallization. By linking the data to the molecular nature of the additives a relationship between the aliphatic chain length and the minimum concentration needed to produce the first visible change in crystal habit was shown. In particular, the

effectiveness of the additives was seen to reach a maximum with octanoic acid, with further increase in alkyl chain length producing relatively small improvements in performance (Davey et al., 1992).

The growth kinetics of urea in the [001] and [110] directions for both pure and solutions containing biuret were consistent with the habit modification. In pure solutions urea grows very quickly in the [001] direction, with the data on growth kinetics represented adequately by the BCF model. In the presence of biuret growth rate along the [001] direction decreased rapidly to zero over a very narrow impurity concentration range, suggesting that the C–V model was operative. Furthermore, it was envisaged that as a step moves forward it encounters an array of biuret molecules in the surface layer, which reduced the kink site binding energy and hence the step velocity. Accordingly, below a critical supersaturation the growth rate fell to zero (Davey et al., 1986).

2.4.3. Solvent effects

The influence of solvent on the habit of crystalline materials can be explained by two different approaches. One school of thought is that favorable interactions between solute and solvent on specific faces may lead to reduced interfacial tension, causing a transition from a smooth to a rough interface and a concomitant faster surface growth. Alternatively, the preferential adsorption of solvent molecules at specific faces may inhibit their growth as removal of bound solvent poses an additional barrier for continued growth. In the latter case, solute–solvent interactions at the crystal interfaces could be akin to stereospecific interaction of tailor-made impurities. Toward illustrating this, the interaction of a toluene (solvent) molecule at the crystal surface of benzophenone is shown in Fig. 2-12 (Roberts et al., 1994).

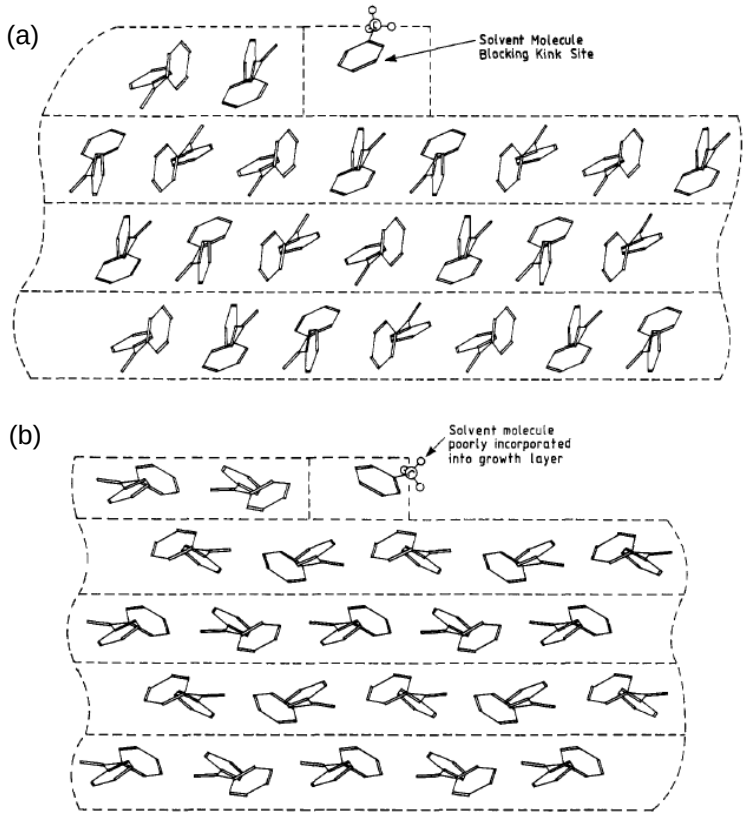

Figure 2- 12 Structural implications for solvent (toluene) binding at surface growth steps of benzophenone: (a) the solvent-modified (021) surface; (b) the unaffected (002) surface (Roberts et al., 1994).

The notion of specific solute-solvent interaction has been rationalized in many ways (Lahav and Leizerowitz, 2001). One, by growing crystalline solvates (where the solvent of crystallization plays the dual role of solvent and crystal solute) in the added presence of tailor-made solvent which is slightly modified version of the solvate solvent. Secondly, by exploiting the principle that a pronounced difference in growth rate at opposite hemihedral faces of a polar crystal must be associated with differences in their solvent–surface interactions. Herein, the difference in the molecular attachment energy at the hemihedral faces is however not significant, and therefore, its effect on morphology must be far less than that of solvent. The third approach involved strong selective adsorption of solvents at a subset of molecular surface sites, and repulsion of solvent at

the remaining set of surface sites on the crystal surface. This involves a cyclic process in which the solvent molecules which are originally bound to specific sites would be repelled after the addition of a solute molecule at an adjacent site. Such a situation, where desolvation is rate limiting (assuming that the free energy of incorporation of a solute molecule aids to displace bound solvent), can lead to fast growth by a kind of "relay" mechanism. Mechanisms involving these principles were demonstrated by determining the growth kinetics of opposite hemihedral faces of polar crystals under different solvents. Solvent interactions at crystal interfaces can also lead to twinning of organic crystals (Williams-Seton et al., 1999).

2.4.4. Implications on product design and process chemistry

In the production of fine organic chemicals and pharmaceuticals, the product crystals have to be separated from their mother liquor. For ease of separation by filtration or centrifugation, the crystals should be of uniform size and have a low aspect ratio. Thin plate crystals tend to form a low permeability layer on the filter medium and hence do not filter well. Likewise, thin needles tend to align with the flow of mother liquor and enter pores in the filter medium, consequently, blocking them. Furthermore, dispersions of thin needles also have high viscosity and can be difficult to pump to the filter or centrifuge. Having said this, habit modification can have significant implications on the filtration behavior. Besides, different morphologies usually influence efficiency of the washing away of impurities and mother liquor, speed of drying, flow properties and bulk density (Wood, 2001).

In commercial manufacturing, impurity levels often change during process development and on scale-up. In addition to its effect on changes in morphology, this can

have potential implications for the yield and productivity. For example, if impurity levels increase, but the time for crystal growth is not adjusted accordingly, then the yield may suffer if the batch is filtered before crystallization is complete. Alternatively, if the impurity levels decrease, crystallization may be completed long before the material is filtered. This is a suboptimal use of production capacity and may also result in unwanted attrition of the product. This, however, can be avoided by the use of in-line technology like the *Lasentec* FBRM (Focused Beam Reflectance Measurement) probe to detect the effects of impurity on the rate of crystallization. The FBRM probe provides a "finger print" of the particle size distribution every few seconds, and hence the course of the crystallization can be followed. Nevertheless, changes in crystal habit may have to be correlated to the FBRM finger print data in order to monitor impurity effects on crystal growth online (Scott and Black, 2005).

2. 5. Crystal Polymorphism

Polymorphism is yet another solid-state attribute which is of central importance to crystallization of organic molecules. Earlier the crystallization of polymorphs from a supersaturated solution was discussed from the viewpoint of nucleation kinetics (cf. section 2.2.5). In this section, the influence of process variables in controlling polymorphism is further elaborated with case studies. The effect of impurities on crystal polymorphism is discussed in greater detail in context to the present study.

2.5.1. Industrial significance

The fact that different packing arrangements of the same molecule within its crystal structure can affect many of the physico-chemical properties of the crystalline product has added in technological importance to polymorphism. In pharmaceuticals, for

example, it is estimated that approximately 40% of all drug compounds discovered have certain delivery limitations due to poor solubility or poor availability (Li and Zhao, 2007). Having said this, different polymorphs will have different solubilities and therefore affect the "bioavailability" vis-à-vis dissolution rate of the active ingredients in the dosage form (Bernstein, 2002). This brings tremendous challenges to scientists working in the field of early formulation.

Crystal polymorphs may also undergo inter-conversion as a result of external influences: in suspension during crystallization, during processing (e.g. elevated temperatures on drying), or under the storage conditions employed (pressure and temperature fluctuations) (Spruijtenburg, 2000). This is highlighted by the issue of so called "disappearing polymorphs", i.e. the sudden appearance of a new structure or the unexplained disappearance of an existing one (Bernstein, 2002). An example of "latent polymorphism" is the case of *Ritonavir*–a drug for HIV treatment from Abbott Laboratories. In this case, a stable form of ritonavir (Form II) crystallized unexpectedly, the presence of which in the formulation caused the semisolid capsules to fail dissolution tests. As a result, the product was withdrawn from the market. In order to tackle this problem, consequently, a formulation was developed to accommodate Form II of ritonavir. Furthermore, a robust crystallization process was developed to produce the metastable polymorph (Form I) consistently through a "super seeding" approach (Chemburkar, 2000).

Polymorphism is also of vital importance in the context of patent protection in the pharmaceutical industry. This was best highlighted by the *Zantac* (GSK's blockbuster drug for peptic ulcers) patent case that involved legal battles fought between major

pharmaceutical companies. In this case, the scientific issues pertaining to solid-state form involved isolation of Form I of ranitidine hydrochloride without concomitant crystallization of Form II, a phenomenon exemplified by the *Ostwald's Rule of Stages* (Davey, 2003).

2.5.2. Thermodynamics and Kinetics

The crystallization of polymorphous crystals is composed of competitive nucleation, growth, and the transformation from a metastable to a stable form. To selectively crystallize polymorphs, the mechanism of each elementary step in the crystallization process needs to be clear in relation to the operational conditions and the key controlling factors (Kitamura, 2004).

In terms of thermodynamics, one of the key questions regarding polymorphic systems is the relative stability of the various crystal modifications at different domains of temperature, pressure, and other conditions and the changes in thermodynamic relationships accompanying phase changes (Bernstein, 2002). Under constant pressure, polymorphic systems come under two categories – *enantiotropic* and *monotropic*. In an enantiotropic system, the *transition temperature* at which two or more polymorphs are at equilibrium falls at a temperature below the melting point of the lower melting form. However, in a monotropic system the free energy curves do not cross at a temperature below the two melting points. In terms of solubility curves, for enantiotropic system the relative solubility of the polymorphs is temperature dependent; whereas, for monotropic system the relative solubilities are independent of temperature (Davey and Garside, 2000).

However, the probability that a particular form will appear is controlled by the rate of some kinetic process associated with the formation of a crystal by molecular aggregation, besides the relative free energies of the possible crystal structures. This concept was clearly reflected in a recent study on the crystallization of glycine polymorphs (Chew et al., 2007). Briefly, their results showed that γ-glycine, which is thermodynamically stable, grows 500 times slower than the metastable α-glycine at the same supersaturation. This difference in growth rate corresponds to a difference in activation energy for growth of ~ 3.6 kcal/mol. In comparison, the thermodynamic difference is small – a solubility ratio of 1.1: 1 corresponds to a difference in lattice energies of approximately 0.05 kcal/mol between the two forms. This large difference in activation energy is consistent with the dissociation of glycine dimers in solution prior to growth of γ-glycine, but their preservation in the α-glycine crystal structure.

The distinction between kinetic and thermodynamic crystallization conditions has been utilized to selectively obtain or prevent the crystallization of a particular polymorph. Recent studies serve to demonstrate this fact. He et al. (2006) have selectively grown γ-glycine crystals via concentrating microdroplets of aqueous glycine solution through *slow* evaporation of water. However, on increasing the rate of evaporation, i.e. supersaturation generation rate, the occurrence of the metastable α-form increased. Rationalizing this observation, the authors proposed that below 'certain' value of supersaturation generation rate the crystallizing solution stays close to the equilibrium, allowing the system to sample the lowest free energy state during the formation of nuclei. A related work achieved selective crystallization of α- or γ-glycine by modulating the solvent evaporation rate for the achievement of supersaturation through a membrane matrix

(Profio et al., 2007). The polymorphic modification was rationalized by stating that the increase in the solvent evaporation rate induced an increase in the metastable zone width with effects on heat and mass transfer during the nucleation kinetics.

In contrast to glycine, with L-glutamic acid and L-histidine the effect supersaturation ratio was less pronounced on the polymorphous composition of the product crystals. However, the temperature effects were different between the systems. In the case of L-Glu, at lower temperatures (e.g. 293 K) only the α form (metastable) crystallized, and as the temperature increased the portion of β form in the crystals increased. The temperature dependence of L-Glu crystallization may be influenced by the change of relative concentration of the conformers (polymorphic embryos) with temperature. However, almost no effect was observed in the L-His system. This difference in the nucleation behavior was rationalized on the basis of molecular structure of each amino acid, and the difference between the crystal structures of the polymorphs of each amino acid. Since L-His has a bulky imidazole group and less number of carbon atoms than L-Glu, it is likely that the conformational difference between the polymorphs is very small in comparison with that of L-Glu polymorphs. Accordingly, the activation energy of the L-His conformer exchange could be very small and therefore the concentration of each conformer corresponding to the polymorphs may be almost the same. This may result in the crystallization of L-His polymorphs *concomitantly* with the same probability (Kitamura, 2004).

Other primary factors affecting polymorphic crystallization may include addition rate of anti-solvent and mixing rate in reactive crystallization. The “stirring rate” can either induce nucleation (of the metastable form) or enhance the rate of solvent-mediated

phase transformation. In a 'solvent-mediated transformation' the metastable phase dissolves while the stable phase renucleates and grows from solution (Davey and Garside, 2000). For example, in the case of L-glutamic acid the solvent-mediated transformation of α to β form proceeds via secondary nucleation in which the surface of the α form acts as a template for the nucleation of the β form (Ferrari and Davey, 2004). A similar mechanism is operative in the case of 2,6-dihydroxybenzoic acid (forms 1 and 2) and is related to the process by which the stable form nucleates at the surface of the metastable crystals (Davey et al., 2002a). In the case of solvent mediated transformation from β to α glycine the mass transfer rate controlled dissolution of the metastable form (Ferrari et al., 2003). In general, the kinetic processes involved in phase transitions between polymorphs could be dissolution (of the metastable form) or growth (of the stable form) controlled (Davey et al., 1986).

2.5.3. Effect of impurities

Having said the role of kinetics in polymorphic crystallization, factors due to external substances such as solvents, additives (impurities), pH, and interfaces also play an important role. A study on the effect of impurities on organic crystal polymorphs begins with the crystal structure analysis which provides information on the detailed packing and intermolecular relationships within the crystal structure. Subsequently, the crystal habit of each of the polymorphic forms is characterized and using this information one may obtain a view of what a molecule in solution 'sees' when approaching the various crystal faces. Combining this information with the interaction mechanisms of tailor-made additives (discussed previously), polymorphic modifications could be rationalized. Classic examples illustrate the application of this strategy.

Blagden et al. (1998) investigated the role of a reaction byproduct (ethamidosulphathiazole, from the final hydrolysis stage) on the appearance of sulphathiazole polymorphs from aqueous solution. While from pure solution the most stable phase (form IV) was isolated, the presence of the impurity at concentrations as low as 1.0 mol% stabilized the metastable modification (form I). In the presence of 1.0 – 0.5 mol% forms II and III were stabilized. From an analysis of the respective hydrogen bonds and crystal morphologies of each phase this was accounted for by a mechanism involving preferential inhibition of the polymorphic modifications by the impurity.

Davey et al. (1997) have successfully selected additives (e.g. trimesic acid) which by virtue of their conformation were able to selectively inhibit the appearance of the stable β polymorph of L-glutamic acid and hence stabilize the metastable α structure. Towler et al. (2004) in an attempt to rationalize the effect of molecular "self-poisoning" on glycine polymorphism have used malonic acid (1.0 wt %) and ethylene diamine (2.0 wt %) to obtain the polar form of γ-glycine, in preference to the centrosymmetric α-form.

The principle of selective inhibition of centric versus non-centric polymorphic structures has been demonstrated using tailor made additives in a number of systems: for example, in glycine, using racemic hexafluorovaline (Weissbuch et al., 1994) and α-amino acids such as DL-phenylalanine, DL-tryptophan and DL-methionine (Torbeev et al., 2005); in N-(2-acetamedo-4-nitrophenyl) pyrolidene using polymeric additives (Staab et al., 1990); and in dihydroxybenzoic acid using benzaldehyde (Davey et al., 2002). Recently, a similar approach has been extended for chiral separations in which additives (e.g. phenyl acetic acid and phenyl propionic acid) were designed to discriminate

between the racemic compound and the pure enantiomer of mandelic acid (Mughal et al., 2007).

Mukuta et al. (2005) have reported the influence of impurities on the solution-mediated phase transformation of an active pharmaceutical ingredient. It was proposed that the kinetic stabilization of the metastable phase in the presence of impurity is a result of its ability to disrupt the nucleation and crystal growth of the stable polymorph and its enhancement in the solubility of form B, which in turn leads to a reduction in the driving force. Sonoda et al. (2006) have reported selective crystallization of the metastable From IV of tolbutamide (a hyperglycemic agent) from aqueous solutions containing cyclic oligosaccharide derivative (impurity), in preference to the stable Form I crystallized in the absence of the cycoldextrin. This was attributed to the inhibition of the solution-mediated transformation of the metastable form to the stable form by the complexation with the impurity.

Literature is replete with case studies where the action of impurities on crystal growth process, by and large, is rationalized based on a 'growth inhibition' mechanism. Nevertheless, the impurity effect on the solubility of the primary solute may have profound implication on the nucleation behavior by changing the supersaturation or the interfacial tension between the crystal–solution interfaces. For example, in electrolyte solutions, the presence of a common ion might cause "salting-in" (wherein the solution becomes undersaturated with respect to the saturation temperature) or "salting-out" (wherein the solution becomes supersaturated) effects (Mullin, 2001). On account of this, experiments should have to be performed at various supersaturation levels and impurity

concentrations so as to confirm the mechanism of impurity action (Rodríguez-Hornedo and Murphy, 1999).

2.5.4. Solvent and pH effects

The choice of solvents is known to influence the relative occurrence of polymorphic modifications. The mechanisms by which solvents can influence the polymorphic outcome of a crystallization process may broadly fall into three categories: (a) solvent molecules could interact preferentially with the crystalline precursors akin to tailor-made impurities and consequently inhibit its growth; (b) induce the self-assembling of solute molecules; (c) influence the relative supersaturation available for nucleation through effects on solubility. The *case (a)* has been exemplified by the approach used to develop solvent choice for the selective growth of polymorphs of sulphathiazole (Blagden et al., 1998a). A similar rationale was proposed for the induced crystallization of the least stable β glycine, in preference to the more stable α and γ forms, by the addition of methanol or ethanol to aqueous solutions (Weissbuch et al., 2005).

case (b) has been exemplified with the example of 2,6-dihydroxybenzoic acid, in which the solvent self-assembly of this molecule is directly linked to the relative occurrence of its two polymorphic forms from toluene and chloroform solutions (Davey et al., 2002). This mechanism is also revealed in the case of tetrolic acid – chloroform solutions rich in dimers nucleate the α form, whose crystal structure consist of a classic dimer motif; and ethanol solutions (polar solvent) in which dimer formation is disrupted nucleate the catemeric β structure (Parveen et al., 2005).

An illustration of *case (c)* is the anti-solvent crystallization of a thiazole-derivative pharmaceutical, BPT (an enzyme inhibitor), in which the thermodynamic

stability of each polymorphs and the transformation behavior between the polymorphs is affected by the methanol composition (Kitamura, 2004). Threlfall (2000) has given a thermodynamic insight into the role of solvent on the nucleation of polymorphs based on the theoretical framework of metastable zone widths. It is argued that under "certain" experimental conditions, the effect of solvent may be related to the concentration attainable in that solvent at a certain temperature rather than a specific effect of solvent–solute interaction.

Jones et al. (2005) demonstrated that the pH factor, combined with the effects of supersaturation and temperature of crystallization was influential in the crystallization behavior of a polymorphic organic salt (ethylenediammonium 3,5-dinitrobenzoate). In this case, by altering the pH of crystallization independently of other factors the polymorphism and morphology of the crystal produced could be controlled. Towler et al. (2004) have rationalized the effect of pH on the polymorphic behavior of glycine through a "self-poisoning" effect.

2.5.5. Nucleation control and polymorph screening

From the above discussion, it is clear that a large number of factors can influence crystal nucleation and growth process, including the composition of the crystallizing medium and the processes used to generate supersaturation. Therefore, solid form screening is used to understand the effects that these variables have on the polymorphic outcome of a crystallization experiment, so that a robust process can be identified to produce the desired crystal form. Traditionally, the study of solid form diversity of active pharmaceutical compounds has relied on the use of a combination of solvent recrystallization (cooling or evaporative, as well as slurry conversion) and thermal

analysis (e.g. hot stage microscopy, differential scanning calorimetry) experiments. Such methods are inherently slow and only allow exploration of a small fraction of the composition and processes space that can contribute to form diversity. Accordingly, it is not surprising that unexpected and undesired outcomes can, and do, occur later on in development. Therefore, in an effort to understand form diversity in a more comprehensive manner, high-throughput (HT) crystallization systems have recently been developed. This methodology uses a combinatorial approach to solid form generation, where large arrays of conditions and compositions are processed in parallel. Supersaturation and induction time are independently controlled by these conditions, resulting in highly non-linear time dependence of crystallization. In addition, the combinatorial approach permits exploration of a chemical continuum, where use of many solvent mixtures may allow one to access what underlying physical or chemical processes are required to produce a particular solid form. Sample analysis in HT crystallization systems typically use Raman spectroscopy and/ or powder X-ray diffraction. Experiments are performed at small scale to reduce the material demand and to afford the largest number of conditions possible (Morissette et al., 2004).

Once a variety of conditions that can be used to produce a given crystal form on the microscale are identified in the HT screen, scale-up studies have to be conducted to optimize the process. At this stage, for a given solvent system, monitoring and control of the process variables such as the temperature at the onset of crystallization, the rate of crystallization, and the degree of supersaturation can contribute to a robust process yielding the desired solid form.

2. 6. Molecular Modeling and Simulation

Having said the importance of crystal habit and polymorphism on product specification and process development, recent work is geared towards predicting these solid-state properties using a molecular modeling approach. Crystal structure prediction can aid in performing targeted crystallization experiments for polymorph screening. However, the fact that organic molecules can adopt different conformations within the predominantly hydrogen bonded crystal structures has limited its application (Blagden and Davey, 2003; Price, 2004; Coombes et al, 2005). Besides it is well known that the structural outcome of a solution crystallization process is dictated by kinetics in most but not all cases, and hence, limited in its prediction success (Chew et al., 2007).

Habit modeling involves the prediction of growth morphology of organic crystals from its molecular crystal structure, and is an equally challenging task (Brunsteiner and Price, 2001). Habit modification by impurities can be rationalized by modeling the interaction of impurities with the crystal faces of the growth morphology, and subsequently, by calculating their interaction energies within the host crystal. The theories in habit modeling and the prediction of impurity effects are discussed in this section along with some case studies.

2.6.1. Habit modeling

In the prediction of the crystal habit (growth morphology) of an organic material, primarily, two of the basic information is derived from its molecular crystal structure. One, is the symmetry constraints (the point group) in the asymmetric unit, and, the second is the inter-atomic distances between the molecules. Having obtained this, the growth morphology can be predicted by employing either the *BFDH (Bravais-Freidel-*

Donnay-Harker) method or the *Attachment Energy* method. The assumptions underlying both these methods is that a *(hkl)* crystal surface grows by the addition of a complete molecular layer of thickness d_{hkl} (i.e. the interplanar spacing along [hkl] direction) having the same orientation and structure as the bulk crystal structure. Further, the energy released when a layer is added to a crystal surface (i.e. attachment energy) is directly proportional to the growth rate of a given face (Bennema, 1995).

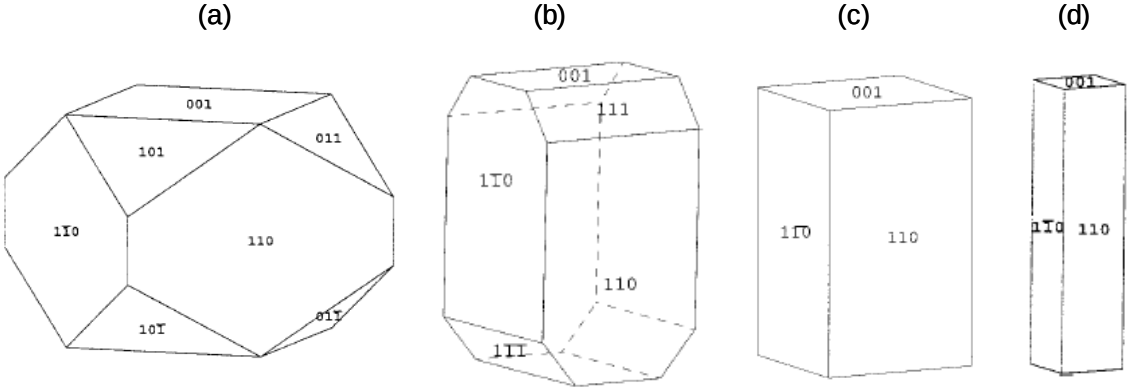

Figure 2- 13 Urea crystal shape: (a) predicted by the BFDH method; (b) experimental (vapor grown) crystal habit; (c) predicted by the attachment energy model; (d) predicted habit after accounting for solute-solvent interactions (Bisker-Leib and Doherty, 2001).

The BFDH theory is based on a purely structural approach and assumes that the binding energy between crystal planes is inversely proportional to the interplanar spacing, i.e. the closer the molecules, the larger are their interaction energies. The morphology of urea crystals predicted using this method is shown in Fig. 2-13 and compared with the crystal habit grown form vapor (Bisker-Leib and Doherty, 2001). Clearly, there is a significant difference between the two shapes; the predicted shape is elongated along the *b* direction, exhibiting faces {110}, {101}, {001}, and {011}. In contrast, the observed morphology is prismatic, elongated along the *c* direction and bounded by faces {110}, {001}, and {111}. This poor prediction is attributed to the fact that the BFDH model

takes into account only cell parameters while ignoring the nature of the chemical interactions between the molecules in the lattice.

The *Attachment Energy* model was proposed by Hartman and Perdok (1955) which successfully related the energies of the bonds between the crystal building units to its external shape. The authors identified uninterrupted chains of "strong" bonds, called periodic bond chains (PBC), and classified crystal faces as one of three types: F (flat) face, S (step) face, or K (kink) face. One of the most useful concepts developed from this analysis was that of the "slice" and "attachment" energies. The slice energy (E_{sl}) is the energy released on the formation of a stochiometric growth slice, and the attachment energy (E_{att}) is the energy released when the slice is attached to the surface of the growing crystal. The sum of the two is the lattice energy, which equals the sublimation enthalpy of the substance corrected for the difference between the gas-phase enthalpy and the solid-state enthalpy (Bisker-Leib and Doherty, 2001).

$$E_{latt} = E_{sl} + E_{att} = -\Delta H_{sub} - 2RT \qquad \textbf{2- 12}$$

The interaction energies E_{ij} between the individual *i*th and *j*th non-bonded atoms of the molecules that constitute the crystal are usually calculated in terms of van der Waals and electrostatic contributions through an equation of the form:

$$E_{ij} = \frac{-A}{r_{ij}^{6}} + \frac{B}{r_{ij}^{12}} + \frac{q_i q_j}{\varepsilon r_{ij}} \qquad \textbf{2- 13}$$

in which the vdW energy is expressed in terms of the well known 6–12 Lennard-Jones function and the electrostatic term as a function of the fractional charges q on the *i*th and *j*th atoms, their separation r_{ij}, and the dielectric constant ε. Specific force fields and partial atomic charges are employed while computing the atom–atom potential energies

by molecular mechanics calculations. It is important to note that the attachment energy predictions are sensitive to choice of force field potentials. Variations in both the repulsion–dispersion parameters and in the accuracy of the electrostatic model (including the atomic point charges) can affect the predictions (Brunsteiner and Price, 2001). Therefore, the accuracy of an intermolecular potential to model morphologies of organic crystals should be verified by comparing the computed values of the lattice energies with the experimental values of sublimation enthalpies.

Clydesdale et al. (1996) were one of the pioneers to develop a computer program – *HABIT95* to simulate the crystal morphology of organic crystals via computational molecular modeling-based techniques. The shape of urea crystal as predicted using the attachment energy model in *HABIT* is shown in Fig. 2-13 (c) (Bisker-Leib and Doherty, 2001). A *Wulff* plot is used to obtain the crystal shape, in which the (hkl) faces are constructed from the centre-to-plane distances of the respective faces. The predicted shape is in reasonable resemblance to the vapor-grown shape, with the assumption made that the {101} face is not morphologically important and does not appear in the final habit. Since this model accounts for the interactions between the molecules in the lattice it provides a reasonable improvement over the BFDH model. However, it does not take into account interactions with a solvent, and therefore, is of limited use for solution crystallization. Moreover, in the case of polar crystals (e.g. urea), the solute–solvent interactions at the crystal–fluid interfaces are relatively stronger and therefore affect the crystal habit. By incorporating such interactions into the kink and edge free energy calculations, the predicted crystal shape of urea, grown from polar solvents (e.g. water and methanol), resulted in a prismatic elongated shape (see Fig. 2-13 (d)) that resembled

the experimental habit. Likewise, in the theoretical approach of Liu et al (1995), it was proposed that the important parameters controlling the growth rate are the energy required to create a step at the crystal surface and the free energy barrier for an adsorbed solute molecule to be incorporated into the crystal. Applying this principle to the case of urea crystals grown from aqueous solution, a needle-like shape was predicted, consistent with experimental observations.

Berkovitch-Yellin (1985) calculated the habit of organic crystals (e.g. benzamide, benzoic acid, α-glycine, cinnamide and succinic acid) according to the *attachment energy* method using *ab inito* calculations. Calculated morphologies were in good agreement with observations for crystals grown by sublimation. Solvent effects on the habit of crystals were explained through preferential adsorption of solvent molecules on specific crystal faces, whose relative polarities were comprehended from the electrostatic potential maps at closest approach distances.

Cuppen et al. (2004) have used Monte Carlo simulations to predict the needle-like morphology of aspartame (an artificial low-calorie sweetener) form II-A. Calculations for all connected (F) faces resulted in a sticking fraction plot which indicated three faces to have a nucleation barrier for growth. Below the nucleation barrier of the slowest growing face, crystals cannot nucleate and grow to a size large enough to observe. A high supersaturation is needed due to the huge nucleation barrier of the slowest growing side face. Consequently, at these high supersaturations, all top faces having a relatively smaller nucleation barrier grow extremely fast, whereas the side faces still grow relatively slowly, resulting in a needle-like morphology.

2.6.2. Impurity interactions: Binding energy

The aforesaid methods for calculating surface attachment energies have been developed to be able to treat the effects of impurity species on the growth morphology. For this, an additional factor, the "differential binding energy", is introduced in order to assess the likelihood of impurity incorporation into the host crystal lattice. It is defined as the difference between the incorporation energies of solute (E_b) and the impurity molecule ($E_{b'}$):

$$\Delta b = E_{b'} - E_b = (E_{sl'} + E_{att'}) - (E_{sl} + E_{att}) \qquad \textbf{2- 14}$$

In this equation $E_{sl'}$ is the slice energy calculated with an impurity molecule at the centre of the slice; $E_{att'}$ is the attachment energy of a growth slice containing an impurity onto a pure surface. This equation shows that the impurities are likely to incorporate on crystal faces where there is a minimum change in the binding energy. If Δb is strongly dependent upon crystal orientation then the incorporation will be specific to one crystal face and vice versa. A modified attachment energy parameter $E_{att''}$, reflecting the energy released on the addition of a pure growth slice onto a surface on which an impurity molecule has adsorbed, is used as a measure of growth rate of a crystal face "poisoned" with an impurity molecule. This methodology has been included into the *HABIT* program so as to enable calculation of the crystal morphology with an impurity present (Clydesdale et al., 2005).

The pioneering work by Berkovitch-Yellin et al. (1985) used atom-atom potential energy calculations to probe into fine intermolecular interactions that caused controlled modification of the morphology of organic crystals. Besides, the induced morphological effects were used to obtain information on molecular interactions and conformations of

the adsorbed impurities at the crystal surface. For example, it was shown that adsorbed impurities benzamide and picolinamide assume twisted and planar conformations, respectively, on the affected faces of host benzoic acid, which is planar in the solid. In contrast, p-aminobenzoic acid tends to be planar when interacting with the growing faces of the nonplanar p-aminobenzamide.

Clydesdale et al. (2005a) have applied the differential binding energy method to predict habit modification in a number of organic systems: naphthalene (host) – biphenyl (impurity), phenanthrene (host) – biphenyl (guest), adipic acid in the presence of succinic acid, glutaric acid and caproic acid as impurities, ε-caprolactam in the presence of cyclohexane, cyclohexanol, cyclohexanone and caprolactim as impurities. As an illustration, the predicted morphologies of naphthalene when modified by the biphenyl impurity are shown in Fig 2-14. The predicted morphologies suggest that the impurity finds the {110} faces as the most favorable faces for incorporation, with low differential binding energy values.

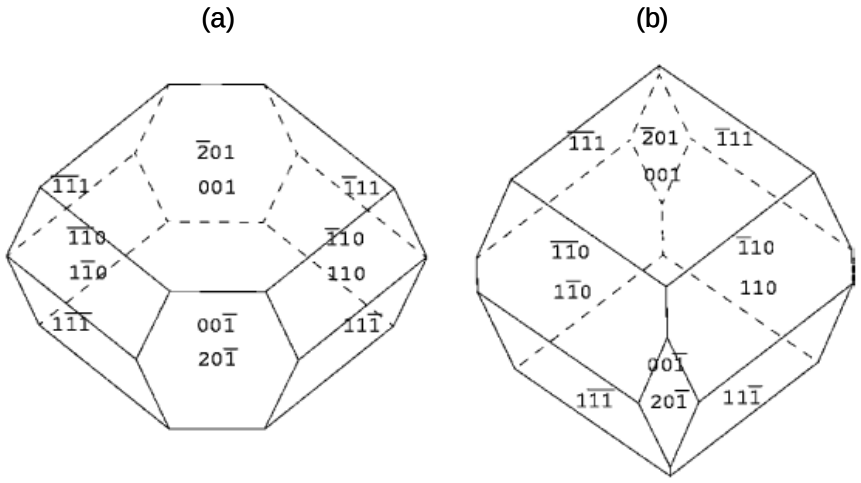

Figure 2- 14 Predicted morphology of: (a) pure naphthalene; (b) effect of biphenyl on the crystal habit (Clydesdale et al, 2005a).

By using the attachment energy model, Mukuta et al. (2005) have rationalized the experimental observations on the solution-mediated phase transformation of an active pharmaceutical ingredient in the presence of tailor-made impurities. The simulation results indicated that the order of the relative incorporation energies of the structurally similar impurities was identical to the order of the percentages of the amount of impurities incorporated into the crystal lattice (as determined by HPLC).

Weissbuch et al. (2006) performed binding energy calculations in order to elucidate a "self-poisoning" mechanism which might explain the unidirectional growth of α-resorcinol in the vapor phase. It was elegantly shown that a molecular misorientation (of the resorcinol molecule) at the growing crystal interface can cause an effect akin to the action of a tailor-made impurity, and therefore, result in growth inhibition.

2. 7. Closing Remarks

With structurally related impurities affecting crystal growth process and bringing about dramatic changes in the product crystal attributes, understanding of the mechanisms is a requisite so as to design and control robust crystallization processes. Experimental investigations combined with molecular modeling studies provide a promising tool toward a better understanding of crystal growth from impure solutions. A direct implication is in pharmaceutical manufacturing where increased control of physical attributes of the bulk drug substance is mandatory to meet formulation needs for reproducibility and bioavailability.

CHAPTER 3

Experimental – Materials and Analytical Techniques

In this chapter, the crystal growth experimental procedures, and the methods used for characterization of solid-state and solution chemistry of the model compound are discussed. The working principle of the state-of-the-art analytical techniques used in this study is briefly reviewed.

3.1. Model System

Pharmaceutical active ingredients, drug excipients and fine chemical compounds are typically organic small molecules, which are frequently purified by crystallization from solution. Considering this fact, glycine was chosen as the model system for this study, with higher homologous α-amino acids added in to glycine solutions as the structurally–related impurities.

3.1.1. Glycine – the primary solute

Glycine (H_2NCH_2COOH), the simplest amino acid, is a prochiral molecule and is commercially available with high purity levels. In aqueous solution it exists in the zwitterionic form (pI = 5.97), and undergoes speciation to form cations and anions in acidic (pK_a = 2.34) and basic (pK_b = 9.60) solutions, respectively (Kirwan and Orella, 2002; Lide, 2004) (Fig. 3.1).

In its solid phase glycine is predominantly hydrogen bonded ("molecular" crystals) with three known crystal structures (polymorphs): α β and γ forms (Weissbuch et al. 1983, 1994; Ferrari et al., 2003; Towler et al., 2004). The polymorphs differ in the packing arrangement of glycine zwitterions via hydrogen bonding in the crystal lattice. In

α-Glycine crystal structure (space group $P2_1/n$; monoclinic with cell dimensions a = 5.10 Å, b = 11.97 Å, c = 5.46 Å and β = 111.8º (Jönsson and Kvick, 1972)), centrosymmetric dimer molecules are laterally H-bonded to form bilayer sheets, which are stacked along the b-axis by Van der Waals interactions (Fig. 3.2a). In the β-polymorph (space group $P2_1$; monoclinic with cell dimensions a = 5.07 Å, b = 6.26 Å, c = 5.38 Å and β = 113.2º (Iitaka, 1960)), individual parallel layers are linked by H-bonds in a three dimensional network (Fig. 3.2b). In the γ-polymorph (space group $P3_2$; cell dimensions a = 7.04 Å, b = 7.04 Å, c = 5.49 Å and γ = 120º (Kvick et al., 1980)), the zwitterions are linked to each other in a three dimensional polar helical network (Fig. 3.2c). The relative stabilities of the polymorphs have been related to the crystal lattice energies vis-à-vis the strength of hydrogen bonding in different polymorphic forms and arranged in the descending order of stability: γ > α > β-polymorph (Perlovich et al., 2001). Recently, the δ-polymorph of glycine has been reported to form under the application of high pressures (Dawson et al., 2005).

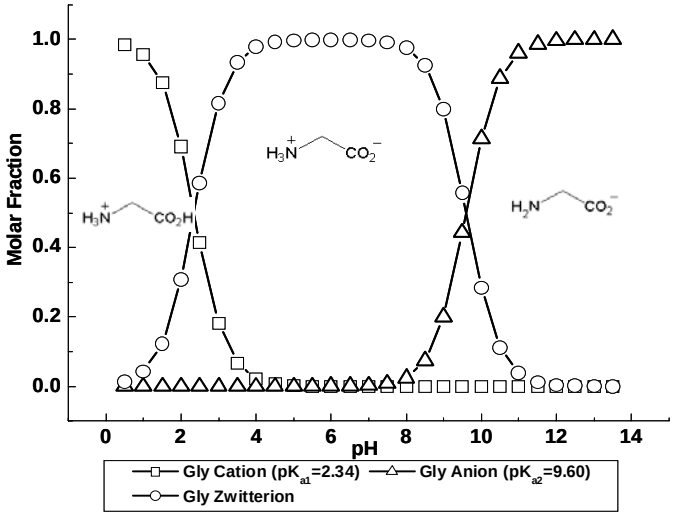

Figure 3- 1 Solution Speciation of glycine as a function of pH.

Glycine has provided a classic example in earlier studies for elucidating the mechanisms by which structurally related impurities impact crystal growth process (Weissbuch et al., 1983, 1994, 2003; Towler et al., 2004). Besides, the rationale behind choosing glycine as the model compound is partly because of its simple molecular structure, which is of advantage in studies pertaining to molecular modeling and simulation.

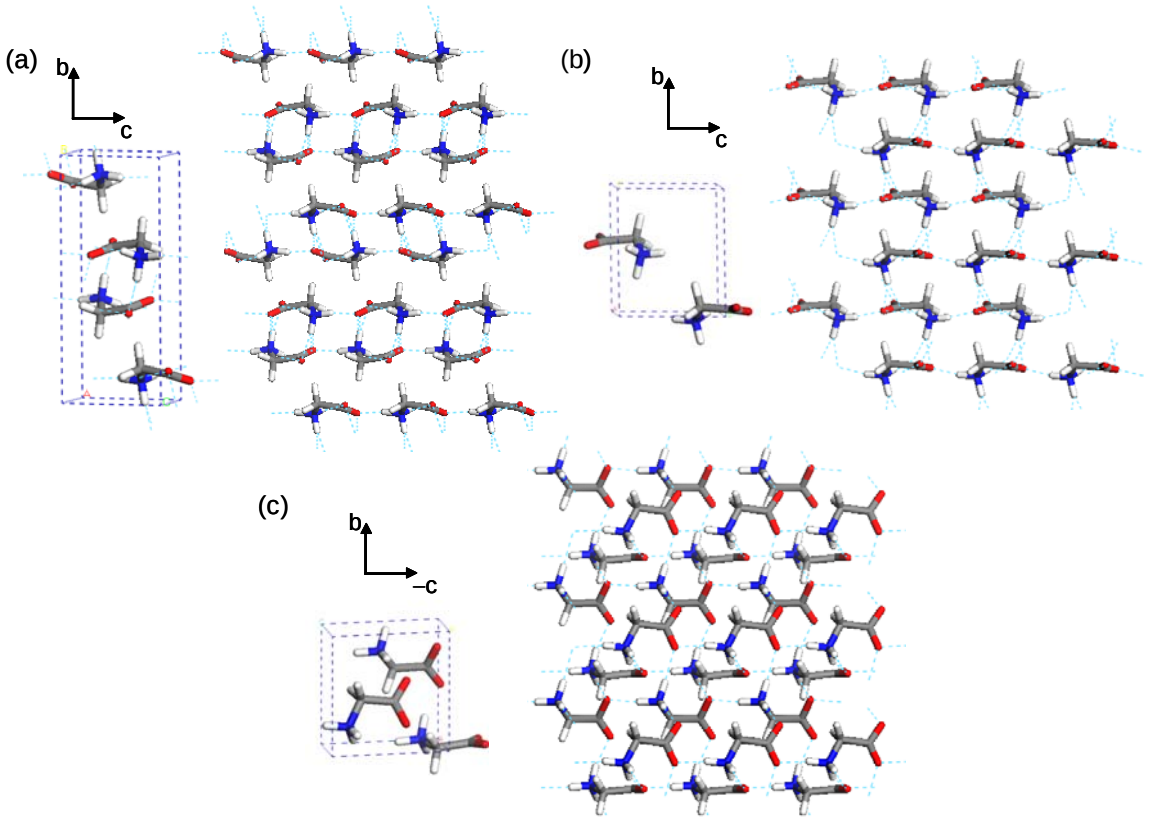

Figure 3- 2 Unit cell structure and molecular packing arrangement of glycine polymorphs: (a) α-form; (b) β-form; (c) γ-form.

3.1.2. Homologous α-amino acids – the impurities

α-amino acids form a family of molecules that have a common functionality at one end (NH_3^+ COO^-) coupled to a range of gradually differentiated functionalities at the other end (Fig. 3.3). The higher homologous α-amino acids (impurities) are, therefore,

structurally similar to the primary solute (glycine). The side chain functionalities of the impurities can be non-polar (hydrocarbon chains), polar (hydroxyl and sulphide groups), acidic (carboxylic group) or basic (ammonium group). In addition, the latter functional groups (polar, acidic and basic) can undergo speciation to exist in ionic and neutral forms (via protonation or deprotonation) under different solution pH conditions (Kirwan and Orella, 2002).

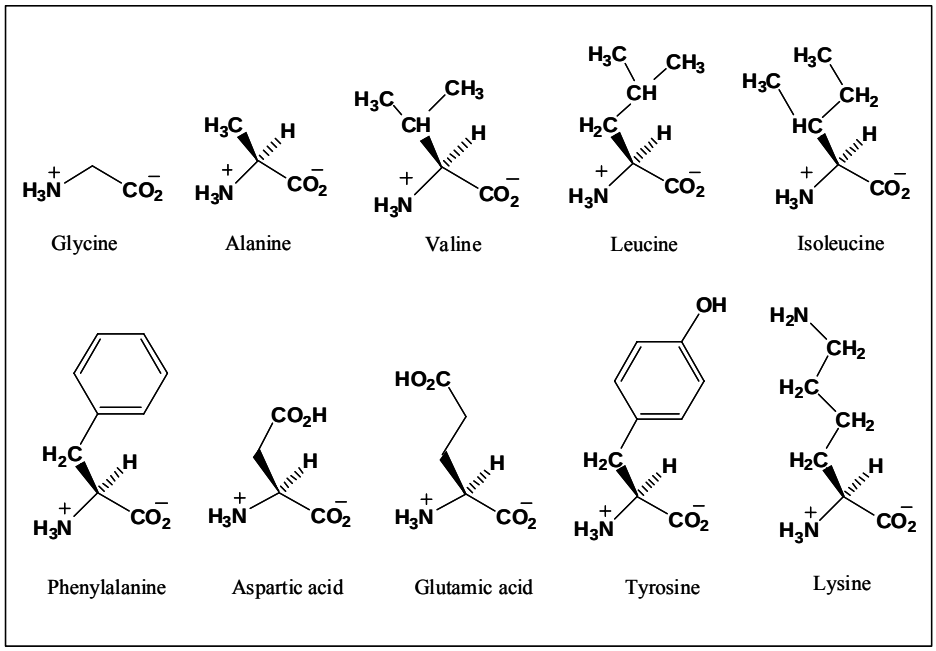

Figure 3- 3 Structural formulae of α-amino acids with common substrate functionality and differentiated residual groups.

3.2. Crystallization Experiments

3.2.1. Materials

Glycine and other α-amino acids (used as the impurities) were obtained from Sigma-Aldrich with 99.0+ % purity and were used as received. The impurities present in the starting material (glycine) were inorganic elements (for example, Na, Al, Ca, Cr, K, Cl) of approximately 100 ppm and salts (for example, NH_4^+ and SO_4^{2-}) of approximately

1000 ppm. It is noted that these trace impurities in solution may not influence the growth of glycine crystals. This was verified by comparing the shapes of glycine crystals grown from solutions prepared with 'as received' and that of recrystallized glycine. Besides, from previous work (Weissbuch et al. 1983), it is also known that the chosen impurities (amino acids) can have a more pronounced effect on glycine crystals in comparison with the trace impurities present in the starting material.

Deionized, 0.22 μm filtered water was used in preparing glycine solutions. Hydrochloric acid and sodium hydroxide were used for pH adjustment.

3.2 2. Recrystallization

Two experimental protocols were used: stirred and unstirred crystallizations, depending on the suitability of the crystals for microscopic analysis. Under stirred conditions, crystallization experiments were performed in an agitated, 250 ml thermostated glass vessel. Glycine solution was prepared by dissolving 27.5 g of glycine in 100 g of water (3.67 M) at 40 °C, with appropriate amounts of impurities added, and then cooled at 0.5 °C/min until visible crystals nucleated from the supersaturated solution (final crystallization temperatures were in the range 15–20 °C). The cooling rate was set to be consistent with the experiments for metastable zone width measurements (section 3.2.3). For the unstirred crystallization, glycine solutions were prepared by dissolving 3.3 g of glycine in 10 g of water (4.4 M) at 50 °C, with appropriate amounts of impurities added. The solutions were filtered through a 0.22 μm Millipore PVDF Durapore® membrane filter and cooled to room temperature (25 °C) in crystallization dishes that were covered with a parafilm® in order to prevent any contamination with atmospheric dust particles. Single crystals of α-glycine with distinguishable crystal faces (1-3 mm

size) were obtained from the supersaturated solution in 12 – 24 h time, allowing for detailed morphological analysis.

In further experiments, glycine solutions were prepared at two different initial concentrations (C = 0.3375 and 0.4555 g/g water) by dissolving required amounts of glycine in 10g of water at elevated temperatures (50 and 70 °C). The impurities were doped into glycine solution at concentration levels 1–4 wt % (w/w glycine). The solutions were filtered and allowed to cool down naturally to room temperatures (25 °C) resulting in two different supersaturation levels: $\sigma = \ln (C/ C_s) = 0.3$ and 0.6 (C = actual concentration of glycine and C_s = glycine solubility at 25 °C = 0.25 g/ g water (Mullin, 2001)).

3.2.3. Metastable zone width measurements

The experimental set up for metastable zone width (MZW) measurements consisted of a 250 ml, jacketed glass crystallizer equipped with a circulating water bath (Julabo FP50 HL). A paddle-type PTFE impeller driven by an overhead motor was used to provide agitation. A turbidimeter (Brinkmann Colorimeter, model PC 920) with a fiber optic probe was used for in situ measurement of solution transmittance. A commercial data logging software (*Windmill Software Ltd*) was used to collect the transmittance data from the turbidimeter online.

Saturated glycine solution (150 ml) (C_s = 0.275 g/ g water at 30 °C)[12] was prepared by dissolving 41.25 g of glycine in 150 g of water. Complete dissolution was ensured by stirring and maintaining the solution at an elevated temperature (40 °C) for 30 min. The solution was then cooled at a rate of 0.5 °C/ min with constant stirring (125 rpm). The nucleation event was detected by a sharp decrease in the solution transmittance

(due to explosive nucleation of crystals), and the corresponding temperature was read as the "cloud point" (Fig. 3.4). The difference between the saturation and the cloud point temperatures was computed as the MZW (Nývlt et al., 1985) of the pure glycine solution. The same procedure was followed for solutions with impurities (L-amino acids: Alanine (Ala), Valine (Val), Leucine (Leu), Isoleucine (Ile), Phenylalanine (Phe), Aspartic acid (Asp) and Glutamic acid (Glu)) added at different concentration levels to the saturated glycine solution. For each data point, the experiment was repeated at least 3 times in order to obtain statistically consistent results.

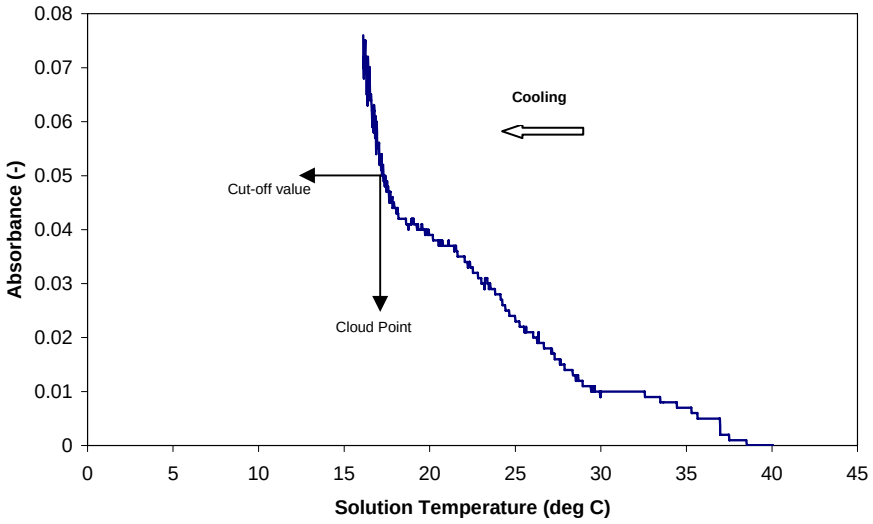

Figure 3- 4 Cloud point measurement using online turbidimeter.

3.3. Characterization Techniques

3.3.1. Optical microscopy

The crystal habit was examined using an optical polarized light microscope (Olympus, BX51) connected to a CCD camera. The images were recorded using Soft Imaging System's *Analysis* image capture software.

3.3.2. X-ray diffraction

For crystal structure confirmation, X-ray powder diffraction analysis was carried out using a Bruker D8 Advance X-ray Diffractometer with Cu $K_{\alpha 1}$ radiation of $\lambda = 1.54$ Å. The samples were scanned in the 2θ range 10° to 50°, at the rate of 0.02°/ second. Glycine polymorphs were identified by comparing the characteristic 2θ peaks ("fingerprints") in the experimental powder XRDs with that of the XRD patterns (Fig. 3.5) simulated from its crystal structures using *Mercury* software (Cambridge Structural Database).

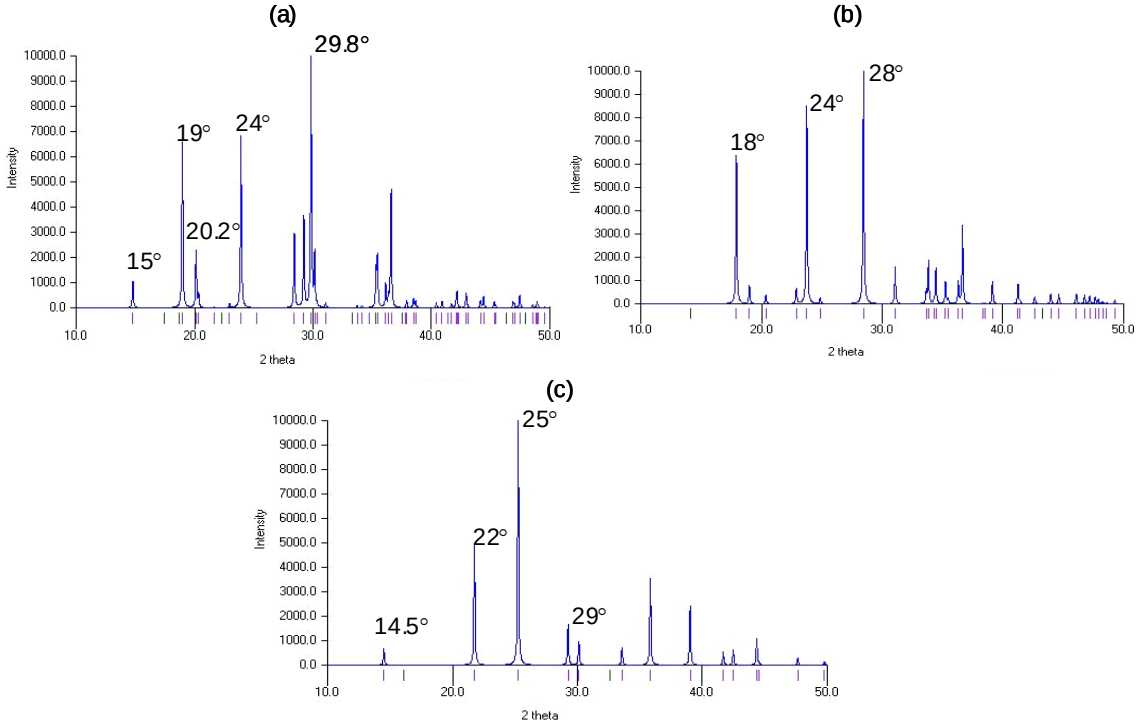

Figure 3- 5 Simulated X-ray diffraction patterns of glycine polymorphs: (a) α-glycine; (b) β-glycine; (c) γ-glycine. The diffraction peaks characteristic of the polymorphs is labeled.

3.3.3. Infrared Spectroscopy

Infrared (IR) spectroscopy was used for two different studies. In the first, solution speciation of the impurity molecules, accompanied with changes in its molecular conformation was investigated. Secondly, the solution infrared spectrum was correlated to the solute concentration using chemometric methods (Togkalidou et al., 2002; Yu et

al., 2006). By this way, the effect of impurities on the solubility of glycine was investigated.

Infrared spectra for the amino acids (L-Asp and L-Glu) and their salts in the solid state were collected with a Thermo Nicolet Avatar 360 Fourier Transform Infrared Spectrometer (FT-IR) using an attenuated total reflectance (ATR) method. A single reflection germanium crystal was employed with a spectral range between 4000 and 675 cm^{-1}. These solid-state spectra obtained were used as a reference for vibration assignments of the IR spectra obtained in solution. The IR spectra of these amino acids in water were collected with a Nicolet Nexus 4700 spectrometer (Thermo Electron Corp.), equipped with a Dipper-210 ATR-FTIR probe with a ZnSe crystal (Axiom Analytical Inc.). Deionized water was used as the background and spectral data were collected in the range between 4000 and 650 cm^{-1}. Solutions of L-Asp and L-Glu (2 wt % concentration) were prepared at 70 °C and their spectra were collected at pH 3.0, 7.2, 8.9 and 11.7 respectively.

As appropriate to this work, a brief review on IR spectroscopy follows below.

A. Theory

At ordinary temperatures, organic molecules are in a constant state of vibration, each bond having its characteristic stretching and bending frequency, and can absorb light of that frequency. Organic applications of IR are almost entirely concerned with the wavenumber range 650–4000 cm^{-1} (15.4–2.5 μm). The region of frequencies lower than 650 cm^{-1} is called the *far infrared*, and that of frequencies higher than 4000 cm^{-1} is called the *near infrared*. These regions are respectively farther from and nearer to the visible spectrum (Kemp, 1987).

Molecules can have different modes of vibration, each of which may give rise to a different absorption band. For example, the methylene (CH_2) groups give rise to two stretch bands at the frequencies ν_{symm} (symmetric) and ν_{anti} (antisymmetric) (Fig. 3.6). Nevertheless, for an absorption band to appear in the IR spectrum, it is necessary that the particular vibration should produce a fluctuating dipole (and thus a fluctuating electric field); otherwise it cannot interact with the fluctuating electric fields of the infrared light. Thus the stretching of a symmetrically substituted bond (for example C≡C in acetylene) produces no change in the dipole of the system, and therefore this vibration cannot interact with infrared light. Besides, some vibrations may not give rise to absorption if their frequencies are the same ('degenerate'), or if the frequencies fall outside the normal IR region being examined.

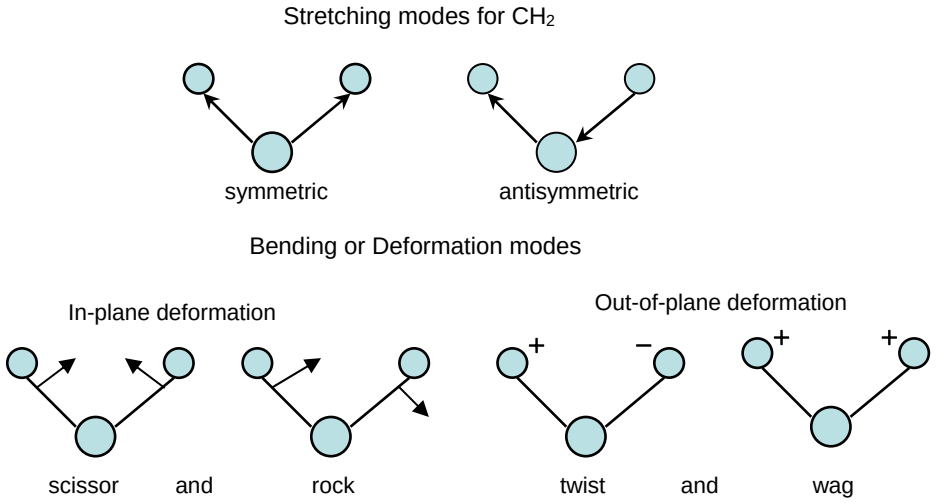

Figure 3-6 Illustration of vibration modes in methylene groups (Kemp, 1987)

B. Applications

As an IR spectrum contains many absorption bands associated with the complex interacting vibrating systems in the molecule, it is uniquely characteristic of each molecule. Therefore, the absorption band pattern serves as a fingerprint of the molecule

being examined. However, while deducing the structure of an unknown compound, other characterization techniques such as mass spectroscopy might have to be used in conjunction with IR.

A second application of IR, which is of relevance to the current study, is to identify the functional groups of a molecule. The IR absorptions associated with different functional groups have been established by examining a large number of compounds known to contain the functional group. Therefore, for an unknown compound, its functional groups can be identified by examining its infrared spectrum together with the correlation data available in the literature (Kemp, 1987; Bellamy, 1980). Furthermore, conformational changes in the molecular structure can be examined by comparing the shifts in the absorption bands of its functional groups under different solid state and solution environments (Parveen et al., 2005).

C. ATR–FTIR spectroscopy

In the conventional sampling techniques (such as using KBr discs, mulls, solution cell, etc.) for IR spectroscopy, light spectrum is transmitted through the sample before analyzed by the detector. However, for materials such as polymer films or foams, fabrics, coatings, etc., these sampling techniques are inapplicable. In this case, the spectrum can be recorded using a modified reflectance technique which depends on the total internal reflectance of light. This technique known as *attenuated total reflectance* (ATR) is frequently used for both solid-state and solution IR spectra measurements. The working principle is illustrated in Fig. 3.7. Provided the refractive index of the prism 1 (usually germanium, diamond, zinc selenide crystals are used) is greater than that of the sample medium 2, and if the incidence angle θ is greater than the critical angle, the infrared light beam will suffer *total internal reflectance* at the interface between 1 and 2. In medium 2

the light beam travels a very short distance (a few μm) during which it is partly absorbed before re-emerging into the ATR crystal. Thus, the re-emerging beam will be attenuated (weakened), rather than totally reflected. In this method, a weak spectrum is obtained because of the very short path length within the sample on a single reflection. Therefore, a multiple reflectance is usually obtained using an optical arrangement.

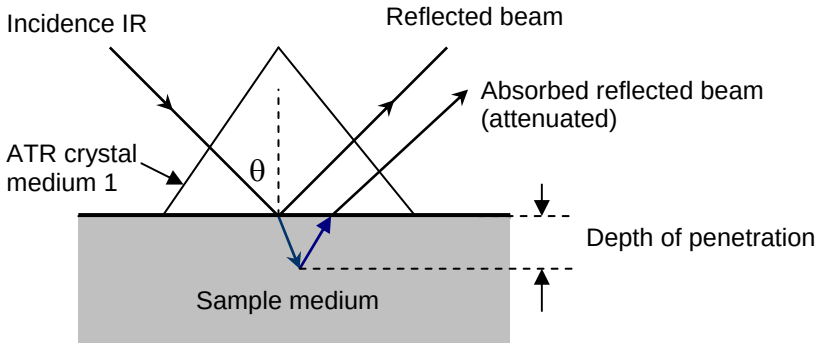

Figure 3-7 Operational mechanism of an ATR-FTIR spectrometer

Conventional IR spectroscopy suffers from disadvantages in sensitivity, speed and wavelength accuracy. This had led to the *Fourier Transform IR* spectroscopy, in which the working principle centers on a *Michelson interferometer*. In this case, the sample compound placed along the beam (either before or after the interferometer) absorbs particular frequencies, so that their intensities are reduced in the interferogram and the ensuing Fourier transform is the infrared absorption spectrum of the sample. Built on this technology, FTIR spectrometers provide more intense signals (typical signal-to-noise ratios are of the order 10^5 : 1) and a high resolution (less than 0.1 cm^{-1}) (Kemp, 1987).

3.3.4. pH measurements

Solution pH measurements were made at room temperature (~25 °C) using a Seven Multi model (Mettler-Toledo) pH meter fitted with a glass calomel electrode and an ATC probe for temperature compensation.

3.4. Solubility measurements

The Beer-Lambert law relates the molar concentration of the solute (c) to the absorbance of the solution (A) by $A = \varepsilon cl$, where ε is the molar absorptivity (constant for the solute causing absorbance) and l is the path length of the sample medium (Kemp, 1987). On the basis of this principle, quantitative determination of solute concentration can be made through solution absorbance measurements using IR.

ATR-FTIR spectroscopy was used for measuring glycine solubility in pure water and in the presence of an impurity (L-Aspartic acid). In situ measurements of solution concentration was carried out using a Nicolet Nexus 4700 spectrometer (Thermo Electron Corp.), equipped with a Dipper-210 ATR-FTIR probe with a ZnSe crystal (Axiom Analytical Inc.). A circulating water bath (Julabo FP 50 HL) was used for heating and cooling the solution contained in a 500 ml jacketed glass crystallizer.

3.4.1. Calibration of ATR-FTIR

Initially, a calibration model relating the solution IR absorbance to glycine concentration in water + glycine + L-Asp mixture was developed. In this case, because the characteristic vibrational frequencies of the carbonyl groups (at 1600 and 1400 cm^{-1}) and the NH_3^+ groups (at 1500 cm^{-1}) of glycine (solute) and L-Asp acid (impurity) overlapped in the IR spectra, a two component calibration model (water + glycine) could not be used. Hence, a calibration model accounting for the presence of impurity was obtained as follows. Appropriate amounts of glycine corresponding to five different concentration levels (viz. 0.2, 0.25, 0.3, 0.35 and 0.4 g/ g H_2O) and L-Asp (1 wt %, w/w water) were dissolved in 100 g of water in a jacketed glass crystallizer. IR spectra of the

solution were collected (32 scans/ spectrum) for the temperature interval 20–60 °C at the corresponding glycine concentrations. DI water at 30 °C was used as the background.

Regression coefficients for glycine concentration were obtained from the IR spectra using chemometrics method (Yu, 2006). For this, the absorbance in the range of 651–1812 cm^{-1} (including 605 discrete wavelengths) and temperatures were used as predictor variables. The calibration model for glycine concentration in the three component system was obtained with a mean width prediction interval (or error value) of ± 0.002 g/ g of solution (Fig. 3.8). It is noted that the prediction interval is maximum at the higher values of solute concentration.

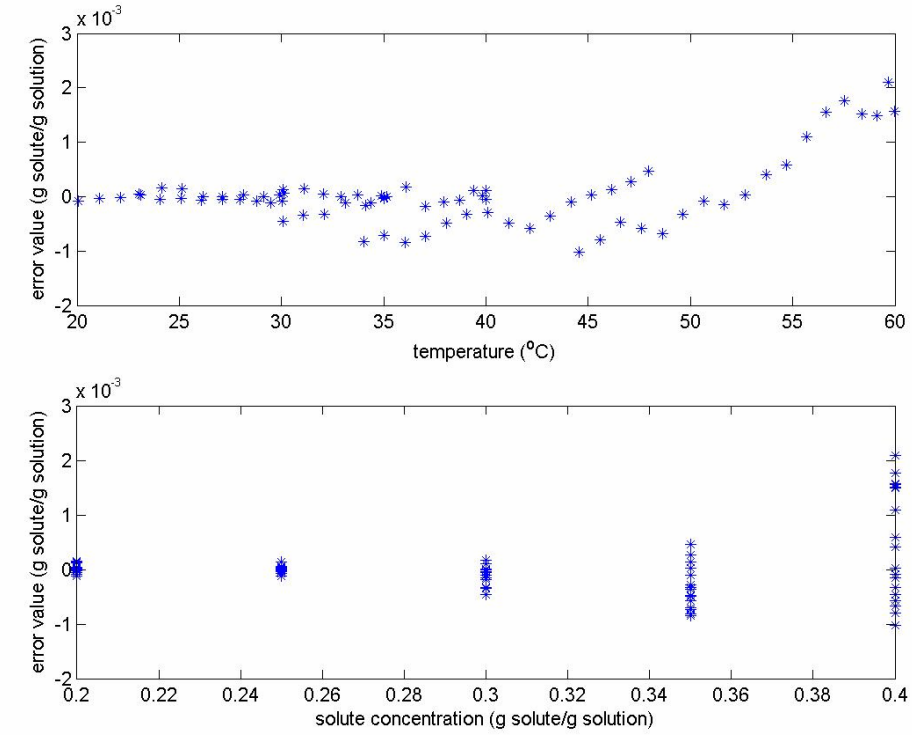

Figure 3- 8. Error values in the calibration of ATR-FTIR for glycine concentration measurement.

3.4.2. Glycine solubility in the presence of impurities

Solubility of the impure system was determined by preparing slurry solutions of α-glycine (recrystallized) in water containing 1 wt % (w/w water) of L-Asp in the temperature range 20–50 °C. This impurity concentration corresponded to 4.3 wt % with respect to the concentration of glycine in a saturated solution at 20 °C. The solutions were stirred for 4 h at the respective saturation temperatures, and IR spectra were obtained for the last 2 h of equilibration time. Glycine concentrations were calculated from the IR spectra collected at every 15 min time interval using the regression coefficients that were obtained from the calibration models earlier. After the solution concentrations became constant, the saturated slurry solution was vacuum filtered and the solid sample was oven dried at 60 °C and collected for PXRD analysis. By following a similar procedure, the solubility of α-glycine in pure water was determined using a calibration model developed for the glycine-water system.

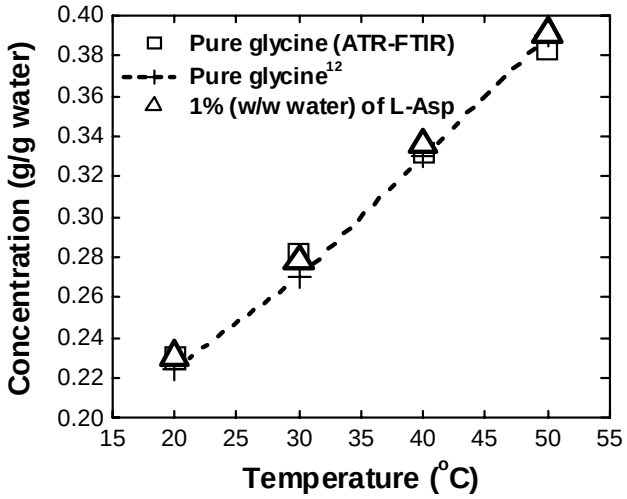

Figure 3- 9 Solubility of α-glycine in the presence of L-Aspartic acid (impurity)

From the above measurements, we could confirm that the solubility of the metastable α-form was unaltered by the presence of L-Asp impurity (Fig. 3.9). Furthermore, we could deduce that L-Glu, which had a lower impact on the pH of glycine solution as compared to L-Asp (refer to chapter 4, section 4.4), may also not affect the solubility of α-glycine at the concentration levels used. Herein, it is significant to note that the solubility of γ-glycine has been determined earlier to be 0.02 g/g of water lower than that of α-glycine (Sakai et al. 1992).

3.5. Atomic Force Microscopy

3.5.1. Working principle

The underlying principle in atomic force microscopy (AFM) involves measurement of the small inter-atomic forces created when an ultra-sharp micro fabricated tip is brought into proximity to the surface of the sample. Lateral and vertical movements of the tip (mounted on the end of a flexible cantilever) or the sample are controlled by piezoelectric positioners with sub-Å precision. The cantilever movement is detected by a 'beam-bounce' method using a laser light. AFMs are usually operated in either contact or tapping mode. In contact mode, the AFM tip is in close contact with the sample during the scanning. The force on the tip is repulsive with a mean value of 10^{-9} N. This force is set by pushing the cantilever against sample surface with a piezoelectric positioning element. In contrast, in the tapping mode, the tip oscillates 50–150 Å above the sample surface, tapping it only during a short interval in its oscillation cycle. The spacing between tip and sample is controlled by monitoring the resonant frequency of the cantilever. Tapping mode minimizes tip–sample interactions and greatly reduces lateral forces; hence, is essential for examining soft samples where tip contact could change the

topography. In both tapping and contact modes, a feedback mechanism adjusts the vertical height of the sample (or AFM tip) using the piezoelectric transducer so as to maintain a constant tip oscillation amplitude (tapping mode) or a constant cantilever deflection (contact mode) (Quate, 1994; Malkin and Thorne, 2004).

A fluid cell arrangement can be used for in situ AFM imaging of surfaces in liquid samples (Fig. 3.10). The supersaturated solution (growth medium) is circulated into the fluid cell with an O-ring sealing which is mounted on the piezoelectric translator. By this method, crystal growth processes can be investigated at the molecular level in the native solution environment (Carter et al., 1994; Gidalevitz et al., 1997; Land et al., 1999).

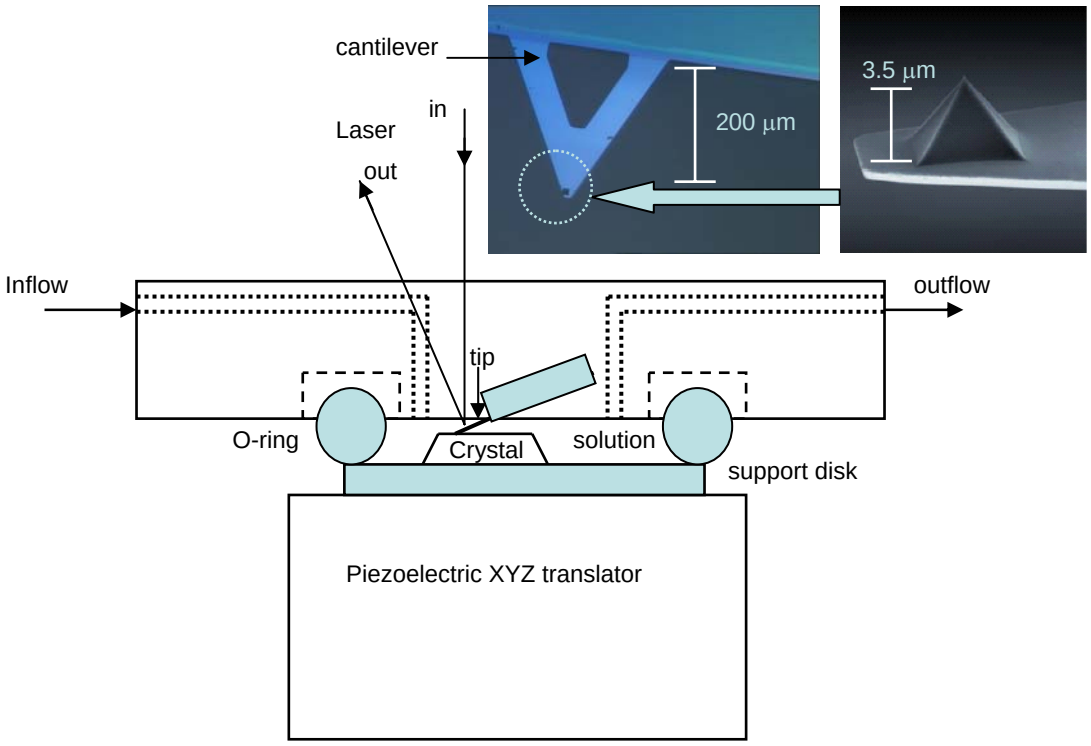

Figure 3- 10 Schematic diagram of an atomic force microscope. A laser beam is reflected from the upper surface of the cantilever and detected with a four-quadrant photodetector. Scanning takes place in a fluid cell of about 50–70 μl volume. The sample is scanned relative to the tip by a piezoelectric positioner upon which the fluid cell is mounted. The inset shows the images of a cantilever tip (Malkin and Thorne, 2004).

3.5.2. Apparatus

A Multimode® Scanning Probe Microscope (Nanoscope® IV, Digital Instruments, Vecco Metrology Group, USA) with an E-type piezo scanner (13 μm scanning range) was used for surface imaging. Images were obtained in contact mode using cantilevers equipped with integral silicon nitride tips (Olympus) of spring constant 0.39 N/m (cf. Fig. 3.10). The tip scan rate during image acquisition was maintained at 2.98 Hz with a scan size of 5 μm x 5 μm. A minimum tip-sample contact force of ≤ 10 nN (during ambient scanning) and ≤ 1nN (during solution scanning) was applied by adjusting the set point voltage for tip deflection. This ensured minimum tip induced etching of crystal surface during scanning. The acquired images were post-processed offline using Nanoscope® software (Digital Instruments).

3.5.3. Sample preparation

An α-glycine crystal was cleaved parallel to the *ac* plane so as to expose a smooth (010) surface. The crystal was then mounted with epoxy onto a magnetic stainless steel sample disk for AFM imaging. A quartz-body fluid cell (Digital Instruments) with an O-ring sealing was placed over the sample disk. 30-50 μl of supersaturated glycine solution ($\sigma = \ln (C/ C_s) = 0.118$ and 0.256, where C and C_s are the actual and saturation glycine concentrations at 23 ºC respectively) was injected into the fluid cell covering the sample crystal surface. Subsequently, the crystal surface was scanned in the solution medium for 15–30 min. Similarly, supersaturated glycine solutions with different concentrations of D- + L-Phe (impurity), viz. 0.5, 0.75, 1.0, 1.5 and 2.0 wt % (w/w glycine) respectively, were prepared and used for in situ AFM imaging.

CHAPTER 4

Effect of Impurities on α-Glycine Crystal Habit

While impurities affect the crystal growth kinetics, often, it is manifested by a macroscopic change in the crystal habit. In this chapter, the experimental observations on the habit modification in α-Glycine crystals caused by impurities are presented. Based on this, the interactions of impurities with the specific facets of α-Glycine crystal are investigated using molecular modeling. Furthermore, the role of solution speciation in controlling the impurity interaction at the crystal interfaces is exemplified through some newly observed habit modification in α-Glycine crystals.

4.1. Symmetry Relations in α-Glycine Crystal Structure

Glycine packs in its crystalline α-form in a centrosymmetric space group $P2_1/n$. In the crystal structure (ref. code GLYCIN03, Cambridge Structural Database (CSD), Ver. 5.26), zwitterionic glycine molecules form centrosymmetric dimers through N–H···O hydrogen bonds; and chains of these dimers are formed along the c-axis by additional N–H···O hydrogen bonds. The dimer layers are stacked along the b-axis through C–H···O interactions. The α-Glycine crystal is delineated by {010} facets along the b-axis and {011} facets along the c-axis (Fig. 4-1a).

In the α-Glycine crystal structure, various symmetry relations exist between the glycine molecules at the four different crystallographic sites (numbered 1–4 in Fig.4-1a). The glycine molecules within a dimer layer, (viz. “1” and “2” or “3” and “4”) are related by a center of inversion symmetry, and those in the alternate layers (viz. “1” and “3” or

"2" and "4") are related by a 2-fold screw symmetry. Given this, the glycine molecules on the (010) face are related to each other by 2-fold screw symmetry and to that on the $(0\bar{1}0)$ face by a center of inversion (Weissbuch et al., 1983).

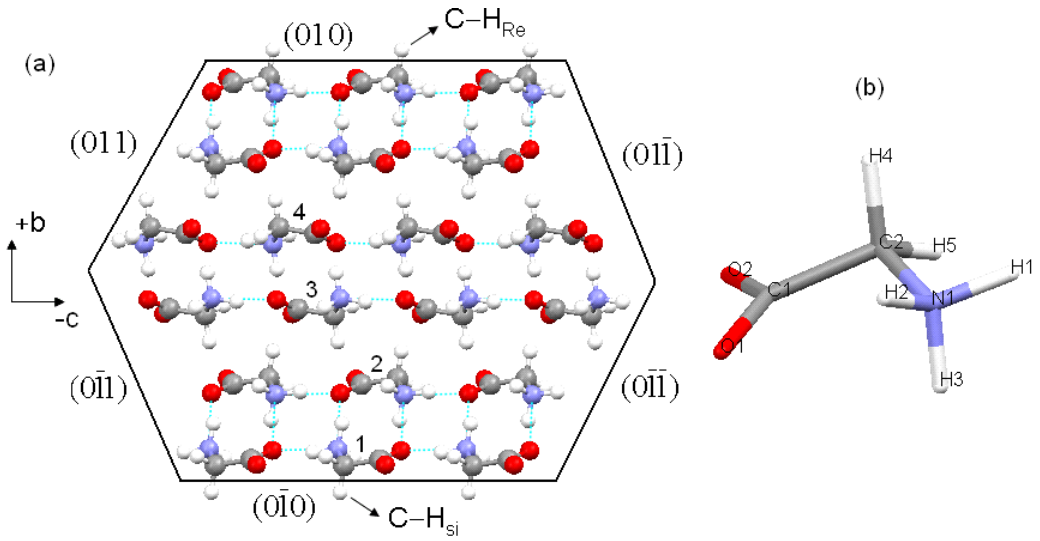

Figure 4-1 (a) Packing arrangement of α-Glycine viewed along the a-axis, delineated by the dominant crystal faces. The hydrogen atoms on the (010) surface (C-H$_{Re}$) and $(0\bar{1}0)$ surface (C-H$_{Si}$) are enantiotopic (Weissbuch et al., 1983); (b) molecular structure of a glycine molecule with the atoms labeled.

Furthermore, in the crystal structure, the orientation of a glycine molecule is such that one of its two C–H bonds, the C_2–H_4 bond (refer to Fig. 4-1b), which forms the C–H···O contact, is parallel to the b axis, whereas the C_2–H_5 bond lies almost in the ac plane. Because of this conformation of the glycine molecule, all those molecules on the (010) face have their C_2–H_4 bonds directed toward the +b axis, away from the crystal bulk. And all those molecules on the $(0\bar{1}0)$ face, through a center of inversion or glide symmetry have their C_2–H_4 bonds directed towards the –b axis. Besides, a glycine molecule is prochiral, meaning replacement of one of the hydrogen atoms at its central carbon atom by a different group yields a chiral molecule. On account of this, the C_2–H_4

bond of a glycine molecule on the (010) face could be assigned an absolute configuration of "pro R", and of those on the $(0\bar{1}0)$ face "pro S" (henceforth, these C–H bonds will be referred to as $C–H_{Re}$ and $C–H_{Si}$ bonds, respectively). As a result, the crystallographic b-axis of α-Glycine is enantiopolar, and the $\{010\}$ facets are enantiotopic.

4.2. Stereoselective Habit Modification in α-Glycine

Typically, α-Glycine crystallizes with a prismatic bipyramidal habit from pure aqueous solution (Fig. 4-2a). The crystal habit is elongated along the c-axis, which is the direction of fast growth. The dominant crystal facets – $\{010\}$, $\{011\}$ and $\{110\}$ are identified by referencing to the theoretical crystal habit of α-Glycine (Fig. 4.2b).

In the presence of chirally resolved impurities (D- and L-amino acids) a prismatic pyramidal crystal habit with a $\{010\}$ basal plane was obtained (Fig. 4-2c, d). When glycine solutions were doped with racemic impurities (either DL-amino acids or D- + L-amino acids) $\{010\}$ plate-like crystals were obtained (Fig. 4-2e, f). These observations were consistent with the previous work (Weissbuch et al., 1983).

In their pioneering work, Weissbuch et al. (1983) have proposed a 'stereoselectivity mechanism' rationalizing the habit modification in α-Glycine crystals. All of the α-amino acids, added to glycine solution as 'tailor-made' additives, adsorb on either of the $\{010\}$ facets of a growing α-Glycine crystal stereospecifically depending on their absolute configuration. This implies that D-amino acids absorb onto the (010) face, and the L-amino acids onto the $(0\bar{1}0)$ face. In other words, the $C–H_{Re}$ bond of a glycine molecule on the (010) surface is enantioselectively substituted by the side chain group

of a D-amino acid (of "R" configuration), and the C–H_{Si} bond on the $(0\bar{1}0)$ surface with that of an L-amino acid (of "S" configuration).

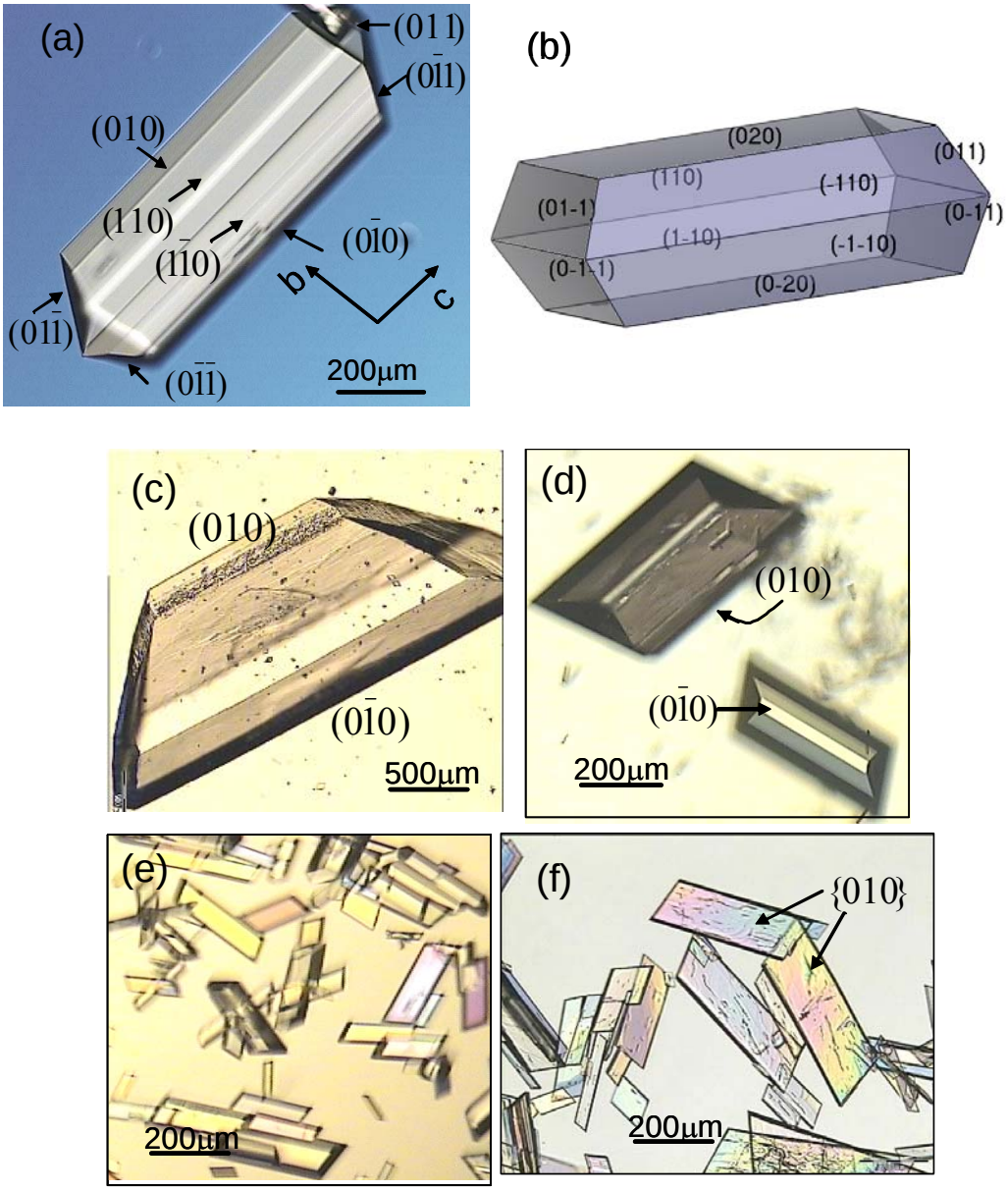

Figure 4-2 Illustration of the stereoselective habit modification in α-Glycine crystals: (a) α-Glycine crystallized from pure aqueous solution; (b) Theoretical crystal habit of α-Glycine[1]; (c) α-Glycine crystallized from solution doped with 0.5 wt % (w/w of glycine) of L-Alanine; (d) 0.5 wt % of D-Ala; (e) 0.5 wt % of DL-Ala; (f) 0.5 wt % of D + L-Ala.

[1] Refer to chapter 5 for details of the habit modeling

Subsequently, the side chain moiety of the imposter molecule perturbs the regular attachment of glycine molecules, resulting in growth inhibition along the enantiopolar b-axis. Therefore, growth inhibition along the –b axis of α-Glycine results in a prismatic pyramidal crystal habit with a $(0\bar{1}0)$ basal plane, and that along the +b axis yields an enantiomorphous crystal habit with a (010) basal plane (cf. Fig. 4-2c, d). Likewise, growth inhibition along the ±b axes results in plate-like crystals with dominant $\{010\}$ facets (cf. Fig. 4-2e, f).

4.3. New Habit Modification in α-Glycine

In the presence of L-Asp and L-Glu (0.5 wt %, w/w of glycine), α-Glycine crystallized with an isometric crystal habit (Fig. 4-3a, b). The dominant facets observed were the $\{011\}$ and $\{110\}$, with the $(0\bar{1}0)$ face slightly developed (Fig. 4-3c), implying that growth inhibition was along the c-axis. This crystal habit was clearly distinguishable from that of the glycine crystal obtained from pure solution (cf. Fig. 4-2a), in which the $\{011\}$ faces showed less morphological dominance. Besides, in this case, the crystal habit of α-Glycine was prismatic bipyramidal, in contrast to the b-axis habit modification reported previously (Weissbuch et al., 1983).

With further increase in L-Asp concentration (between 0.75 – 1.0 wt %), again prismatic bipyramidal crystals were obtained, however, with partial growth inhibition along the –b axis. Interestingly, at L-Asp concentrations between 1.0 – 2.0 wt %, the crystal habit was prismatic pyramidal with dominant $(0\bar{1}0)$ faces (Fig. 4-3d). Likewise, in any of the typical experimental runs with L-Glu, it was observed that the additive action

was dominant along the ±c axes of α-Glycine, prior to the growth inhibition along the −b axis (Fig. 4-3e, f).

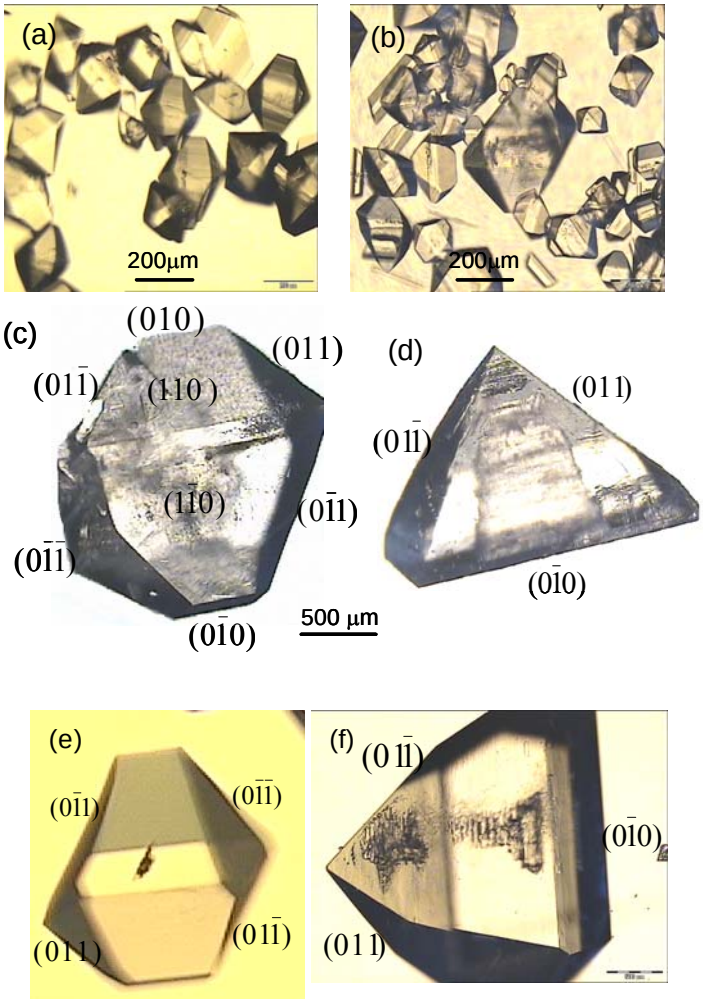

Figure 4-3 New habit modification in α-Glycine crystallized with the impurities: (a) 0.5 wt % (w/w of glycine) of L-Asp; (b) 0.5 wt % of L-Glu; (c) 0.5 wt % of L-Asp (crystal facets labeled); (d) 1.0 wt % of L-Asp; (e) 0.5 wt % of L-Glu; (f) 1.5 wt% of L-Glu.

4.4. Solution Speciation of Impurities

Toward understanding the newly observed habit modification in α-Glycine, firstly, the solution chemistry of impurities is briefly discussed. The species distribution of glycine and aspartic acid as a function of pH were computed from their pK_a values (Lide, 2004) and shown in the speciation chart (Fig. 4-4a). It shows that glycine exists in

three different charged states – viz. zwitterions, cations, and anions; and the diprotic aspartic acid exists as zwitterions, cations, anions and dianions.

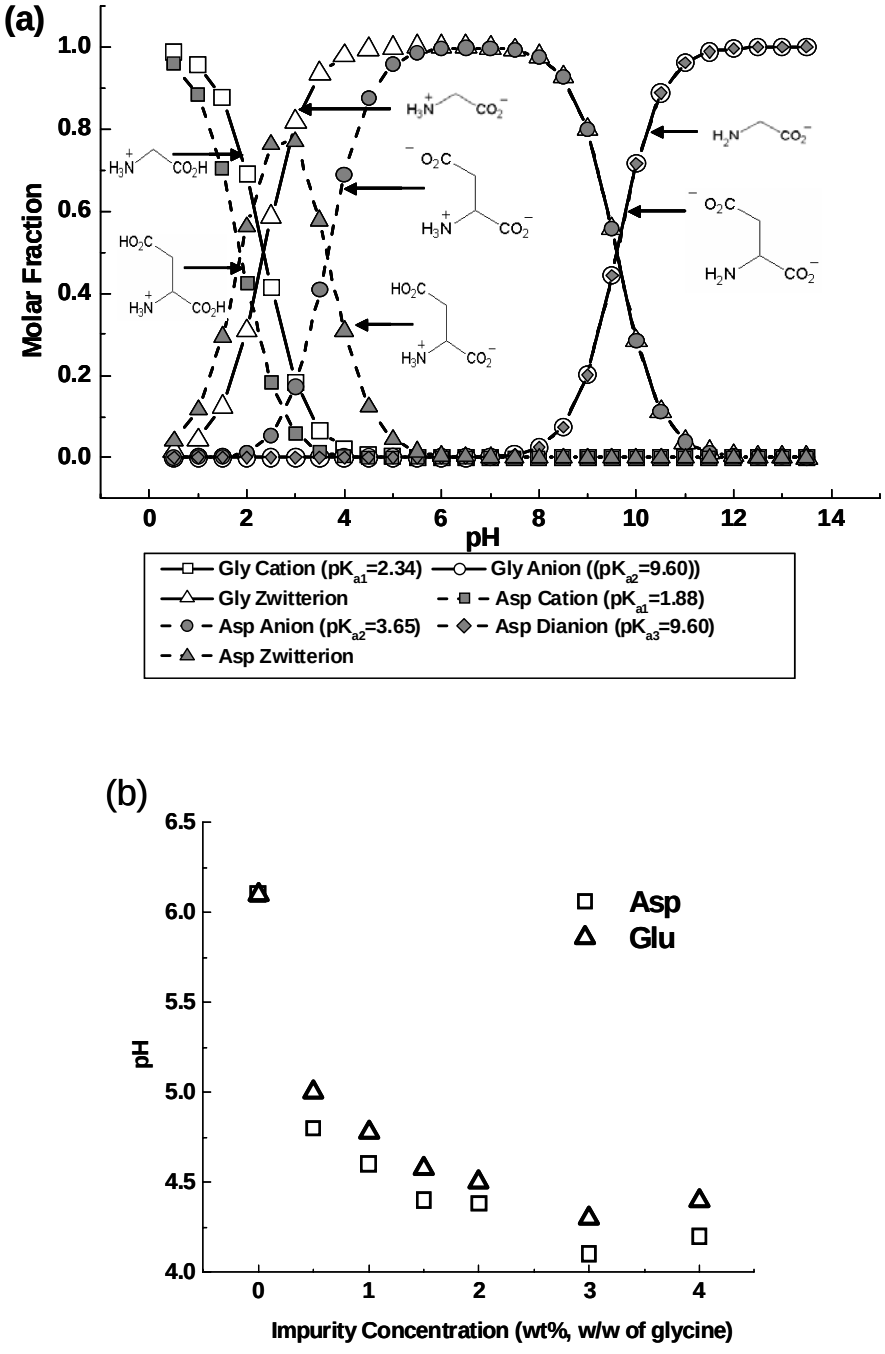

Figure 4-4 (a) Speciation of aqueous glycine (Gly) and aspartic acid (Asp) as a function of pH; (b) Change in glycine solution pH along with the doping of impurities.

Furthermore, in the pH region 4–6, glycine exists predominantly as zwitterions, besides a small fraction of cations (ca. 0.02 mole fraction), while aspartic acid exists as both zwitterions and anions. Therefore, with the addition of L-Asp to glycine solution, the pH gradually decreased from ca. 6.1 to ca. 4.2 (Fig. 4-4b), accompanied by changes in molecular speciation. The resulting ionic equilibrium and species distribution are shown in Fig. 4-5a and Table 4-1 respectively. Similarly, glutamic acid, with a pK_a value (4.25 for the side-chain –COOH group) less than the pI (5.97) of glycine solution undergoes dissociation to form zwitterions and anions in the pH domain 4-6 (Fig. 4-5b). In contrast, alanine, with no carboxylic acid moiety in their side chain, predominantly exists as zwitterions in this pH region (Fig. 4-5c).

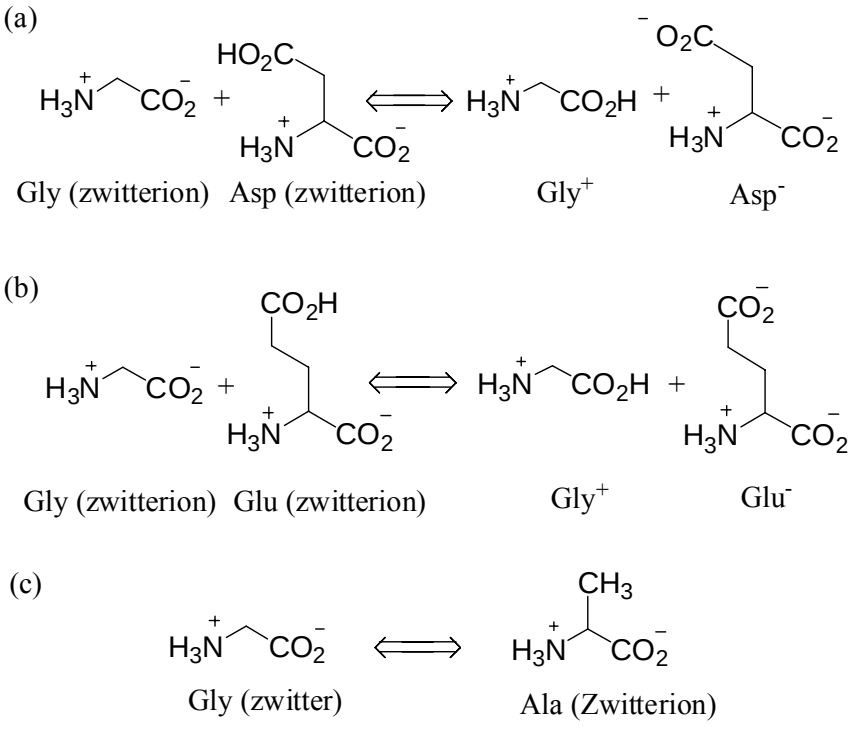

Figure 4- 5 Ionic equilibrium in glycine solution in the pH domain 4–6 of: (a) Aspartic acid; (b) Glutamic acid; (c) Alanine.

Table 4- 1 Glycine and impurity (L-Aspartic acid) species distribution in solution (mol %).

molecular species type	pure solution (pH 6.0)	0.5 wt% of L-Asp (pH 5.0)	1.0 wt % of L-Asp (pH 4.5)
Gly zwitterion	100.0	99.44	98.15
Gly cation	0.0	0.27	0.85
Asp zwitterion	0.0	0.015	0.15
Asp anion	0.0	0.27	0.85

4.5. Impact of Solution Speciation on the Habit Modification

The habit modification in α-Glycine that were reported in section 4.3, in principle, could be resulting from the interactions of the molecular species, viz. L-Asp zwitterion, L-Asp anion and glycine cation (Gly^+) with the specific facets of α-Glycine crystal. Firstly, in accordance with the stereoselectivity mechanism (Weissbuch et al., 1983), the action of L-Asp zwitterions should be confined to the –b axis of α-Glycine. Indeed, this was observed experimentally, with partial to complete growth inhibition along the –b enantiomorphous crystal half of α-Glycine (cf. Fig. 4-3c, d). The dominant {011} facets (cf. Fig. 4-3c), could then be attributed to growth inhibition along ±c axes, possibly, either by the Gly^+ or L-Asp anions.

4.5.1. Isolating the effect of Gly^+ on the habit modification

In this context, Towler et al. (2005) have conjectured a 'self-poisoning' mechanism, explaining the role of Gly^+ species on the growth inhibition of {011} facets of α-Glycine at low pH values. This self-poisoning effect has led to the nucleation inhibition of α-Glycine and subsequent crystallization of the more stable γ-form (at pH<3.8). However, the authors were unsuccessful in observing habit modification in α-Glycine crystals in the transitional pH range (viz. pH 6.0 to 4.0). To this end, in this

study, some additional crystallization experiments were performed with pure glycine solution at pH 6.2 (the control sample) and pH 4.5 (adjusting the pH using HCl). In these experiments, at pH 4.5, the harvested α-Glycine crystals were more isometric with dominant {011} faces, in comparison with those crystallized at pH 6.2 (Fig. 4-6). These observations reveal growth inhibition of α-Glycine along the fast growing c-axis, and hence corroborate the proposed self-poisoning mechanism. Besides, given this observation, the implication is that very low concentrations of Gly^+ species are required to produce an effect on the crystal habit of α-Glycine. Therefore, it is implied that α-Glycine crystals had to be obtained at pH 6.0 (viz. near the pI of glycine) in order to isolate the effect of Gly^+ on the impurity induced habit modification.

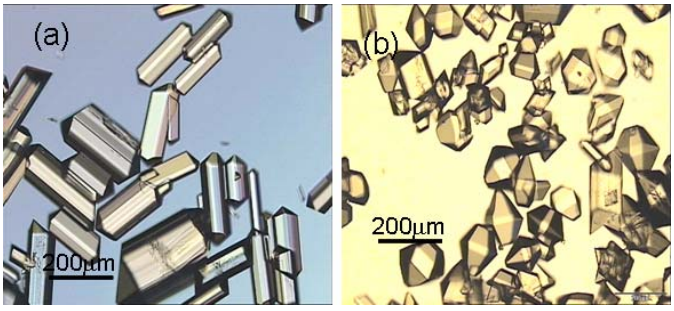

Figure 4- 6 Effect of Gly^+ species on the habit modification in α-Glycine crystals: (a) pH 6.2 (nil Gly^+); (b) pH 4.5 (ca. 0.7 wt % Gly^+, w/w of glycine).

4.5.2. Confirming impurity action along the c-axis

Consequently, α-Glycine crystals were obtained at pH 6.0 (using NaOH to adjust pH), with the impurities added in at the same concentration levels as in section 4.3. In the absence of Gly^+ species (after pH adjustment), α-Glycine crystals exhibited dominant {011} faces, indicating growth inhibition along the ±c axes (Fig. 4-7a). In turn, this could imply that the L-Asp anions interact with these crystal facets and subsequently result in the habit modification. Furthermore, from a closer observation (see the crystal labeled

"1" in Fig. 4-6a), it was possible to distinguish that the $\{0\bar{1}1\}$ faces on the $-b$ enantiomorphous half of α-Glycine (viz. $(0\bar{1}1)$ and $(0\bar{1}\bar{1})$ faces) were morphologically more significant than those on the $+b$ enantiomorphous half (viz. (011) and $(01\bar{1})$ faces). Similar habit modification was also observed with L-Glu (Fig. 4-7b, see crystal labeled "1" for the difference in morphological importance between the $\{011\}$ faces). Analogously, with the D-forms of the amino acids, it was observed that the $\{011\}$ faces of α-Glycine were morphologically more significant as compared with the symmetrically related $\{0\bar{1}1\}$ faces. These subtle, but significant observations on the habit modification demonstrate the specific interaction of impurities with the crystal facets of α-Glycine. This is explained further using the stereoselectivity mechanism in the subsequent sections.

At higher impurity concentrations, prismatic pyramidal crystals were obtained with well developed $(0\bar{1}0)$ basal faces, indicating growth inhibition along the –b-axis (Fig. 4-6c, d). These results are consistent with the observations made earlier (cf. section 4.3). Further, it was verified that the Na^+ ions of NaOH did not have any pronounced effect on the $\{011\}$ faces at the concentration levels used to adjust the solution pH.

In a subsequent experiment, racemic aspartic acid (DL-Asp or an equimolal mixture of L- and D-Asp) was doped into glycine solution. α-Glycine was crystallized with equally well developed $\{011\}$ faces on both the ±b enantiomorphous halves, confirming that the action of additives were along the c-axis (Fig. 4-7 e). If, on the other hand, the additive action had been confined to the enantiotopic crystal faces (viz. (010) and $(0\bar{1}0)$ faces), plate-like crystals should have been obtained on account of growth

inhibition along the ±b axes. However, with racemic glutamic acid, both isometric (Fig. 4-7f) and plate-like crystals (Fig. 4-7g) were obtained either simultaneously or from different batches. These observations revealed that the action along the c-axis was predominant in the case of aspartic acid as compared to glutamic acid. The reason behind this disparity in impurity action is explained in the following sections using molecular modeling, speciation and spectroscopic data.

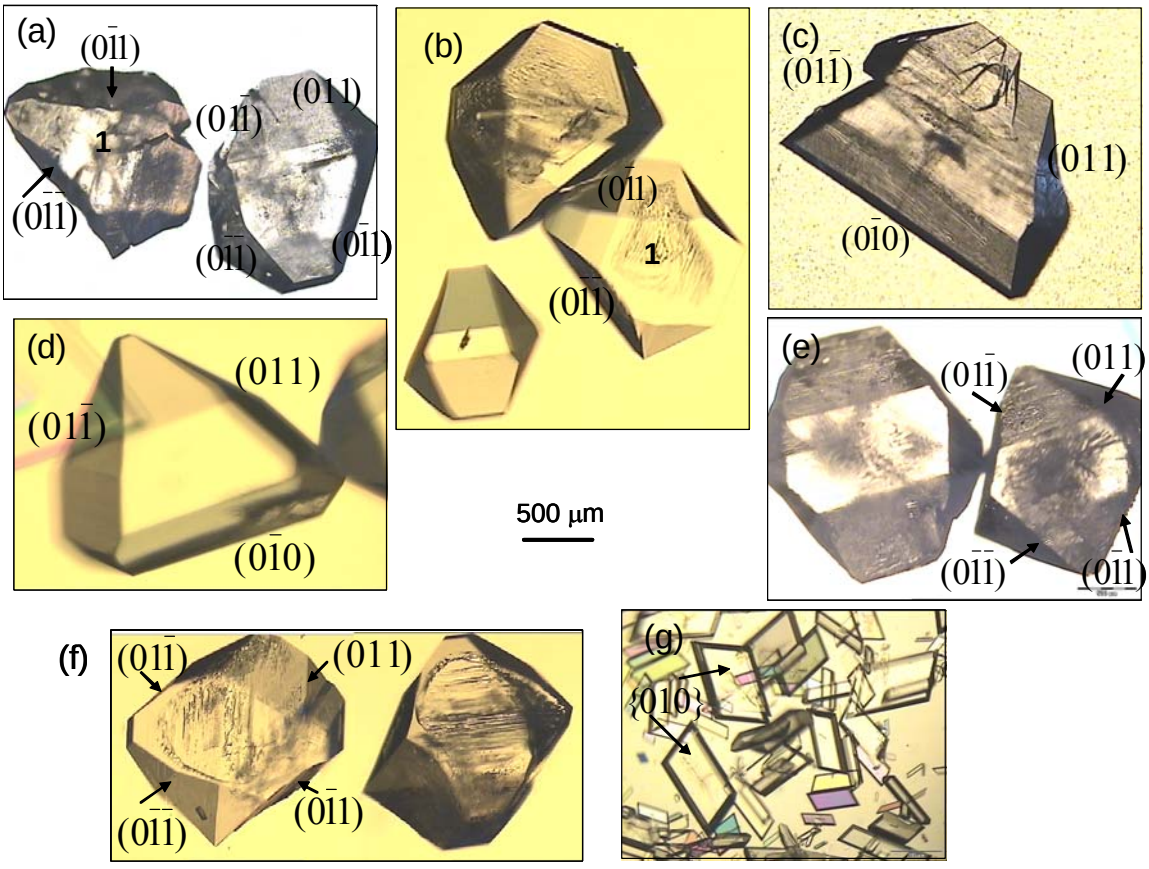

Figure 4-7 α-Glycine crystals obtained at pH 6.0: (a) and (b) 0.5 wt % (w/w of glycine) of L-Asp and L-Glu; (c) and (d) 1.5 wt % of L-Asp and L-Glu respectively; (e) and (f) 0.5 wt % of D + L-Asp and D+ L-Glu respectively; (g) 2 wt % D + L-Glu.

4.6. Mechanism of Molecular Differentiation

From the experimental observations, it is clear that habit modification along the *b*- and *c*-axes of α-Glycine crystals were stereospecific in nature. Combining this information with the known solution chemistry of the impurities, it is surmised that molecular speciation controls the stereoselectivity of impurities on the α-glycine crystal faces. This proposition is represented in Fig. 4-8, wherein, the zwitterions make a stereospecific interaction on the enantiotopic faces (i.e. along the *b*-axis), and the anions interact along the *c*-axis. Nevertheless, according to the stereoselectivity mechanism, molecular recognition along the enantiopolar *b*-axis of α-Glycine should be like for both the zwitterionic and anionic species. Therefore, the mechanism of differentiation between the impurity species at the α-Glycine crystal interfaces is further investigated so as to rationalize the newly observed habit modification.

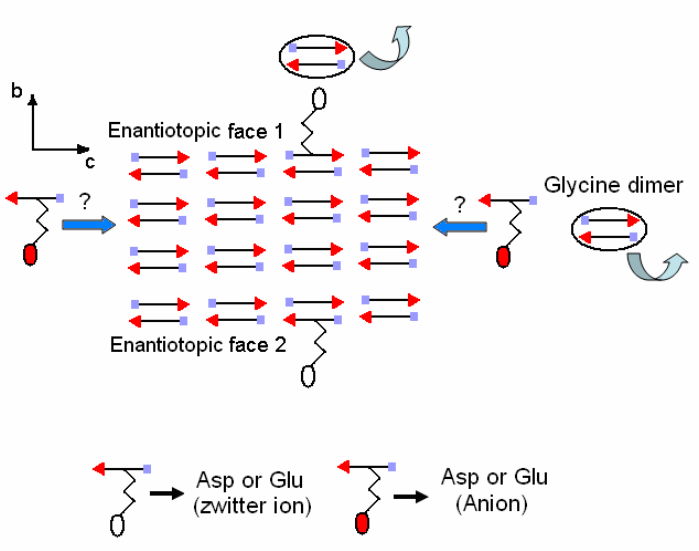

Figure 4- 8 Interaction of impurity molecular species with the α-Glycine crystal. The dimer growth unit of α-Glycine is shown as a pair of centrosymmetric glycine zwitterions.

4.6.1. Interaction of impurity species with the α-Glycine crystal

Interaction of the impurity molecular species with the crystal faces of α-glycine was modeled and visualized in Materials Studio molecular modeling (Accelrys Software Inc.). First, an L-Asp zwitterion was modeled in accordance with the stereoselectivity mechanism by replacing the C-H_{Si} bond of a glycine molecule on the $(0\bar{1}0)$ face with the side chain moiety of aspartic acid ($–CH_2COOH$) (Fig. 4-9a). On building the molecule, the conformation of the side-chain was kept intact as found within the crystal structure of L-Aspartic acid (ref. code. LASPRT, CSD, Ver. 5.26). Subsequently, the anion was modeled by deprotonating the side chain carboxylic acid group. As a result, a lone pair electron is introduced onto the carboxylate moiety (Fig. 4-9b), which could cause repulsive effects at the crystal interface. The O···O contact length between the side chain $–COO^-$ group and the carboxylate group of a glycine molecule at an adjacent site was measured to be ca. 2 Å. Note that at such short contacts, repulsive forces due to lone pair electrons of the oxygen atoms can be significantly stronger (ca. 1–2 kcal/mol; Berkovitch-Yellin et al., 1985). Therefore, the anion molecule could be prevented from incorporating into the crystal lattice along the *b*-axis due to the unfavorable interactions. These intermolecular interactions between the impurity species and glycine molecules on the crystal surface were calculated using atom-atom potential energy method and reported later in chapter 5.

Subsequently, the interaction of L-Asp anion was envisaged along the *c*-axis by making a stereospecific docking on the $(0\bar{1}1)$ and $(0\bar{1}\bar{1})$ faces (Fig. 4-9c). Apparently, at these crystallographic sites, the anions have no electrostatic repulsive effects on account of the oblique nature of the crystal faces delineating the glycine dimer motifs along the *c*-

axis. An analogous explanation holds for the interaction of D-Asp anions with the (011) and $(01\bar{1})$ faces of α-Glycine. This mechanism is akin to the interaction of racemic hexaflurovaline ($(CF_3)_2$–CH–$CH(NH_3^+)CO_2^-$), a 'tailor-made' auxiliary molecule, with the crystal faces of α-Glycine (Weissbuch et al. 1994). This additive molecule, being prevented from adsorbing along the *b*-axis due to steric and electronic repulsions of the hexafluroisopropyl moiety on the {010} faces, preferentially interacted with the {011} faces.

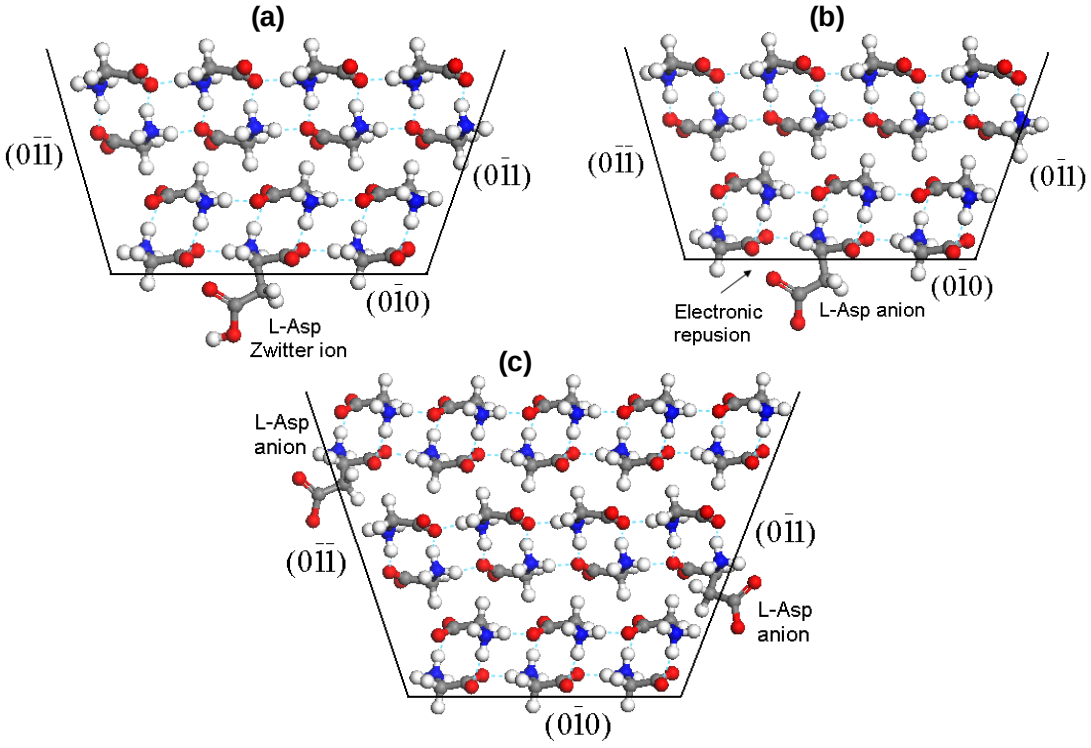

Figure 4-9 Molecular modeling of the interaction of the additive species with α-glycine crystal: (a) L-Asp zwitterion and (b) L-Asp anion on the $(0\bar{1}0)$ face; (c) L-Asp anion on the $(0\bar{1}1)$ and $(0\bar{1}\bar{1})$ faces.

Another likely mechanism is that the Asp anion molecule can preferentially incorporate at the (010) step instead of the flat crystal surfaces of α-Glycine, thereby circumventing the repulsive effects (Fig. 4-10a). Such an interaction mechanism for the adsorption of additive molecules has been demonstrated in previous studies for

centrosymmetric crystals by applying second harmonic measurements (Weissbuch et al. 1989). The anion molecule adsorbed on the step face can subsequently block an adjacent site and cause growth inhibition along the *c*-axis. Similar to this mechanism, in a recent work, Torbeev et al. (2005) have explained the role of the 'perturber' moiety (viz. bulky side chain moieties of α-amino acids such as phenylalanine, tryptophan and methionine) in controlling the stereoselective interactions with the (010) step planes of α-Glycine. The selective interactions of the additive molecules had resulted in nucleation inhibition of the α-Glycine crystal and, thereafter induced the crystallization of either β or γ-forms.

In the context of the proposed mechanism, it is noted that an L-Asp anion could not incorporate on the (011) and $(01\bar{1})$ faces, due to constraint imposed by the packing arrangement of the host molecules within the crystal structure. In principle, both types of host prochiral molecules (viz. of pro-R and pro-S absolute configurations) are expressed at all the four $\{011\}$ faces, in contrast to the (010) and $(0\bar{1}0)$ faces that individually express only one of the prochiral forms (cf. Fig. 4-1a). However, on incorporation of an L-Asp anion on the (011) or $(01\bar{1})$ faces at the symmetrically related sites, its side chain moiety would encounter a steric hindrance. A surface vacancy could be created to allow incorporation of L-Asp anion on these facets; however, in that case, it will be required to remove a host molecule on the $\{010\}$ step below the current growth layer. Therefore, docking on these facets would be less significant, as supported by the experimental habit modification (cf. Section 4.5.2). Consequently, considering the growth inhibition mechanism for the $\{011\}$ faces, it is one of blocking of an adjacent site in the current

growth layer on the {010} step plane, whereas in the case of {010} faces, the additive blocks the subsequent growth layer and not the current one.

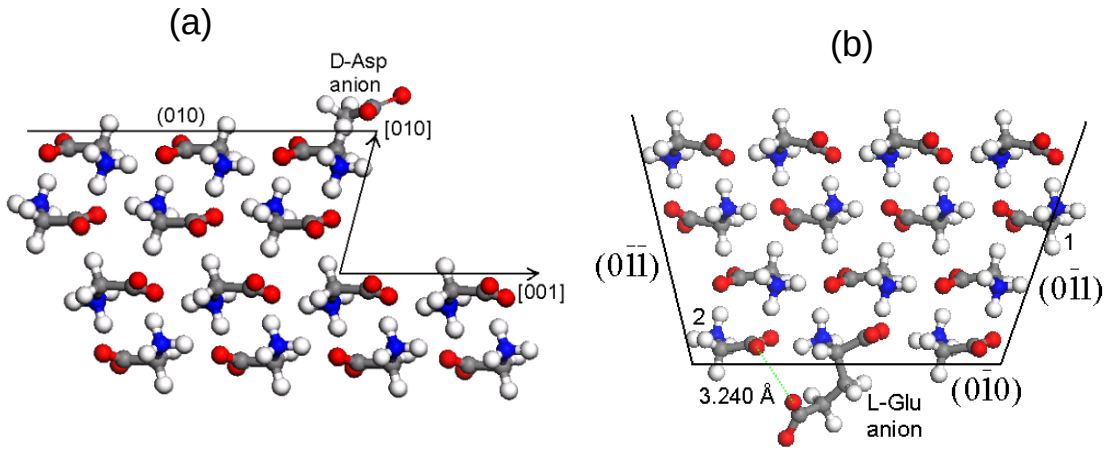

Figure 4-10 Molecular modeling of the interaction of: (a) D-Asp anion on the (010) step plane of α-Glycine; (b) L-Glu anion with the $(0\bar{1}0)$ face of α-Glycine.

Likewise, an L-Glu anion was modeled on the $(0\bar{1}0)$ face by stereospecifically docking an L-Glu zwitterion molecule taken from its crystal structure, and subsequently, deprotonating the distal –COOH group (Fig. 4-10b). This methodology was preferred over the construction of the side chain moiety, because, the substrate moieties ($^{+}H_3N–C^{\alpha}H–CO_2^{-}$) of the glycine molecule in the host crystal lattice and in the L-Glu zwitterion were stereospecifically superimposable. Besides, by this method, the side chain conformation of L-Glu was kept intact as found within its crystal structure (ref. code LGLUAC11, CSD Ver. 5.26). According to the aforesaid mechanisms, it could then be expected that the L-Glu anion is likely to experience electronic lone pair repulsions between its distal COO^{-} group and the carboxylate group of a glycine molecule at the adjacent site on the $(0\bar{1}0)$ facet (the O···O distance was measured as 3.240 Å). However, the L-Glu anion can favorably occupy either the crystallographic site "1" on the

$(0\bar{1}1)$ face or site "2" on a $(0\bar{1}0)$ step plane of α-Glycine (cf. Fig. 4-10b) , and subsequently result in growth inhibition along the *c*-axis.

4.6.2. Factors controlling impurity interactions

From the molecular models discussed above, it is understood that the repulsive effects described therein, is caused because of the partial delocalization of negative charge on the side chain carboxylate group of the impurity anions. Primarily, this factor could contribute to the energy penalties associated with the incorporation of the impurity species on the $\{010\}$ faces of α-Glycine. The values associated with these interactions could be determined by calculating the binding energies for the impurities on the various faces of a α-Glycine crystal. The results of these calculations are reported in chapter 5. Theoretically, the partial delocalization of negative charge is reflected by the pKa values of the distal –COOH group of the two acids – Asp anion has a higher ionization constant ($K_a = 2.2*10^{-4}$) as compared to the Glu anion ($K_a = 5.6*10^{-5}$). Therefore, as per the proposed model, this difference could result in greater repulsive effects at the $\{010\}$ faces in the case of the former anionic species as compared to the latter. Indeed, this was reflected in the extent of habit modification along the *c*-axis of α-Glycine in the presence of these two impurities, with aspartic acid having a greater impact on the $\{011\}$ faces.

Furthermore, it could be reasoned that the side chain length and conformation of the impurity anions can influence the interactions at the crystal interfaces, insights into which were gleaned through IR spectroscopic studies and conformation analysis.

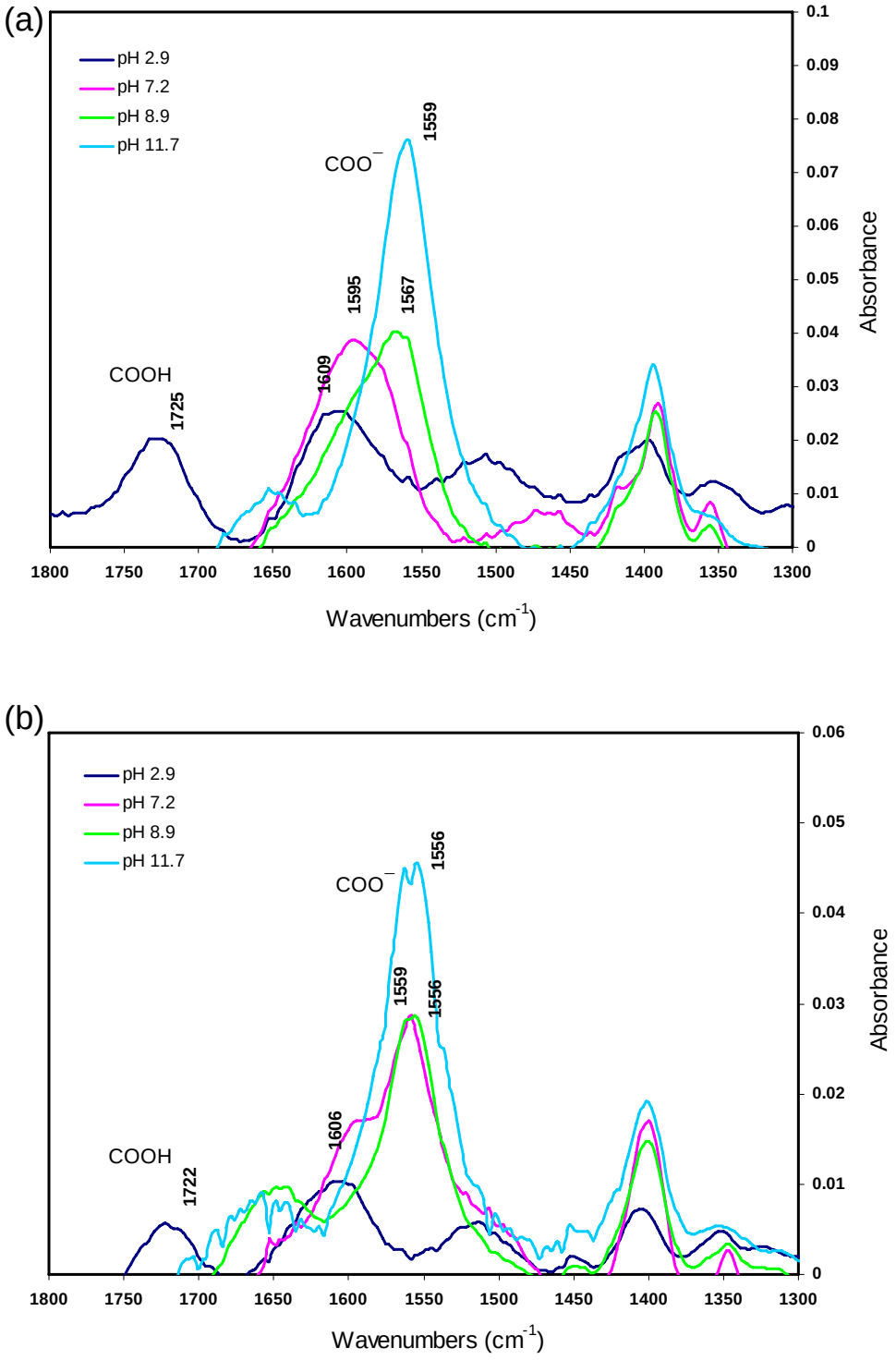

Figure 4-11 ATR-FTIR spectra of aqueous amino acids at different solution pH: (a) L-Asp and (b) L-Glu.

4.6.3. IR spectroscopy – solution speciation and molecular conformation

An implication of the partial delocalization factor is that intramolecular interactions could be effected within the molecular structures of the aspartic and glutamic acid anions. In this context, previous IR spectroscopic studies of these two amino acids in solution (water and D_2O) have shown intramolecular charge transfer interactions between the C^{α}-NH_3^+ group and the distal COO^- group of the anions (Pearson and Slifkin, 1972). To this end, in order to provide evidence for such interactions, IR spectra for L-Asp and L-Glu in water were obtained at different pH conditions: pH 3.0 (mostly zwitterions), pH 7.2 (anions), pH 8.9 (anions and dianions) and pH 11.7 (dianions only). The IR spectra showed a shift in the antisymmetric stretching frequency of the COO^- groups on increasing the solution pH (Fig. 4-11a, b). A similar shift of the carbonyl antisymmetric stretching frequency was observed in the solid-state spectra of these two amino acids and their salts; viz. 1614 cm^{-1} and 1586 cm^{-1} for DL-Aspartic acid and magnesium DL-Aspartate respectively, and 1645 cm^{-1} and 1594 cm^{-1} for L-Glutamic acid and sodium L-Glutamate respectively.

Of interest here, the change in the carbonyl antisymmetric stretch frequencies of the amino acids at different solution pH is redrawn in Fig. 4-12. Note that at pH 7.2, when Asp and Glu exist predominantly as anions, the antisymmetric stretching frequency of the COO^- groups for the two amino acids differ by 36 cm^{-1} (viz. 1595 cm^{-1} and 1559 cm^{-1} for Asp and Glu respectively). In contrast, the zwitterionic forms (pH ~3.0) show little difference in the antisymmetric stretch of the α-COO^- groups. Again, the difference of the antisymmetric stretching frequencies of COO^- groups between Asp and Glu diminishes at higher pH values; at pH 8.9, the difference is only 11 cm^{-1}, and at pH 11.7

it is further decreased to 3 cm^{-1}, in the absence of the influence of NH_3^+. This spectral shift is consistent with the previous observation for the anions of these two mono amino dicarboxylic acids in D_2O at neutral pD (Pearson and Slifkin, 1972), and hence corroborates the intramolecular charge-transfer interaction. As reasoned earlier, the nearer the charged NH_3^+ is to the COO^- group, the greater the wavenumber at which the antisymmetric COO^- absorption occurs, viz. 1595 cm^{-1} for Asp anion, and 1559 cm^{-1} for Glu anion.

The inferences from these findings on the molecular conformation of the impurity anions, and, in turn, the intermolecular interactions at the glycine crystal surface are further discussed in the following section.

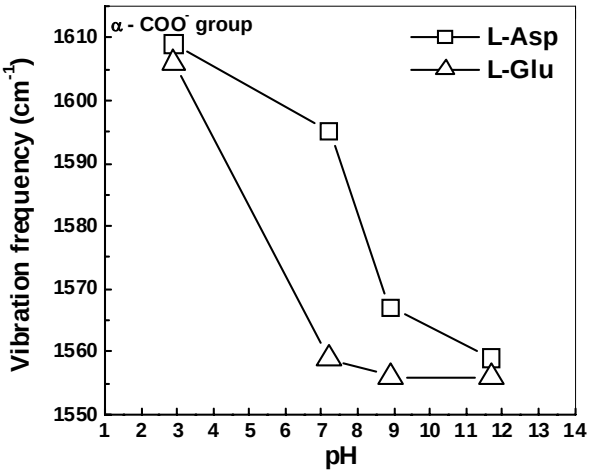

Figure 4- 12 Molecular vibration (–COO^- antisymmetric stretch) frequencies of the impurities at different solution pH. The data points corresponding to pH 2.9 are of the α-COO^- group. Lines are drawn to aid the eye.

4.6.4. Conformational analysis – implications on the proposed model

On analysis of the molecular structures of the zwitterions and anions within their crystal structures, some specific observations were made. First, in the L-Asp anion

structure, a conformational change of ca. 10° torsion in the side chain fragment was observed as compared to the zwitterions. On account of this, the side chain moiety was preferentially orientated towards the C^{α}-NH_3^+ moiety. Second, the formation of intramolecular H-bridge in the Asp anion molecular structures (in ca. 50 % of the hits) was observed between the C^{α}-NH_3^+ group and the distal COO^- group, absent in the L-Asp zwitterion molecular structures (Fig. 4-13a, b; molecular structures were extracted from CSD (Ver. 5.26); L-Aspartic acid – ref. code LASPRT, L-Ornithine D-Aspartate monohydrate – ref. code VUYHII). These observations, in turn, correlate to the intramolecular charge transfer interactions in L-Asp anion, as evinced by the IR spectroscopic studies. The implication of this on the proposed model is that an L-Asp anion with the modified conformation is likely to have higher repulsive effects along the *b*-axis, when attempting to dock on the $(0\bar{1}0)$ face of α-Glycine.

Further, continuing with this line of thought, a conformational analysis was made for an L-Glu anion using the torsions τ_1 and τ_2 as defined in Fig. 4-13c. These calculations were performed at molecular mechanics level using the DREIDING force field (Mayo et al., 1990) and Mulliken charges (Leach, 1996). It resulted in minimum energy conformers that showed the expected orientation in the anion side chain (in comparison with the zwitterion) due to favorable Coulombic interactions between the C^{α}-NH_3^+ group and the side chain $-COO^-$ group (Fig. 4-13d). However, in a solution environment, it is anticipated that the solvation effect would considerably stabilize the charged moieties through intermolecular H-bonding with surrounding water molecules. Nevertheless, it is reasonable that any considerable amount of conformational change in the side chain of L-Glu anion (as a consequence of the partial delocalization of negative

charge and the subsequent intramolecular charge transfer interaction), could increase the repulsive effects on the $(0\bar{1}0)$ face of α-Glycine.

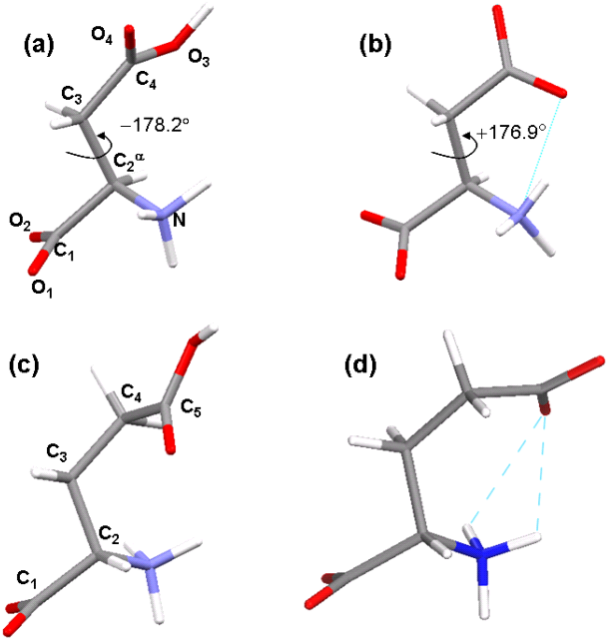

Figure 4-13 Molecular structures illustrating conformational changes in the side chain: (a) L-Asp zwitterion; (b) L-Asp anion; (c) L-Glu zwitterion; (d) minimum energy conformer obtained from the conformational analysis of L-Glu anion. The intramolecular H-bridge between the C^{α}-NH_3^+ and the distal COO^- group in the anion molecular structures is represented by the dash lines. The torsions τ_1 and τ_2 are defined by the carbons C_1, C_2, C_3, C_4 and C_2, C_3, C_4, C_5 respectively of the glutamic acid molecule.

Finally, what could be the energy penalties associated with relieving the repulsive effects for the incorporation of anions on the {010} faces of α-Glycine? From the conformation analysis made earlier, the energies associated with the changes in the molecular conformation of the anion side chain were in the order of 1.0 kcal/ mol and 6.0 kcal/ mol for L-Asp and L-Glu respectively. If these energy penalties were to be imparted by relatively subtle but cooperative changes in the torsion angles that describe the orientation of the anions side chain, it may be possible to relieve the repulsions due to close O···O contacts. However, two of the factors may restrain changes in the molecular

conformation of the anion side chain at the crystal interfaces. Firstly, because of highly stereospecific intermolecular interactions between the adsorbed additive and the neighboring molecules at the host crystal surface, the side chain fragment would be less flexible (Berkovitch-Yellin, 1985). Secondly, the favorable intramolecular charge transfer interactions in the additive anions may also limit changes in their conformation, while attempting to dock into the crystal lattice.

4.7. Summary

While the interactions of added α-amino acid impurities with the α-Glycine crystal faces are in general stereoselective in nature, however, molecular speciation of some amino acids (viz. aspartic and glutamic acids) in glycine solution could control such interactions. This was demonstrated using the stereoselective habit modification in α-Glycine crystals in the presence of these impurities, which revealed growth inhibition along the *b*- and *c*-axes respectively, depending on the pH conditions. The habit modification was explained based on solution speciation of the impurities, and subsequent interaction of the molecular species (viz. zwitterions and anions) with the α-Glycine crystal faces. The change in impurity action from the crystallographic *b*-axis (viz. {010} faces) to the *c*-axis (viz. {011} faces) was proposed to be the result of electrostatic repulsive interactions between the anionic species and glycine molecules at the {010} faces. The study further highlighted that the conformation and pK_as of the residual groups of the impurity species are important factors controlling the intermolecular interactions at the α-Glycine crystal interfaces. This proposition was successfully corroborated by exploiting the speciation data of the impurities, together with IR spectroscopy and molecular modeling.

CHAPTER 5

Molecular Modeling and Simulation

In chapter 4, habit modification in α-Glycine crystals was explained using solution speciation data of the impurities, and some preliminary molecular modeling and visualization of the interaction of impurity species with the crystal facets. In this chapter, firstly, the growth morphology of α-Glycine is predicted using theoretical methods, and compared to the experimental crystal habit. Subsequently, interactions of the impurity species with α-Glycine crystal are estimated quantitatively using atomistic potential energy calculations, in an attempt to rationalize the earlier observations.

5.1. Habit Modeling

In this section, molecular-modeling based simulation techniques – The Bravais-Friedel-Donnay-Harker (BFDH) and the Hartman-Perdok theories are used to compute the growth morphology (vis-à-vis crystal habit) of α-Glycine from its molecular crystal structure. The differences between the predicted growth morphology and the experimental crystal habit are investigated by considering the effect of solvent on crystal growth.

5.1.1. The BFDH morphology of α-Glycine

According to the BFDH theory, the relative morphological importance of the (hkl) crystal faces is proportional to the interplanar distance (d_{hkl}) of the crystallographic lattice planes (Bennema, 1995). The BFDH growth morphology of α-Glycine has been computed from its crystal structure (Jönsson and Kvick, 1972; reference code

GLYCIN03, Cambridge Structural Database (CSD), Ver. 5.26) in Materials Studio (2005) using the *Morphology* program. The predicted crystal habit is bounded by the dominant faces {020}, {011}, {110}, {10-1} and {11-1} (Fig. 5-1). The morphological importance of these facets, as given by the percentage of total facet area, decreased with the d_{hkl} values (refer to Table 5-1). This morphology is defined using the Wulff Plot construction, in which the distance from the origin to the (hkl) face (centre-to-plane distance) is inversely proportional to the d_{hkl} values (Bennema, 1995).

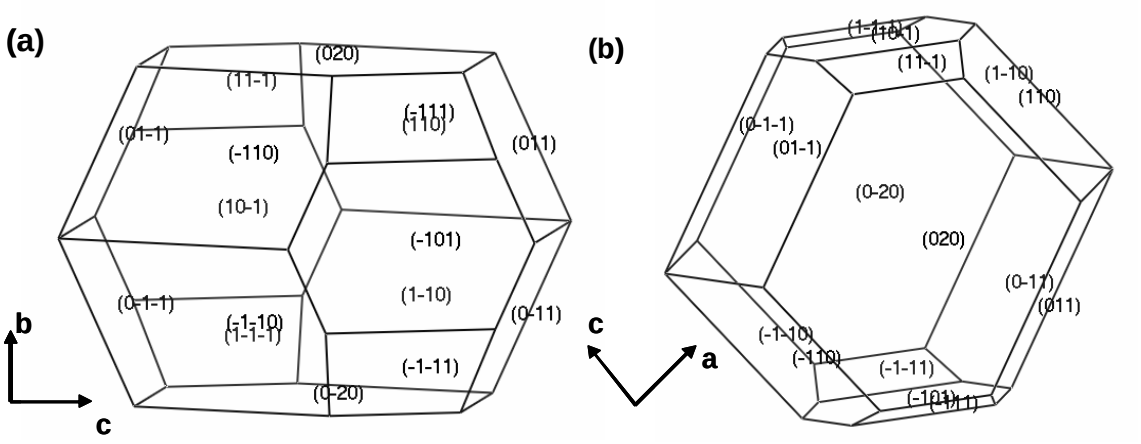

Figure 5- 1 Growth morphology of α-Glycine computed using the BFDH method: (a) view along the *a*-axis; (b) view along the *b*-axis.

Table 5- 1 Morphological data of α-Glycine crystal computed using the BFDH method.

Face (hkl)	Multiplicity	d_{hkl} (Å)	Centre-to-plane distance (Å)	% Total facet area
{020}	2	5.984	16.71	29.6
{011}	4	4.674	21.39	28.4
{110}	4	4.410	22.67	24.1
$\{10\bar{1}\}$	2	4.363	22.91	10.5
$\{11\bar{1}\}$	4	4.099	24.39	7.8

5.1.2. Comparison between theoretical and solution grown crystal habit

On comparing with the experimental α-Glycine habit (Fig. 5-2a) the BFDH morphology adequately described the dominant facets. All those facets that were

expressed in the solution grown crystal habit (viz. {010}, {011} and {110} faces) were found to be expressed in the predicted morphology. However, there were some striking discrepancies between the predicted and observed morphologies. Firstly, the $\{10\bar{1}\}$ and $\{11\bar{1}\}$ faces of the predicted α-Glycine morphology were not expressed in the experimental crystal habit. Secondly, the {010} faces were not observed in several of the as grown α-Glycine crystals (Fig. 5-2b). Thirdly, the aspect ratio of the predicted morphology (b/c ratio=1.72) was lower when compared to the experimental crystal habit (b/c ratio = 2.62 ± 0.5 for a sample size of 20 crystals). The differences between the predicted and experimental crystal morphologies are explained in the following paragraphs.

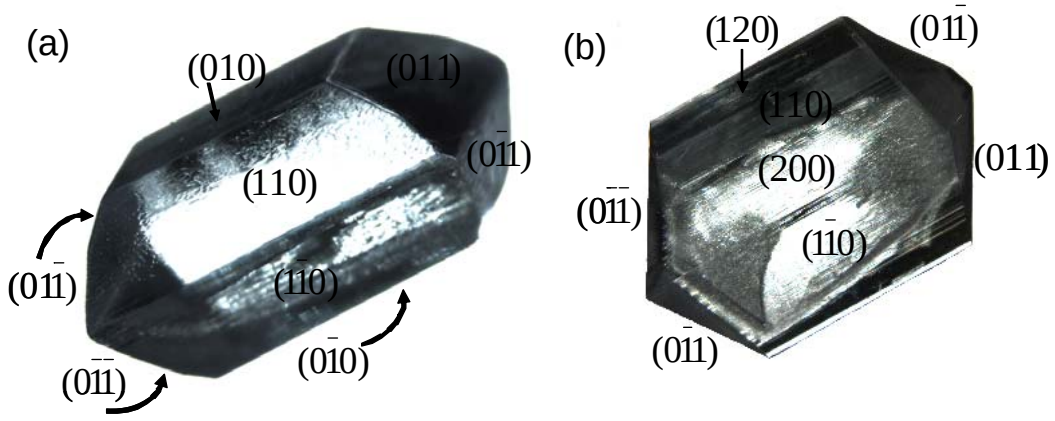

Figure 5- 2 (a) and (b) Stereomicroscope images of α-Glycine crystals grown from pure aqueous solution.

In the BFDH theory, neither the intermolecular interactions in the crystal structure, nor the thermodynamics of crystal interfaces, nor the crystal growth mechanisms are taken into account (Bennema, 1995). It only takes into consideration the unit cell parameters and interplanar spacing in the prediction of crystal habit. However,

from previous experimental studies it is known that the {011} faces of α-Glycine are usually fast growing (Li and Rodríguez-Hornedo, 1992), a fact evident from the *c*-axis elongated crystal habit (cf. Fig. 4-2a, 4-5a and 5-2a). It is along the c-axis of α-Glycine that the centrosymmetric glycine dimers are packed through strong hydrogen bonds (cf. Fig. 4-1a). This may explain the observed variation of aspect ratios between the predicted BFDH morphology and the experimental crystal habit.

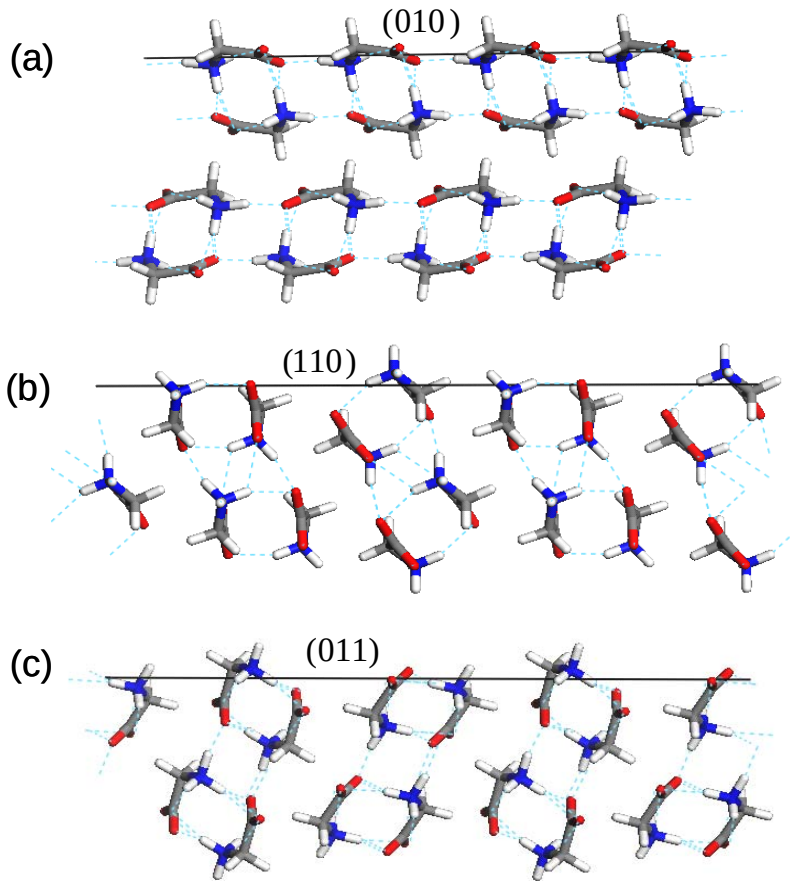

Figure 5- 3 Edge-on view of the molecular packing arrangement on the various facets of α-Glycine crystal: (a) the (010) face; (b) the (110) face and (c) the (011) face.

The absence of the $\{10\bar{1}\}$ and $\{11\bar{1}\}$ in the experimental crystal habit can be reasoned by considering the relative growth kinetics of the {110} faces. The well developed {110} facets in the experimental crystal habit (cf. Fig. 5-2 (a)) suggest that

these facets are slow growing. This can be understood on the basis of solvent-solute interactions at these crystal interfaces. The surface chemistry of the {110} faces (Fig. 5-3b) is made up of charged amino and carboxylate groups that can form strong hydrogen bonds with water molecules at the crystal interface. During crystal growth, the solvation layer had to be broken before glycine molecules could attach to the crystal surface (Lahav and Leiserowitz, 2001). On account of this, growth rate normal to that surface could be decelerated, consequently resulting in dominant {110} facets, and less developed $\{10\bar{1}\}$ and $\{11\bar{1}\}$ facets.

In the BFDH morphology, the {020} faces are the most morphologically significant (cf. Fig. 5.1 and Table 5-1). In comparison, α-Glycine obtained from the solution crystallization experiments were of two distinct crystal habits. While, one of them exhibited dominant {010} facets (cf. Fig. 5-2a), in the other, these facets were less developed (cf. Fig. 5-2b). The absence of {010} facets in the solution grown α-Glycine crystal habit as against the vapor grown crystals could be explained through solvent-substrate interactions (Weissbuch et al., 1995). First, it is essential to study the surface chemistry of the various facets of α-Glycine in order to explain this difference between the crystal habits. The {010} faces are made up of cyclic hydrogen bonded glycine dimers with the C–H group oriented normal to the surface (Fig. 5.3a) (Gidalevitz et al., 1997). In contrast, both the {011} and {110} faces consist of NH_3^+ and CO_2^- groups exposed normal to the surface (cf. Fig. 5-3b and c). As a result, the {010} faces are less hydrophilic when compared to the later facets, with the amino and carboxylate groups oriented on the {011} and {110} faces having strong affinity for water molecules. Supporting of this argument, Coulomb potential maps computed for these facets using *ab*

inito methods have shown the {011} facets to be strongly polar (Berkovitch-Yellin, 1985). On the basis of these premises, as crystal growth along the b-axis is relatively less impeded by the solvent interactions the {010} facets tend to grow faster than the prediction, and hence, are not expressed in the solution grown morphology.

In an attempt to overcome some of the above mentioned limitations of the BFDH theory the Attachment Energy (AE) method (Hartman and Perdok, 1955) was used to predict the α-Glycine crystal habit, which will be discussed in the later section. Prior to this, a rational method was adopted for the selection of an appropriate force field and a description of charge set that can define the intermolecular interactions in a molecular crystal precisely.

5.1.3. Force field selection

For a potential set to be considered accurate, it should mimic the lattice energy (often referred to as the crystal binding or cohesive energy) of the system satisfactorily (Docherty, 1996; Clydesdale et al., 2005). Lattice energy (E_{latt}) is the energy of formation of a crystal from the isolated (gas phase) molecules and for molecular crystals can be calculated by summing all the interactions between a central molecule and all the surrounding molecules within a limiting sphere at which the system energy converges. The calculated lattice energy can be correlated to the sublimation enthalpy (ΔH_{sub}) of the substance, after correcting it by a factor of 2RT that accounts for the difference between the gas-phase enthalpy and the vibrational contribution to crystal enthalpy.

Furthermore, in the case of glycine, which crystallizes as zwitterions, the “proton transfer” energy (ΔE_{pt}) should be included in the calculation of the corresponding lattice energy (Bisker-Leib and Doherty, 2003). It is the energy associated with the transfer of a

proton from the NH_3^+ group to the COO^- group of the glycine zwitterion molecule to form the neutral molecule. The relationship between the lattice energy, sublimation enthalpy, and proton transfer energy can be described as follows:

$$E_{latt} = -\Delta H_{sub} - 2RT + \Delta E_{pt} \qquad \textbf{5- 1}$$

In equation 5-1, E_{latt} and ΔE_{pt} were calculated using the procedures as given below:

(a) Following the method proposed by Voogd (1981), the proton transfer energy was calculated as the difference between the *ab initio* molecular energies of the gas (neutral form) and the crystal (zwitterionic form). The calculations were performed at the Hartree–Fock theory level (Leach, 2001) using the DMol^3 program (Delley, 2000) in Materials Studio, which employs a density functional theory (DFT) quantum mechanical code. The BLYP gradient-corrected correlation potential (Becke, 1998; Lee et al., 1998) with an "all electron" core treatment and the DNP basis set were used in the energy calculations as suggested by Gnanasambandam et al. (2007). The ΔE_{pt} value of glycine was calculated to be –33.0 kcal/mol. In comparison, the proton transfer energies of glycine were estimated previously at –34.3 kcal/mol (No et al., 1994) and –37.3 kcal/mol (Voogd et al., 1981). As noted before (Bisker-Leib and Doherty, 2003), the calculated proton transfer energies showed high dependency on the basis set selected.

(b) The lattice energy of α-Glycine was computed by energy minimization of its crystal structure using the *Forcite* program in Materials Studio. To this end, the asymmetric unit cell of α-Glycine (Jönsson and Kvick, 1972) consisting of 4

glycine molecules as rigid bodies was built as a periodic system. The net atomic charge distributions of the glycine zwitterion molecule (cf. Table 5-3) were determined using the Mulliken population analysis or by fitting to molecular electrostatic potentials (ESP). The energy expression was set up using different forcefield potentials available within the *Forcite* program viz. Dreiding (Mayo et al. 1990), Universal (Rappé et al., 1992), COMPASS (Sun, 1998) and CVFF (Dauber-Osguthorpe et al., 1998). All of these are generic force fields and have been parameterized for small organic molecules in the gas phase and in molecular crystals. The Ewald summation method (Ewald, 1921) was used to calculate the non-bonded interactions between the glycine molecules, including the van der Waals and electrostatic contributions (note that the Dreiding forcefield employs an additional expression to compute hydrogen bond energies separately). The conjugate gradient algorithm was used in energy minimization.

Table 5- 2. Lattice energies (kcal/mol) of α-Glycine crystal computed using different force fields and charge sets.

Force field	Charge set	Lattice energy	Percentage error
Dreiding	Mulliken	–65.96	2.8
	ESP	–57.83	14.8
Universal	Mulliken	–44.65	34.2
	ESP	–34.22	49.6
COMPASS	Mulliken	–68.47	0.81
	ESP	–63.06	7.1
CVFF	Mulliken	–65.57	3.4
	ESP	–58.96	13.1
Experimental		–67.92	

Table 5- 3 Calculated point atomic charge distributions of glycine and impurity molecules.

Atom label	Molecule					
	Glycine zwitterion		Aspartic acid zwitterion	Aspartic acid anion	Glutamic acid zwitterion	Glutamic acid anion
	Mulliken	ESP	Mulliken			
C_1[a]	0.483	0.729	0.498	0.487	0.501	0.491
C_2 (C^{α})	0.007	–0.223	0.015	0.041	0.031	0.035
O_1	–0.578	–0.666	–0.563	–0.617	–0.567	–0.612
O_2	–0.552	–0.647	–0.524	–0.603	–0.544	–0.584
N_1	–0.127	–0.245	–0.165	–0.127	–0.152	–0.141
H_1	0.199	0.268	0.250	0.225	0.184	0.181
H_2	0.218	0.264	0.203	0.195	0.218	0.203
H_3	0.224	0.287	0.218	0.165	0.228	0.197
H_4	0.064	0.128	…	…	…	…
H_5	0.061	0.106	0.067	0.024	0.077	0.059
C[b]			–0.079	–0.065	–0.056	–0.039
H			0.117	0.059	0.097	0.069
H			0.125	0.062	0.076	0.051
C			0.495	0.481	0.531	0.474
O			–0.450	–0.637	–0.495	–0.677
O			–0.523	–0.691	–0.442	–0.648
H			0.315	…	0.311	…
C					–0.128	–0.096
H					0.059	0.020
H					0.072	0.017

[a] The atomic numbering is as given in Fig. 4-1b. [b] The atom labels refer to that in the side chain group of the impurity molecules.

The calculated lattice energy values of α-Glycine are listed in Table 5-2. It is observed that the values show high sensitivity to both the potential and the charge sets

used. The Dreiding and COMPASS force fields in conjunction with the Mulliken charge set show small differences with respect to the experimental lattice energy, which can be computed using Eq. 5-1 with a sublimation enthalpy value of –33.69 kcal/mol (Svec and Clyde, 1965). Consequently, these two force fields were used to predict the crystal habit using the attachment energy method.

Givand et al. (1998), in a similar work, have used semiempirical solution techniques to the quantum mechanical theory in order to determine the atomic point charges for L-isoleucine molecule. The authors used the root mean square deviation of the atomic positions to characterize the deviation of the energetically minimized crystal structure from the initial structure determined using X-ray data. The smaller the RMS value, the more the minimized structure resembled the experimental structure, and hence, the more accurate the atomic charge description and governing energy expression were considered.

5.1.4. Attachment Energy method

Within the framework of the Hartman-Perdok theory (Hartman and Perdok, 1955), it is assumed that the rate of growth of a face (hkl) is proportional to the attachment energy. The attachment energy (E_{att}) is defined as the energy released on the addition of a growth slice to the (hkl) surface of a growing crystal. E_{att} is complementary to the 'slice energy' (E_{sl}) or the 'layer energy' (E_l), which is defined by the intermolecular bonding energy contained within the surface growth slice of depth d_{hkl}. In line with this theory, crystal morphology is bounded by the slow growing facets that have lower E_{att} values. The summation of the E_{att} and E_{sl} energies gives a measure of the crystal lattice energy (Berkovitch-Yellin, 1985; Bennema, 1995; Clydesdale et al., 2005).

The Dreiding and COMPASS force fields were used to predict the growth morphology of α-Glycine as the lattice energies computed using these two potentials conformed to the experimental value (cf. Table 5-2). The following procedure was followed. Initially, the α-Glycine crystal structure was energy minimized with glycine molecules constrained as rigid bodies. Subsequently, the growth morphology was computed using the attachment energy method as implemented within the *Morphology* module in Materials Studio. The parameters used for the calculation of attachment energies were set similar to the one used for the crystal structure minimization. The attachment energies for the morphologically significant facets of α-Glycine crystal as computed using the intermolecular force field potentials are shown in Table 5-4. The calculation results indicate that the {020}, {110, {011} and {002} faces have increasing E_{att} values, and hence, are in the decreasing order of morphological importance (M.I.) in the α-Glycine crystal habit.

Table 5- 4 Attachment energies of the α-Glycine crystal facets calculated using the force field potentials.

Face (hkl)	E_{att} (kcal/mol)				Centre-to-plane distance (Å)	% Total facet area
	Total	vdW	Electrostatic	H-bond		
Dreiding						
{020}	–13.7	–6.0	–7.7	0	13.7	61.5
{110}	–43.4	–5.5	–27.2	–10.7	43.4	22.7
{002}	–61.7	+3.3	–55.0	–10.0	61.7	6.6
{011}	–59.6	+5.7	–55.3	–10.0	59.7	5.4
{012}	–61.5	+4.4	–56.0	–10.0	61.5	3.7
COMPASS						
{020}	–15.6	–8.8	–6.7	0	15.6	61.7
{110}	–53.3	–8.5	–44.7	0	53.3	21.1
{011}	–63.7	–8.2	–55.4	0	63.7	11.7
{002}	–67.1	–12.1	–54.9	0	67.1	5.5

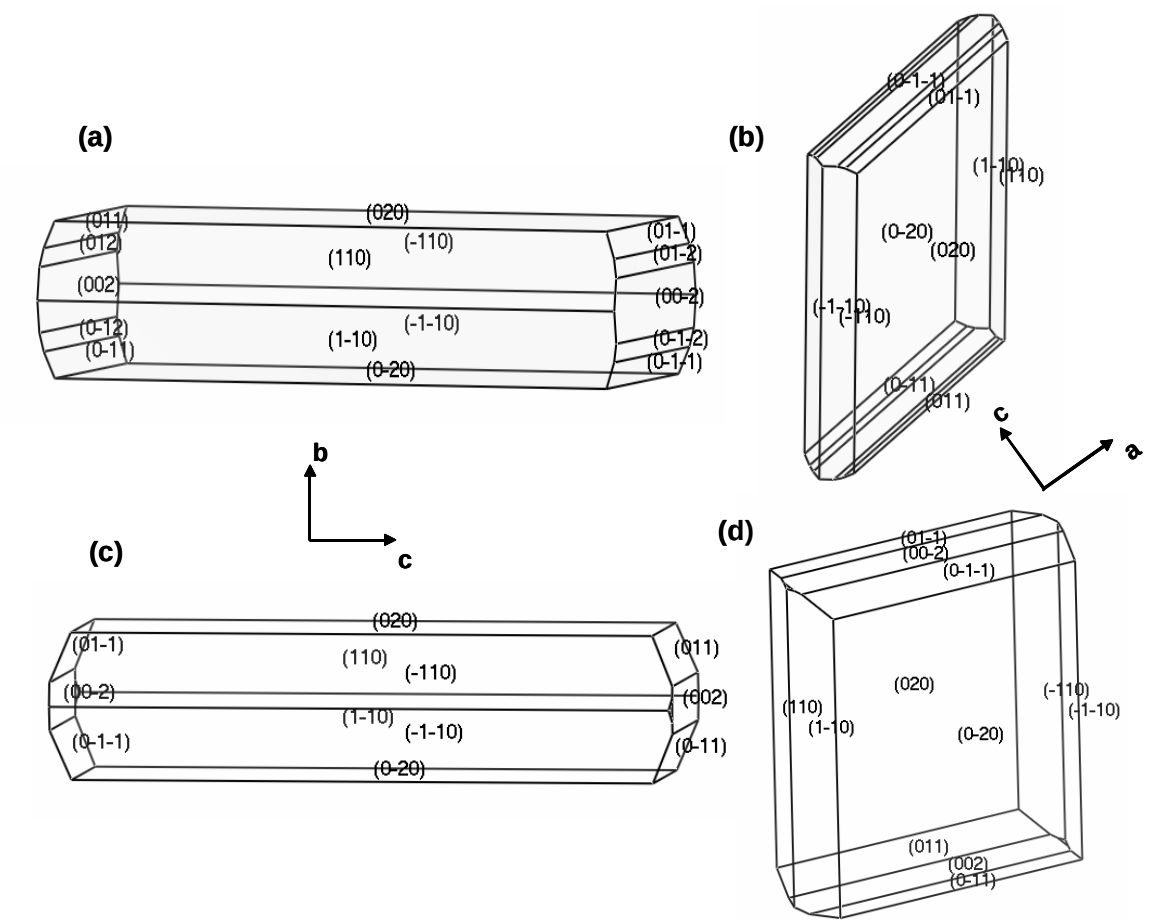

Figure 5- 4 Growth morphology of α-Glycine computed by the attachment energy method using the force field potentials: (a), (b) Dreiding; (b), (d) COMPASS. (a), (c) are views along the *a*-axis; (b), (d) are views along the *b*-axis.

The α-Glycine growth morphology predicted using the attachment energy method is shown in Fig. 5-4. These morphologies have a higher aspect ratio along the *c*-axis and can be clearly distinguished from that of the BFDH morphology (cf. Fig. 5-1). The crystal habits exhibited the {020}, {110}, {002}, {011} and {012} faces, in the order of morphological importance (M.I.). Apparently, they compare well with the experimental crystal habit, with the M.I. of the {010}, {110} and {011} facets (cf. Fig. 5-2a) being in good agreement with the prediction. Nevertheless, the predicted growth morphologies yielded higher aspect (*b*/*c*) ratios (ca. 7.0) as compared to the experimental crystal habit (2.62±0.5). This difference, however, can be explained by considering into account

solvent interactions with the {011} faces. The {011} faces are highly polar in nature (Berkovitch-Yellin, 1985), and hence, can have strong solvent interactions. In turn, it can cause a delay in the rate at which solute molecules attach onto these faces through a "relay mechanism" (Lahav and Leiserowitz, 2001). This may explain the reduced growth rate along the c-axis resulting in well developed {011} faces, together with absence of {002} faces in the experimental crystal habit.

5.2. Impurity Effects on Crystal Habit

In chapter 4, habit modification in α-Glycine crystals was explained based on solution speciation of impurities (aspartic and glutamic acids) and the stereoselectivity mechanism. It was proposed that the charged impurity species, viz. zwitterions and anions, adsorbed on the {010} and {011} facets, respectively, and thereafter, resulted in growth inhibition along the *b*– and *c*–axes of the α-Glycine crystal. In this section, the interaction between charged impurity species and glycine molecules at the host crystal surfaces is quantitatively determined using atomistic potential energy calculations.

5.2.1. Approach

Firstly, in order to assess the likelihood of impurity incorporation at the crystal surface, the differential slice energy (ΔE_{sl}) value is computed. It is defined as the difference between the slice energies of a pure glycine (hkl) layer (E_{sl}), and that of a impurity incorporated (hkl) layer (E_{sl}'). E_{sl} and $E_{sl}^{'}$ are computed as the intermolecular interaction energies associated with the incorporation of a single glycine molecule and of an impurity molecule, respectively, at the centre of the host crystal slice. The impurity incorporation will be favored where ΔE_{sl} is at its minimum (Weissbuch et al., 2006;

Clydesdale et al, 2005). If the differential slice energies are strongly dependent upon crystal orientation then the impurity incorporation will be specific to one crystal face and vice versa. The attachment energy is computed as the sum of all intermolecular energy between a reference molecule on the (hkl) face and all other molecules outside the layer in a single direction. A modified version of the attachment energy (E_{att}'), defined as the energy released on the addition of a pure growth slice onto a surface on which an impurity has adsorbed, can be used to infer the growth rate of a crystal face with an impurity molecule present. This parameter, in turn, can be corroborated with the habit modification due to the impurity.

5.2.2. Computational details

For the slice energy calculations, the α-Glycine crystal structure was cleaved parallel to the (010) plane with a depth of one unit cell (11.97 Å). A crystal slice was constructed as a periodic superstructure of 7 x 7 unit cells comprising 196 molecules. A 25 Å thickness vacuum slab was built in above the crystal slice (Fig. 5-5a). Similarly, for the (011) crystal slice (d_{hkl} = 4.67 Å), a superstructure of 7 x 3 unit cells comprising 168 glycine molecules was constructed along with a 25 Å thickness vacuum slab. In both cases, fractional positions of the symmetry-related glycine molecules within the cleaved surface layer were kept the same in all calculations.

For the pure glycine layer, E_{sl} was calculated as the sum of intermolecular interactions between one glycine molecule as a rigid body placed in the center of the host crystal slice in the crystallographic sites on either (010) or (011) surfaces. The orientation of the docked glycine molecule was optimized by minimizing the energy of the slice with all the neighboring host molecules constrained as rigid bodies. In the case of impurities,

the zwitterions were modeled by constructing the side chain moiety superimposed on a glycine molecule comprising a common substrate molecular structure. The impurity molecules were then inserted as a rigid body in the center of the slice at the crystallographic sites on the (010) and (011) surfaces respectively, with the side chain protruding from the host lattice into the vacuum slab (Fig. 5-5b). In this context, note that while the (010) and $(0\bar{1}0)$ faces individually express only one of the prochiral forms of the host molecules, at the {011} faces, both types of host molecules (viz. of pro-R and pro-S configurations) are expressed (cf. Fig. 5-3a, c). However, due to steric effects imposed by the side-chain moieties of the impurity molecules, stereoselective interactions are possible only at one of the crystallographic sites on the {011} facets. The Mulliken point atomic charge distributions were determined and assigned for the impurity zwitterion molecules (cf. Table 5-3).

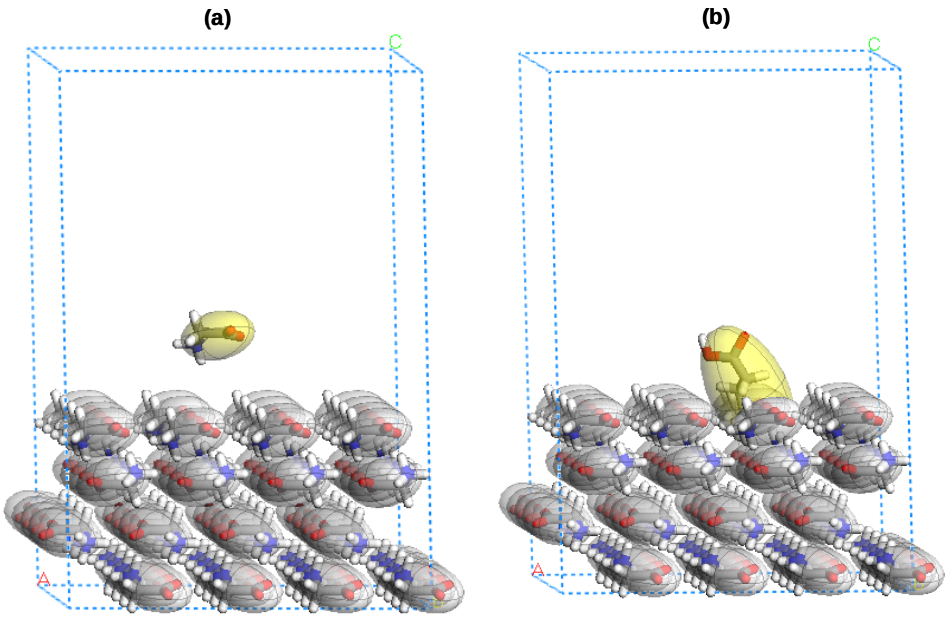

Figure 5- 5 Superstructures of the (010) face of α-Glycine crystal consisting of glycine molecules as rigid bodies. (a) The lone glycine molecule shown in the vacuum slab is docked into the growth slice to determine the slice energy; (b) An L-Glutamic acid zwitterion molecule is docked into the growth slice.

After docking the impurity molecules by a stereospecific superimposition, the C-C torsion angles of the side chain fragment of the impurity molecule were adjusted in order to obtain different initial conformations. Subsequently, its position in the host crystal slice was optimized by energy minimization, with the Cartesian coordinates of the neighboring glycine molecules in the 2D crystal lattice constrained. By imposing such a constraint, the intermolecular interactions within the bulk crystal could be reproduced precisely, besides keeping intact the symmetry of glycine molecules within the crystal slice. This procedure was repeated until the minimized energy of the slice incorporated with the impurity zwitterions either approached the E_{sl} value of that a pure glycine slice (the reference system) or was lower than that. In this way, we ensured that E_{sl}' determined for the impure slice was one amongst the many energy minima, albeit not the global minimum.

Following this, the anionic species of the impurity molecule was modeled by deprotonating its residual carboxylic acid group. Their net atomic charges of the impurity anions were computed using the Mulliken population analysis within the DMol^3 program (cf. Table 5-3). Herein, it is understood that calculation of net atomic charges for an anion molecule is somewhat ill-defined and there is no universally agreed 'best' procedure (Cramer, 2004). Nevertheless, the quantum mechanical method was used to compute net atomic charges for the anion so as to be consistent with the calculations for zwitterions. Subsequently, the interaction energies of the anions with the (010) and (011) crystal faces were calculated through an energy minimization procedure. Depending on the pH, the dynamic equilibrium between solution and surface can maintain a fixed proportion of surface molecules as protonated or deprotonated species (Towler et al., 2004). Given this,

although the impurity anion could not incorporate into the crystal lattice to form a solid solution, it can interact with the growing crystal surface in dynamic equilibrium with the solution. Based on this premise, the relative interaction energies of the impurity zwitterions and anionic species at the α-Glycine crystal faces could be compared.

5.3. Results and Discussion

5.3.1. Stereospecific impurity interactions on the (010) surface

The stereospecific interactions occurring at the (010) face were evaluated from the difference between the slice energies (ΔE_{sl}) of the impurity molecules and that of a glycine molecule (Table 5-5). Except for the particular case of glutamic acid with the Dreiding force field, the results indicate that interaction of the impurity molecules with the crystal slice are more favored when compared to glycine molecule itself. In line with this, earlier studies using *ab initio* calculations have shown that incorporation of alanine, which exists in the zwitterionic form under the solution pH conditions, was energetically more favored on the (010) face (Berkovitch-Yellin et al., 1985). This can be explained on the basis of stereospecific interactions of the "binder" moiety of the impurity molecules with glycine molecules on the crystal lattice, plus favorable interaction forces between the side chain groups of the impurity molecule and of glycine molecules on the surface. Nevertheless, comparing the ΔE_{sl} values of Asp zwitterions and anions, it is clear that the anions incur "net repulsive" interaction forces of 5.0 kcal/mol (Dreiding) and 4.9 kcal/mol (COMPASS) respectively (cf. Table 5-5). Similarly, a Glu anion incurs 4.0 kcal/mol (Dreiding) and 4.5 kcal/mol (COMPASS) of repulsive interactions on the (010) face when compared to its zwitterionic form. This corroborates with the proposed model

wherein the repulsive effects were reasoned due to delocalization of negative charge on the anion residue.

5.3.2. Stereospecific impurity interactions on the (010) step face

In the above modeling, the impurity (and glycine) molecules were docked stereospecifically on a flat (010) surface of an α-Glycine crystal. However, from previous experimental studies (Li and Rodríguez-Hornedo, 1992; Carter et al., 1994), it is known that glycine crystal growth proceeds through a "screw dislocation" mechanism, in which solute molecules incorporate into the crystal lattice more preferentially at the 'kink' site on a growing step. This mechanism could be energetically more favorable than adsorption of solute molecules on a flat surface (Davey and Garside, 2000; Nývlt et al., 1985). Furthermore, 'tailor-made' impurity molecules preferentially adsorb at a crystallographic site on the (010) step of an α-Glycine crystal (Torbeev et al., 2005). On the basis of these premises, subsequently, the slice energies were computed with the impurity molecules stereospecifically docked at a kink site on the (010) step (cf. Fig. 4-10a).

In sharp contrast to the impurity interactions on the (010) face, incorporation of Asp and Glu anions at a crystallographic kink site on the (010) step incurred no repulsive effects (cf. Table 5-5). The preferential adsorption of Asp anion at the (010) step was evident from more favorable (attractive) interaction energies gained, viz. 7.0 kcal/mol (Dreiding) and 7.3 kcal/mol (COMPASS) respectively, when compared to the zwitterions. Similarly, interaction of the Glu anion at the (010) step was preferred over the zwitterions by 4.5 kcal/mol (Dreiding) and 4.8 kcal/mol (COMPASS) of attractive intermolecular energies, respectively. Furthermore, analyzing the non-bonded

interactions, it became evident that Coulombic forces contributed significantly to the differentiation of impurity zwitterions versus anions at the crystal surfaces.

Table 5- 5 Slice energies (kcal/mol) of pure and impurity incorporated glycine layers

Molecule	(010) flat face			
	Force field type			
	Dreiding		COMPASS	
	E_{sl}	ΔE_{sl}[a]	E_{sl}	ΔE_{sl}
Glycine	–47.3	…	–50.0	…
Aspartic acid zwitterion	–54.5	–7.2	–59.3	–9.3
Aspartic acid anion	–49.5	–2.2	–55.2	–5.2
Glutamic acid zwitterion	–43.0	4.3	–56.1	–6.1
Glutamic acid anion	–39.0	8.3	–51.6	–1.6
(010) step face				
Glycine	–43.8	…	–43.4	…
Aspartic acid zwitterion	–54.6	–10.8	–54.6	–11.2
Aspartic acid anion	–61.6	–17.8	–61.9	–18.5
Glutamic acid zwitterion	–45.6	–1.8	–49.2	–5.8
Glutamic acid anion	–50.1	–6.3	–54.0	–10.6
(011) flat face				
Glycine	–37.2	…	–39.5	…
Aspartic acid zwitterion	–41.8	–4.6	–47.6	–8.1
Aspartic acid anion	–46.8	–9.6	–52.9	–13.4
Glutamic acid zwitterion	–32.2	5.0	–40.5	–1.0
Glutamic acid anion	–36.0	1.2	–45.0	–5.5

[a]Difference in slice energies of the impurity molecules compared with that of a glycine molecule.

The favorable interaction of the impurity anions at the (010) step can be reasoned as follows. The delocalization of negative charge on the residual carboxylate group of the Asp/ Glu anion can introduce attractive interactions with glycine molecules along the

(010) step ledge (viz. along the a-axis). In contrast, on a flat surface, the Asp and Glu anions incur repulsive Coulombic interactions with glycine molecules at an adjacent crystallographic site (viz. along the c-axis).

5.3.3. Stereospecific impurity interactions on the (011) surface

Continuing further, the impurity molecules were stereospecifically docked on a flat (011) surface and then its slice energies computed (cf. Table 5-5). The Asp and Glu anions gained ca. 5.0 kcal/mol and 4.0 kcal/mol of attractive interaction forces respectively, in excess of their zwitterionic species. In this case, the calculated values of differential slice energies were in agreement with the results obtained previously for impurity interactions at the (010) step layer.

5.3.4. Discussion

The atomistic potential energy calculations so far show preferential interaction of the Asp and Glu zwitterions on the (010) face, and of the impurity anions on the (011) surface. In these calculations, the Asp anion has incurred greater repulsive (on the (010) face) and attractive interactions (on the (010) step face and (011) surface), as compared to the Glu anion. Theoretically, this could be explained based on the pKa values of the residual –COOH groups of these acids (Lide, 2004), with a higher ionization constant for the Asp anion ($K_a = 2.2 \times 10^{-4}$) as compared to the Glu anion ($K_a = 5.6 \times 10^{-5}$). From a mechanistic viewpoint, the shorter side chain length of the Asp anion may lead to a conformation which results in greater interactions with the neighboring glycine molecules in the crystal lattice, as compared to the Glu anion (cf. section 4.6).

In all the above molecular models, the incorporation of impurity molecule on the crystal surface was achieved by substituting the side chain of glycine (the H atom) by the

specific residue of the impurity. Other alternatives could be leaving the NH_3^+ and CO_2^- moieties outside the surface and submerging the residue in the slice underneath. However, in that case, vacancy sites have to be created in order to accommodate the residual moiety without encountering short atom-atom contacts. Besides, because it known that the basic growth unit of α-Glycine is a centrosymmetric cyclic dimer (Gidalevitz et al., 1997) the topography of a growing surface will consist of glycine molecules with the unique H atoms oriented on the surface. Therefore, it is more likely that the impurity molecules dock with its specific residue protruding out of the surface. Besides, symmetry relations between the glycine molecules in the (010) crystal slice allow only for stereospecific impurity incorporation as modeled before.

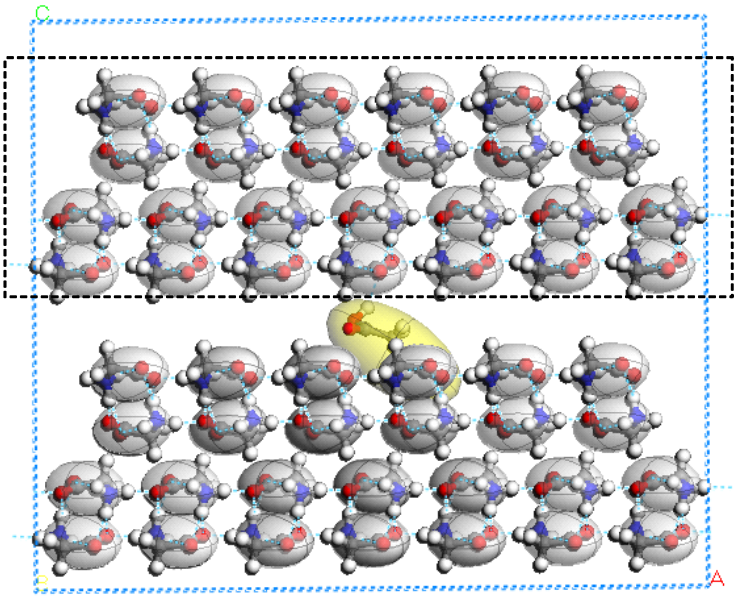

Figure 5- 6 Epitaxy of a (010) glycine layer (within the dashed rectangular box) built on the (010) surface of α-Glycine crystal. The substrate slice is docked with an aspartic acid zwitterion (encircled by yellow solid sphere).

To corroborate the results of the slice energy calculations with the experimental habit modification in α-Glycine crystals, subsequently, the "attachment" energies of a glycine layer approaching the impurity incorporated surfaces were determined. To this

end, an epitaxial glycine layer was constructed above the (*hkl*) crystal surface (using the "Layer Builder" in Materials Studio) (Fig. 5-6). The intermolecular interactions between the layers were calculated and reported in Table 5-6. The results obtained clearly indicated decrease in the attachment energies for an impurity incorporated crystal surface, reflecting upon the energy barrier for adsorption of oncoming solute molecules normal to the facet. However, this methodology is only a metaphor to quantify growth rates and may not reflect upon the actual physical processes involved during crystal growth. For instance, impurity molecules that are adsorbed on the (010) step face of α-Glycine crystal can provide a modified surface energy for the integration of solute molecules and prevent the progress of kink sites along the step. In the process, impurity molecules could get incorporated at the defect sites on a step and growth may still progress unless a "threshold" impurity concentration is reached (cf. chapter 7). Such detailed investigations would perhaps require a molecular dynamic simulation so as to account for surface reconstruction upon impurity adsorption (Fiebig et al., 2007). Nevertheless, as reported here, and in several other works (Clydesdale et al., 2005, Mutuka et al., 2005, Weissbuch et al., 2006), the calculation of a "modified" version of the attachment energy, which takes into consideration the "perturbing" effect of a tailor-made impurity, can help to infer the extent of growth inhibition.

Table 5- 6 Attachment energies (kcal/mol) of an oncoming pure glycine layer onto the impurity incorporated substrate glycine layer.

face	molecule on the substrate glycine layer		
	glycine	aspartic acid	glutamic acid
(010)	–7.0	13.0	18.7
(011)	–84.5	–50.0	–68.1

Continuing further, we explore other possible mechanisms by which interaction of the impurity species at the crystal surface could be influenced. From previous reports (Leunge and Rempe, 2005), it is known that glycine zwitterions in solution are associated with the formation of a hydration layer (comprising ca. 5 water molecules) around the COO^- group bonded to the α-carbon atom. Taking clue from this, it is likely that that the impurity anions are "hydrated" with water molecules bonded to the oxygen atoms of the side chain COO^- group. Consequently, the hydration layer can introduce "steric effects" upon incorporation of the impurity anion on the (010) surface of α-Glycine. To test this proposition, assuming a hydration shell radius of 2.5 Å (Leunge and Rempe, 2005), 5 water molecules were constructed around the side chain COO^- moiety of the Asp anion molecule. The geometry of the hydration structure was locally optimized so as to maximize its interactions with the oxygen atoms of the COO^- moiety through hydrogen bonding. Subsequently, the "hydrated" Asp anion molecule was docked onto the glycine crystal surface stereospecifically as modeled before. By visualization, it was apparent that the hydration shell can impose short atom contacts with the glycine molecules on a flat (010) face (Fig. 5-7a); in contrast, such steric effects were less probable when the hydrated anion molecule was docked either onto to a kink site on the (010) step or on the (011) face (Fig. 5-7b, c). This effect was also inferred from the calculated values of intermolecular interactions between the hydrated Asp anion molecule and of glycine molecules on the crystal surface. However, as these calculations involved static energy minimization restructuring of the hydration layer after incorporation of the anion molecule on the crystal surface was not accounted for.

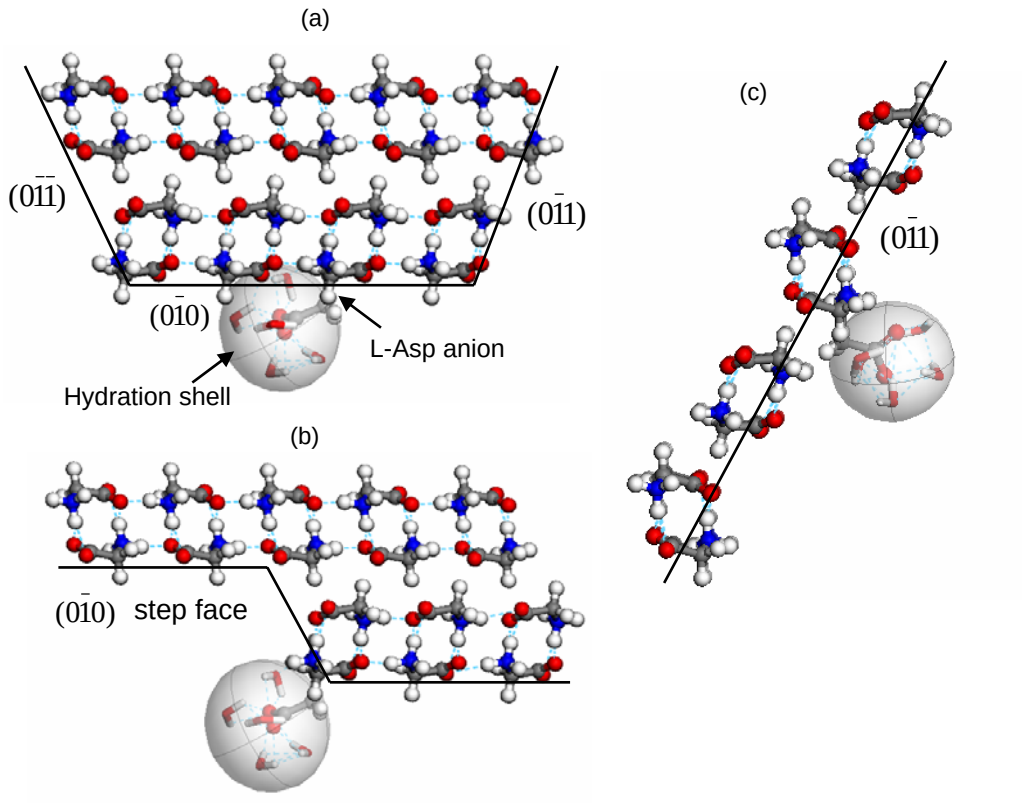

Figure 5- 7 Molecular modeling of the interaction of a hydrated aspartic acid anion molecule with the α-glycine crystal faces (edge-on-view along the a-axis): (a) $(0\bar{1}0)$ flat face; (b) $(0\bar{1}0)$ step face; (c) $(0\bar{1}1)$ flat face. The hydration shell formed around the side chain carboxylate group of the Asp anion prevents its docking on the $(0\bar{1}0)$ flat face, but has a lesser impact on the interactions with the $(0\bar{1}0)$ step face and the $(0\bar{1}1)$ face.

At this solution pH conditions, it is known that glycine cations coexist along with the impurity anions. Given this, it is possible for the impurity anions to form complex with the glycine cations. The interaction of the "impurity–solute" complex with the glycine crystal surface can be modeled in accordance with the stereoselectivity mechanism. Then, for a given conformation of the impurity–solute complex, it is likely that it can bind preferentially to a kink site on the (010) step face (Fig. 5-8) rather than on the (010) flat face. Subsequently, the "modified" portion of the impurity complex (viz. the glycine cation bonded to the side chain group of the anion through hydrogen bonding)

can introduce disorientation and prevent further attachment of solute molecules at the growing step interface. Future work will be directed toward understanding this mechanism in detail so as to explain the effect of solution speciation on crystal growth inhibition.

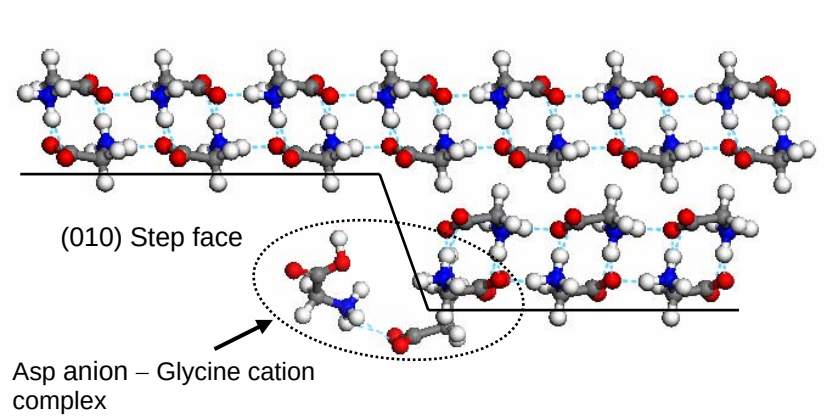

Figure 5- 8 Molecular modeling of the interaction of an "Aspartic acid anion–Glycine cation" complex with the α-glycine crystal at the (010) step face (edge-on-view along the a-axis).

5. 4. Assumptions and Limitations

The assumptions underlying the attachment energy (AE) method can some times lead to less accurate prediction of the crystal habit. Firstly, the AE method predicts the crystal habit based on the ad hoc assumption that the growth rate of F (flat) faces (according to the Periodic Bond Chain (PBC) networks) is directly proportional to the attachment energy (E_{att}). In this, it is assumed that crystal growth proceeds by a layer-by-layer mechanism. However, crystal growth from solutions commonly proceeds either through a 2D surface nucleation or spiral growth (BCF) mechanism (Winn and Doherty, 2000). Furthermore, depending on the supersaturation level, either the 2D surface nucleation via a birth and spread mechanism or the rough interface growth mechanism can be operating. In that case, the boundary condition to grow by a layer mechanism as a

flat face with an orientation (hkl) vanishes. Besides this, different growth mechanisms could be operating on different (hkl) faces (Bennama, 1995).

Secondly, the effects of solvent interactions were not quantitatively considered in the AE method. On account of this, while the growth morphology agrees well with the sublimation grown crystal, it distinctly differs from the solution grown crystal. Recent works (Liu et al., 1995; Bisker-Leib and Doherty, 2001, 2003; Hammond et al, 2007) have, therefore, developed methods to account for the solute-solvent interactions at the crystal-fluid interface along with the growth mechanisms, while predicting the growth morphology of solution grown crystals.

On investigating the interaction of impurities at the crystal surfaces the hydration effect of impurity ions were not quantitatively treated. In principle, the solvation effect would dampen the electrostatic interactions as computed from the Coulomb's law equation using the permittivity of free space. The effect of hydration of ions on the intermolecular interactions can be accounted either through explicit solvent models or implicit dielectric models. For example, from distance-dependent dielectric models, it is suggested that the effective dielectric constant can deviate from the vacuum value by a factor of 3–5 (Leach, 2001). Nevertheless, considering the fact that in the proposed molecular models the O···O contact distances between the residual (carboxylate) group of the impurity anion molecule and of a glycine molecule on the crystal lattice is much smaller (ca.2.0 Å and 3.5 Å for aspartic and glutamic acid molecules respectively, cf. Fig. 4.9b and 4.10b), therefore, the repulsive (or attractive) effects operating at the crystal interfaces could be expected to be significantly stronger even in a solution environment.

5. 5. Summary

The growth morphology of α-Glycine was predicted using the BFDH and the attachment energy methods. The attachment energy method, using various force field potentials, predicted the growth morphologies in better agreement with the experimental habit. However, there was distinct differences between the predicted and solution grown crystal habit indicating the need for more accurate models which will consider the solute-solvent interaction at the crystal interfaces.

Furthermore, our molecular modeling calculations show that habit modification of α-glycine crystal observed in the experiments can be explained by preferential adsorption of impurity species on the crystal surfaces. Simulation results indicate that the impurity anions incur repulsive electrostatic effects on incorporation on the flat (010) surface and, in contrast, gain attractive Coulombic interactions on adsorption at either the kink site on the (010) step, or on the flat (011) surface. The impurity zwitterions, on the other hand, experience favorable interactions on the flat (010) face. This is correlated with the subsequent growth inhibition along the *c*-axis and *b*-axis of α-glycine by the anion and zwitterion impurity species, respectively.

CHAPTER 6

Effects of Impurities on Polymorphism in Glycine

Based upon experimental observations on the habit modification in α-glycine crystals (cf. chapter 4), it is predicted that certain amino acid impurities can operate as stereospecific nucleation inhibitors and in doing so impact crystallization of glycine polymorphs. In line with this prediction, the thermodynamically stable γ-glycine is nucleated, in preference to the metastable α-form, from aqueous solutions containing trace amounts of these impurities. The strategy employed in selecting the impurities and the mechanism by which the polymorphic modification is effected is described in this chapter.

6.1. Impurity Selection Strategy

6.1.1. Stereoselective nucleation inhibition mechanism

Glycine, the simplest of the amino acids, exhibits polymorphism with three known crystal structures – α, β and γ (cf. chapter 3). The metastable α–form is preferentially crystallized from pure aqueous supersaturated solution. This is a kinetically favored process because in supersaturated solution glycine molecules primarily exist as zwitterionic cyclic dimers (Lo and Myerson, 1989; Gidalevitz et al., 1997), which form the growth synthons of the α-glycine crystal structure.

In previous studies a kinetically controlled crystallization process has been utilized to obtain the glycine polymorphs in the presence of "tailor-made" additives or impurities (Weissbuch et al., 1994; Towler et al., 2004; Torbeev et al., 2005). The proposed mechanism was built on a working hypothesis that crystalline nuclei, whose

structures and morphologies resemble those of the various mature polymorphs, exist amongst the clusters that are formed in the supersaturated solution. Consequently, impurity molecules were designed to selectively target the nuclei of the metastable α–form and prevent their growth into crystals. Under such conditions, the stable γ–form can then crystallize from the solution, provided the impurity molecules do not interfere with its growth. To demonstrate this proposition, a tailor-made additive – racemic hexaflurovaline was selected, which, at lower concentrations (1–2 wt % on glycine), preferentially adsorbed on the {011} faces of α-glycine crystal and subsequently inhibited its fast growth along the *c*-axis. This was evident from the modification in α-glycine crystal habit with affected step-like {011} side faces. At the higher additive concentration levels (3 wt %), the γ–glycine was crystallized, an outcome of suppression of nucleation of the α-form. From the morphology of γ-glycine crystals obtained it was inferred that the additive molecule has retarted its growth at only one pole of the polar crystal, thus leaving the crystal free to grow at the opposite pole (Weissbuch et al., 1994).

On the other hand, impurities (e.g. naturally occurring α-amino acids such as DL-Alanine, DL-Valine and DL-Lysine etc.), which inhibited growth along the b-axis of α–glycine crystal were not influential to subdue its nucleation. The reason was, presumably, those impurity molecules prevented the stacking of glycine dimers along the b-axis, and did not disrupt the hydrogen bonding within the glycine dimers bonded along the c-axis. Consequently, the presence of increased concentrations of racemic additives produced thinner and thinner plates but always only the α-form (Weissbuch et al., 1994).

Recently, this kinetically controlled nucleation mechanism was utilized to obtain the β- and γ-polymorphs of glycine from aqueous solutions in the presence of α-amino

acids (e.g. DL-phenylalanine, DL-methionine and DL-tryptophan) operating as stereospecifc nucleation inhibitors. These additive molecules bear "bulky" side chain moieties which imparted the property of an efficient growth inhibitor to the imposter molecule. Because different polymorphs of the trimorphic glycine crystals are delineated by faces of different surface textures, the additive molecules adsorb selectively onto the growing crystal nuclei, and thus prevent the transformation of these nuclei into crystals. This was further corroborated by the stereoselective habit modification and occlusion of additives in the polymorphic crystals obtained in the presence of these auxiliary molecules (Torbeev et al., 2005).

6.1.2. Self-poisoning mechanism

Glycine crystallizes as the metastable α–form from aqueous solutions at the isoelectric point (pI 5.97), while the stable γ–form only nucleates at high and low pH (viz. pH< 3.8 and pH>8.9). Rationalizing this effect, Towler et al. (2004) have proposed a molecular "self-poisoning" mechanism. It is based upon the known solution speciation data of glycine, along with the relative growth kinetics of the glycine dimorphs and molecular packing arrangements within their crystal structures. At and around the isoelectric point, glycine exists in solution predominantly as dimerized centrosymmetric pairs of zwitterions, which is preserved in the α–glycine crystal structure. However, there is a small change in the species distribution in glycine solution at the pH conditions where the polymorphic switch is observed – viz. 0.03 mol fraction of cationic (at pH 3.8) and 0.12 mol fraction (at pH 8.9) of anionic glycine. On investigating the effect of molecular speciation on crystal polymorphism, it seems unlikely that such a small fraction of charged glycine species could either "disrupt" the nucleation of the α–form or

"induce" the nucleation of the γ–form. Alternatively, the potential for the charged species to inhibit the growth of the metastable α polymorph en route to its crystallization is more likely given the following arguments.

The fast growing {011} faces of α-glycine expose both protonated amine and carboxylate functionality at this surface and their fast growth is driven by the strong coulombic interactions within the (010) layer. When either cationic or anionic glycine species are present in solution they may join the surface and in doing so modify the charged nature of the interface preventing the further addition of zwitterions. These ions would thus act as selective 'tailor-made' additives to inhibit the crystallization of α-glycine. However, crystallization of the γ-polymorph cannot be completely inhibited by these charged species since, its major growth (*c*) axis accepts NH_3^+ functionality at its faster growing (carboxylate rich) end and COO^- functionality at its slow growing (amino rich) end. Thus, crystal development along the fast growing –*c* direction will be inhibited at low pH and the slow growing +*c* direction at high pH, which was indeed observed in the experimental crystal morphologies.

The above hypothesis was furthermore strengthened by crystallizing the γ polymorph in the presence of tailor-made growth inhibitors – malonic acid and ethylenediamine, which were chosen to mimic the charged cationic and anionic glycine species.

Nevertheless, in the original work, the author was unsuccessful to observe habit modification in α-glycine crystals in the transitional pH range (viz. pH 6.0 to 4.0). To this end, in this study, some additional crystallization experiments (cf. chapter 3) were performed with pure glycine solution at pH 6.2 (the control sample) and pHs 4.5, 4.0 and

3.6 respectively (adjusting the pH using HCl). At pH 4.5, the harvested α-glycine crystals were more isometric with dominant {011} faces when compared with the control sample (Fig. 6-1a). At pH 4.0 and 3.6 respectively, the crystal habit became thinner and thinner along the fastest growing c-axis resulting in {011} plates. These observations were consistent with the proposed self-poisoning mechanism. Here, it is noted that the observed changes in α-glycine crystals are not due to the effect of chloride ions. In this context, previous studies (Towler et al., 2004) using salts (NaCl, Na_2SO_4, and Na2CO3) has shown that whilst Na^+ (anion) has specific interactions with the carboxylate group of the glycine zwitterions which are exposed on all four fast growing {011} faces of α-glycine, the cations (Cl^-, SO_4^{2-}, CO_3^{2-}) do not exhibit significant effects. This could be due to differences in the hydration of these ionic species in solution phase, and its subsequent impact on interactions with the crystal surface.

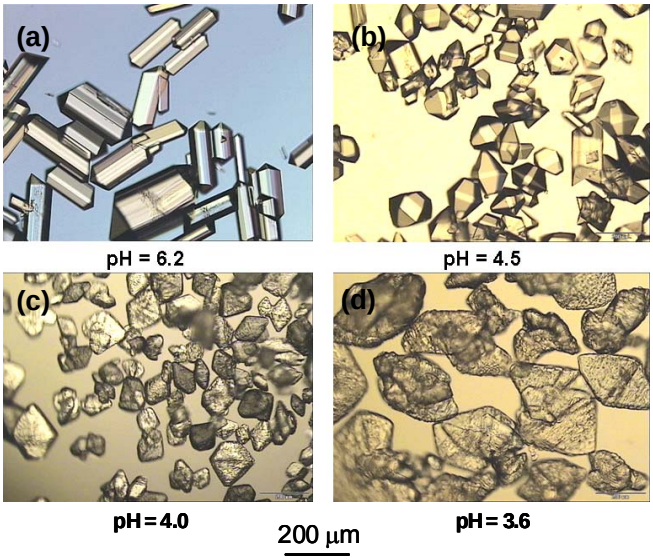

Figure 6- 1 Habit modification in α–glycine crystallized from aqueous solutions at different pH.

6.1.3. Linking solution chemistry to crystal nucleation

The impurities – aspartic (Asp) and glutamic (Glu) acids when doped into glycine solution undergo speciation to form charged molecular species (cf. section 4.4). Given this information, building on the aforementioned nucleation inhibition mechanisms, it is envisaged that Asp and Glu acids can operate as stereospecific nucleation inhibitors. The rationale is explained on the basis of possible interactions of various molecular species present in the solution – viz. Asp zwitterions, Asp anions, and glycine (Gly) cations, with the growing crystal nuclei. Firstly, in accordance with the stereoselectivity mechanism, the Asp zwitterions should interact with the {010} faces of α-glycine, and the Asp anions with the {011} faces (cf. chapter 4). Secondly, according to the self poisoning mechanism, glycine cations should also interact with the {011} faces of α-glycine (Towler et al., 2004). If these predicted interactions were to hold true, then it can be expected that the impurities can selectively inhibit the development of the α-form. Under these solution conditions, the supersaturated glycine solution is likely to equilibrate through induced precipitation of the stable γ-form.

6.2. Nucleation of Glycine Polymorphs

As predicted, from solutions doped with L-Asp acid as the impurity (4.0 wt % on glycine), the γ-polymorph nucleated and grew as a bunch of crystals with a polar morphology (Fig. 6-2a). In comparison, crystallization of pure glycine solutions always produced the α polymorph. As reported previously (Weissbuch et al., 1994), it was observed that the NH_3^+ rich {103} facets of γ-glycine were pointing towards the centre, and the COO^- rich $(00\bar{1})$ face was growing away from the centre. This is an interesting observation given the fact that like charges is in close contact while it is usually expected

that the pointed ends would repel. It is, however, not clear at this stage, and needs further understanding of intermolecular interactions occurring during the nucleation stage.

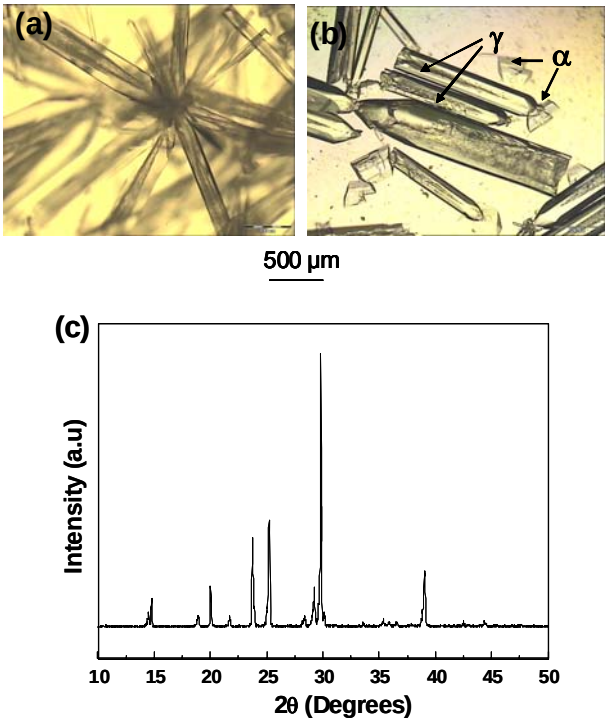

Figure 6- 2 Glycine polymorphs crystallized from aqueous solution doped with 4 wt% of L-Asp: (a) γ-glycine; (b) mixture of α- and γ-glycine; (c) PXRD pattern of a mixture of α- and γ-polymorphs. α-glycine has characteristic peaks at 2θ values 15, 19, 24, 29.8° respectively. γ-glycine peaks correspond to 2θ values 14.5, 22, 25, 29.2° respectively.

Under similar experimental conditions (impurity concentration, temperature, supersaturation), it was also observed that a mixture of both polymorphs nucleated and grew concomitantly from a duplicate crystallization batch (Fig. 6-2b). The polymorphs could be distinguished from their characteristic crystal habits. γ-glycine was pencil-shaped trigonal crystals with the $(00\bar{1})$ face clearly the fastest growing, resulting in a crystal habit elongated along the c-axis. On the other hand, α-glycine crystallized with a typical prismatic pyramidal crystal habit. The polymorphic forms were further confirmed from their PXRD patterns (Fig. 6-2c).

Table 6- 1 Summary of the Glycine polymorphs nucleated from aqueous solution doped with various impurities.

Impurity	Impurity concentration (wt%, w/w glycine)	Supersaturation $\sigma = \ln (C/ C_s)$	Polymorph type Batch 1	Batch 2	Batch 3
	1–4	0.1	α + γ	α + γ	…
L-Asp	1	0.3	α	γ	α + γ
	2	0.3	α + γ	α + γ	α + γ
	3	0.3	α + γ	γ	α
	4	0.3	γ	γ	α + γ
	1	0.6	α + γ	α	γ
	2	0.6	α + γ	α + γ	γ
	3	0.6	γ	α + γ	γ
	4	0.6	γ	γ	γ
L-Glu	1	0.3	α	α	α + γ
	2	0.3	α	α	α
	3	0.3	α + γ	α	α + γ
	4	0.3	α + γ	α	α + γ
	1	0.6	α + γ	α	α
	2	0.6	α + γ	γ	α + γ
	3	0.6	α + γ	γ	γ
	4	0.6	α + γ	γ	α + γ
D-Asp	2	0.3	γ	γ	α + γ
	4	0.3	α + γ	α + γ	γ
	2	0.6	α + γ	γ	γ
	4	0.6	α + γ	α + γ	γ
D-Glu	2	0.3	α	γ	α + γ
	4	0.3	γ	γ	α
	2	0.6	γ	α + γ	α + γ
	4	0.6	γ	α + γ	γ
DL-Asp	2	0.3	α + γ	α + γ	γ
	4	0.3	γ	γ	α
	2	0.6	γ	α + γ	α + γ
	4	0.6	γ	γ	α + γ
DL-Glu	2	0.3	γ	α + γ	α
	4	0.3	γ	α + γ	α + γ
	2	0.6	γ	γ	α + γ
	4	0.6	α + γ	γ	α + γ

Subsequently, additional crystallization experiments were carried out by doping glycine solutions with both chirally resolved and racemic impurities (viz. L-, D- and DL-Asp and Glu) at different concentration levels. All the solutions were prepared at elevated temperatures and naturally cooled down to room temperature (~ 25 °C) resulting in two different supersaturation levels (viz. $\sigma = 0.3$ and 0.6) at the crystallization temperature. In these experiments, whilst a few batches produced either the α- or γ-polymorph exclusively, a mixture of both forms were nucleated in general (Table 6-1).

Here, it should be mentioned that in these experiments crystals were observed to nucleate and grow both from bulk solutions as well as from bottom of the crystallizing dish. Hence, the batch-to-batch variation in the appearance of glycine polymorphs could be only due to the action of impurities on the relative nucleation and growth kinetics of the individual polymorphs (discussed in section 6.3.2). Other factors such as the surface or wall effects of the crystallizing dish (concerning heterogeneous nucleation) or the effect of air–solution interface (concerning induced nucleation due to hydrophobic/ hydrophilic effects) seems less influential, from both our experimental observations as well as previous work (Weissbuch et al. 1983).

6.3. Rationalizing the Form Modification

Having observed nucleation and growth of the γ-glycine in the presence of aspartic and glutamic acids as impurities, their possible role in the polymorphic modification is considered. To this end, the nucleation inhibition mechanisms are corroborated with experimental observations on morphological changes in the glycine polymorphs nucleated, and by molecular modeling of the interactions between the charged molecular species and the developing crystal nuclei. In addition, results of

metastable zone width measurements of pure and impurity doped glycine solutions are provided in support of the proposed mechanism.

6.3.1. Impurity interactions and morphology changes

The primary evidence for the effect of impurities on the growth of the metastable polymorph was gleaned from morphological changes in α-glycine crystals. In the presence of 0.5 wt % of L-Asp, the crystal habit of α-glycine obtained was apparently isometric with dominant {011} faces (Fig. 6-3a), indicating that the impurity inhibited growth along the fastest growing c-axis. This can be clearly distinguished from the α-glycine crystal habit obtained from pure glycine solution (cf. Fig. 6-1a). The changes in the growth morphology is also similar to the one observed previously with a pH change (cf. Fig. 6-1b).

The habit modification was explained earlier on the basis of stereospecific interaction of L-Asp anions with the {011} faces of α-glycine (cf. chapter 4). Summarizing and restating, the L-Asp anions can either adsorb on the $(0\bar{1}0)$ face or the {011} faces along the *–b* enantiomorphous part of the α-glycine crystal structure (Fig. 6-4a). However, on interaction with the $(0\bar{1}0)$ face L-Asp anion is likely to experience O···O electronic repulsive effects between the side chain carboxylate moiety and a glycine molecule at the adjacent site. Alternatively, the anions can selectively interact with the {011} faces in the absence of any such repulsive effects, and in doing so prevent the further addition of glycine zwitterionic dimers (growth unit) on the crystal surface.

Nevertheless, with the type of interactions described above, chirally resolved impurities (viz., L- or D-Asp) can inhibit growth only along either of the enantiomorphous parts of the centrosymmetric α-glycine. This implies that an L-Asp

anion can only adsorb on the $(0\bar{1}1)$ and $(0\bar{1}\bar{1})$ faces, and the D-Asp anion on the (011) and $(01\bar{1})$ faces (cf. Fig. 6-4a). However, as dictated by the crystal symmetry of α-glycine, growth inhibition should occur along all the four symmetry-related {011} facets in order to subdue its nucleation. This aspect of stereochemical control of crystal nucleation, however, can be explained by invoking the self poisoning mechanism (Towler et al. 2004). According to this, glycine cations, which are formed along with the L-Asp anions on doping aspartic acid into glycine solution (cf. section 4.4), may interact with the {011} faces of α-glycine, and consequently, inhibit the development of the α-form. This postulate is indeed justified given that only α-glycine could be crystallized from glycine solutions doped with L-Aspartic acid, but pH adjusted (~ pH 6.0, i.e. near to the pI of glycine), and hence, with practically no glycine cations present.

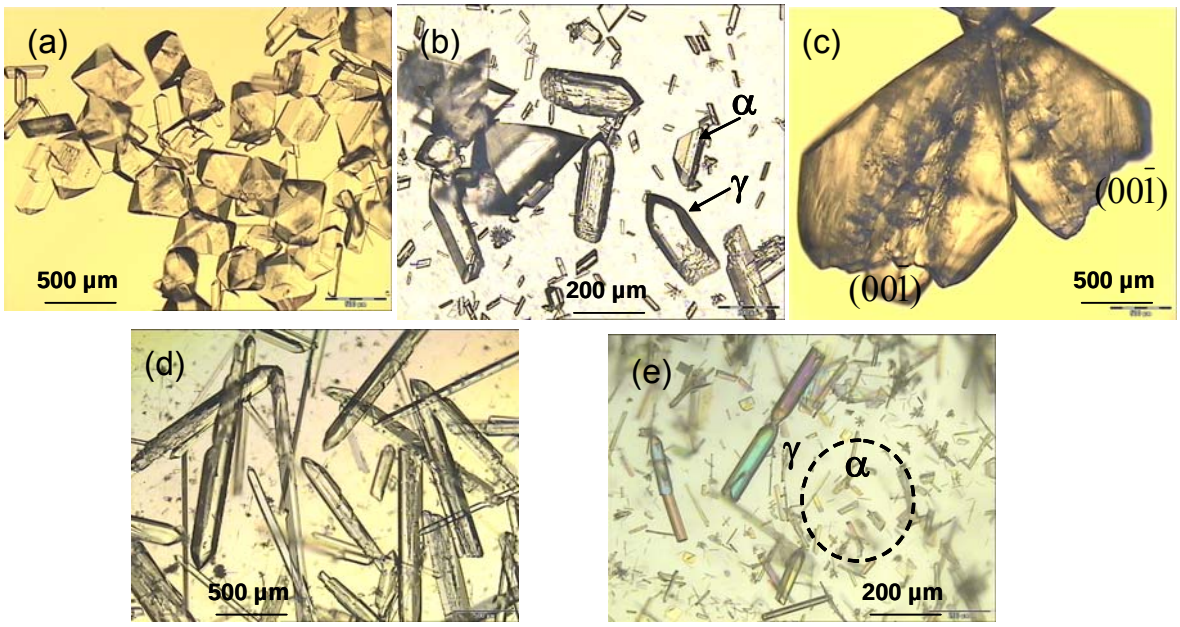

Figure 6- 3 Nucleation of glycine polymorphs from aqueous solution doped with impurities: (a) 0. 5 wt% of L-Asp (α-glycine); (b) 2.0 wt % of L-Glu (α- + γ-glycine); (c) 4.0 wt % of D-Glu (γ-glycine); (d) 6.0 wt% of L-Asp (γ-glycine); (e) 4.0 wt% of L-Asp (α- + γ-glycine).

Following the above analysis, the effect of charged molecular species on the nucleation and growth of the γ-polymorph is considered. The possibility that L-Asp anions and/ or glycine cations either inducing the nucleation of γ-glycine or stabilizing the γ-glycine nuclei seems unlikely from the previous studies (Towler et al. 2004). However, their effect on the growth of γ-glycine was apparent from the changes in crystal habit. Firstly, γ-glycine crystallized in the presence of the impurity exhibited well developed capped faces at the head end of the polar morphology (Fig. 6-2b, 6-3b). From the molecular packing arrangement of the γ-glycine crystal structure (Fig. 6-4b), this can be envisaged as resulting from interactions between the L-Asp anions and glycine molecules at the NH_3^+ rich, head end, and consequently, causing growth inhibition along the +*c* direction. Secondly, γ-glycine also grew as elongated pencil-shaped crystals given the fact that the COO^- rich, $(00\bar{1})$ face is the fastest growing (Lahav and Leiserowitz, 2001). In addition, the morphology became needle-like at higher concentrations of L-Asp impurity (Fig. 6-3d), consistent with the stereospecific interactions of the impurity along the {hk0} side faces of γ-glycine (Weissbuch et al. 1994).

Finally, the impact of glycine cations on the growth morphology of γ-glycine is considered. In principle, glycine cations are likely to interact with the COO^- rich, $(00\bar{1})$ face of γ-glycine, and thereby cause growth inhibition along the –*c* axis as reported previously (Towler et al., 2004). However, this effect was observed only in a few crystallization experiments in which the γ-glycine crystals were shortened along the tail end (cf. Fig. 6-3b, c). This may be justified since the concentration of glycine cations (ca. 0.02 mole fraction at 4 wt % of L-Asp) could be significantly lower to manifest habit

modification along the fastest growing $-c$ direction of γ-glycine. Overall, these observations show that while the impurity (L-Asp) is effective in suppressing the nucleation and growth of the α-form, the nucleation and growth of γ-glycine may not be totally affected.

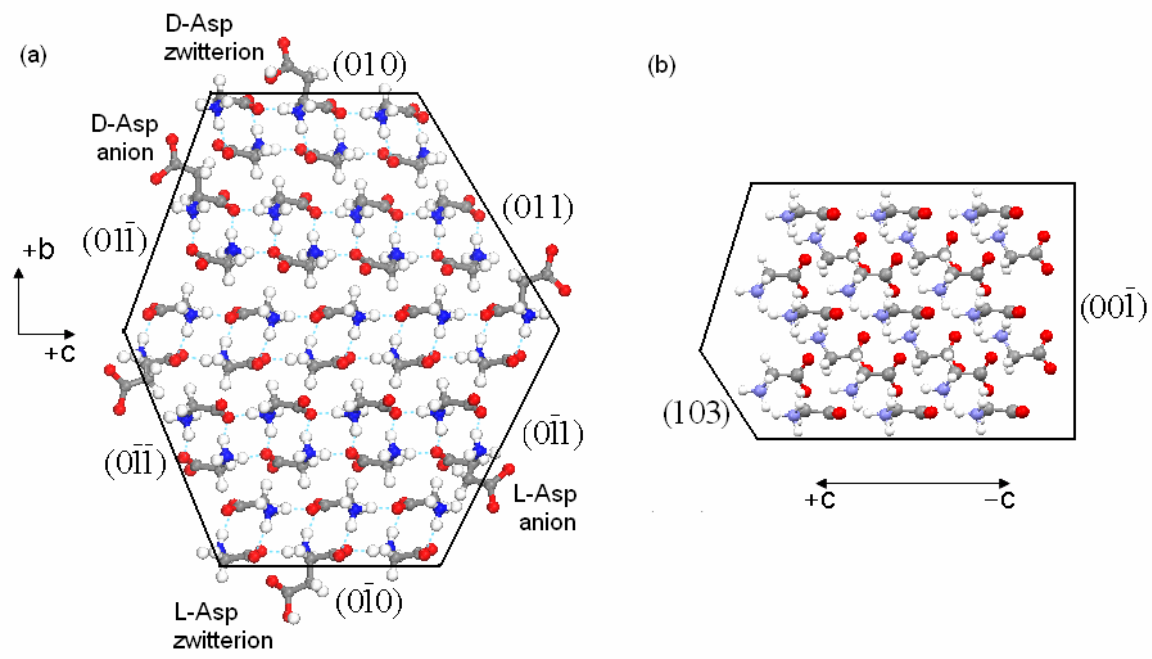

Figure 6- 4 (a) Stereoselective interaction of aspartic acid (Asp) anion with the crystal faces of α-glycine; (b) molecular packing arrangement in γ-glycine showing the polar crystal axis and the fastest growing $(00\bar{1})$ face (molecular modeling done in Materials Studio).

Note that the above arguments hold equally true to explain the nucleation and growth of the γ-polymorph of glycine in the presence of like impurities – D-Asp, DL-Asp, and L-, D-, DL-Glu (cf. Table 6-1). However, it was observed that γ-glycine crystallized more readily from solutions doped with aspartic acid than with glutamic acid. One possible reason could be the extent to which these two amino acids can retard the development of the α-form. In this context, it was earlier observed that growth inhibition along the {011} faces of α-glycine was more dominant in the presence of aspartic acid

than with glutamic acid (cf. chapter 4). The difference in impurity action was ascribed to the preferential interaction of aspartic acid anions with the {011} faces of α-glycine as compared to that of glutamic acid anions.

Further, in order to validate the proposed growth inhibition mechanism, additional crystallization experiments were carried out with α-amino acids such as DL-Alanine and DL-Lysine doped into glycine solution at different concentration levels. Only the α-polymorph of glycine was obtained as plate like crystals, which is consistent with the interaction of these impurities with the {010} faces and resulting in growth inhibition along the *b*-axis of α-glycine.

6.3.2. Some conflicting observations

Even as the above elucidation, by and large, conform to the growth inhibition mechanism, some experimental observations conflicted with the proposed theory. Firstly, nucleation of the γ-polymorph of glycine was not consistent in the experiments carried out. In several batches, whilst the γ- form crystallized from glycine solutions doped with the impurities at a lower concentration (i.e.1.0 wt %), the α-form also nucleated from solutions containing the impurities at a higher concentration (i.e. 4.0 wt %). This is in conflict with the 'growth inhibition' mechanism because nucleation of the α-form should be suppressed effectively at the higher impurity concentrations. The batch-to-batch inconsistency, however, can be attributed to the probabilistic nature of the nucleation process, and to the relative nucleation and growth kinetics of the two polymorphs. As the kinetically favored form, nucleation of α-glycine is facile from aqueous solutions. Given this, crystallization of the α-form could be induced by several other factors, notwithstanding the competitive effect of impurities. For example, heterogeneous

primary nucleation of the metastable form can be induced by the presence of any dust particle or adventitious impurity in the crystallizing solution (Mullin, 2001). Besides, interactions between the charged molecular species and the developing α-glycine crystal nuclei is also significant in determining the structural outcome. If, for example, the action of anionic impurity species were dominant to retard growth along the fastest growing c-axis of α-glycine, it can effectively lead to nucleation inhibition of the metastable form. On the other hand, if the action of zwitterions were dominant, growth inhibition will be along the b-axis of α- glycine, and thus possibly ineffective to suppress its nucleation.

The second observation conflicting with the proposed theory was with respect to the supersaturation effect. With the impurities doped in the glycine solutions, it appeared that a higher solution supersaturation (i.e. $\sigma = 0.6$) favored preferential nucleation of γ-glycine as compared to the solutions at lower supersaturations (i.e. $\sigma = 0.1$ and 0.3) from which, concomitant nucleation of the α- and γ-polymorphs occurred more often (cf. Table 6-1). The influence of supersaturation on the polymorph selectivity may indicate the role of additional factors such as solubility and/ or interfacial tension on the nucleation behavior. Nevertheless, some counter arguments could be made. First, there was no effect of the impurities observed on the equilibrium solubility of glycine (cf. chapter 3). Second, induction times for concomitant nucleation of the glycine polymorphs from the impure solutions was much longer at the lower supersaturations (typically, 1–3 weeks). In contrast, γ-glycine preferentially nucleated from solutions at the higher supersaturation, typically, in a few minutes or hours of induction times. This may indicate that a higher supersaturation has favored the faster growth kinetics of the γ-glycine. In contrast, if supersaturation had influenced the nucleation event, the metastable α-form

should have been favored in accordance with the Ostwald's rule of stages (He et al., 2006). Concurring with these arguments, earlier works have in fact shown that the interplay between nucleation and growth kinetics determine the structural outcome of a crystallization process (Cardew and Davey, 1982; Davey et al., 1997; Weissbuch et al., 1994).

6.3.3. Shifts in MZW – supporting nucleation inhibition

It is of common interest to characterize the operating region of a crystallization system in terms of the metastable zone widths (MZW). From the operational view of an industrial cooling crystallization, an optimal cooling profile designed to be just within the MZW prevents excessive crystal nucleation and growth, and therefore ensures narrow crystal size distribution. From previous studies, impurities are known to impact the nucleation kinetics by either acting as nucleation enhancers to decrease the MZW or as nucleation inhibitors to increase the MZW (cf. chapter 2). However, in general, the metastability of a system is reflected not only in nucleation kinetics alone, but also the growth kinetics. Furthermore, the detection limits on instruments used to observe small crystals also constrain precise delineation of the nucleation event from the subsequent crystal growth process.

In this work, experimental observations on MZWs of pure glycine solutions and that of solutions doped with different impurities provided a qualitative indication of the nucleation conditions. The impurities that were studied can be grouped into two categories, i.e. neutral L-amino acids (viz. Alanine, Valine, Leucine, Isoleucine and Phenylalanine) and acidic L-amino acids (viz. Aspartic and Glutamic acids). Initially, a ratio of MZWs (viz. MZW with impurity/ MZW of pure glycine) was defined for

identification of impurities as nucleation enhancers (for MZW ratio < 1) or inhibitors (for MZW ratio > 1). The average MZW for pure glycine was measured 12.0 ± 1.0 °C. In Fig. 6-5, this was normalized on the MZW ratio scale as 1.0 ± 0.1. In terms of solution supersaturation (σ), this value corresponds to 0.246 ± 0.03. With neutral impurities, statistically significant deviations in MZW could not be observed and no clear effect on the nucleation kinetics could be discerned. However, with acidic impurities, the MZW increased proportionately with the impurity concentration resulting in ca. 49.0 % and 39.0 % increase at 4 wt % (on glycine) of L-Asp and L-Glu respectively (Fig. 6-5). The corresponding values of supersaturation for nucleation of glycine crystals was calculated to be 0.375 ± 0.02 and 0.349 ± 0.03 respectively. From these results, we could infer that the presence of acidic impurities has imposed an additional supersaturation barrier to nucleation of the kinetically preferred α polymorph, and thus exhibited a nucleation inhibition tendency.

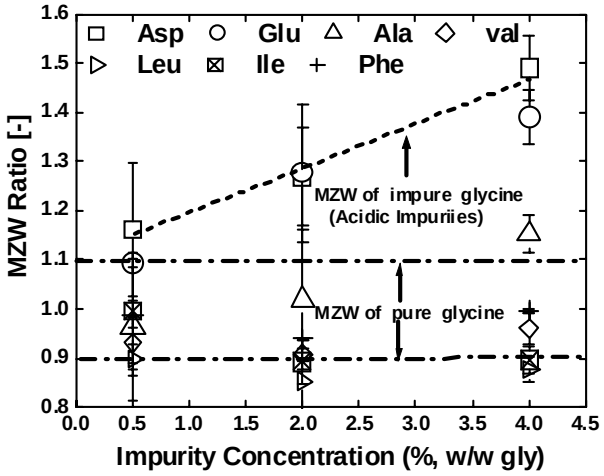

Figure 6- 5 Effect of impurities (L-amino acids) on the Metastable Zone width (MZW) of glycine. MZW ratio is defined as MZW with impurity/ MZW of pure glycine. Pure glycine has a normalized MZW ratio of 1 ± 0.1. The increase in the MZW ratio of glycine solution with acidic impurities (Asp and Glu) is shown by the dashed line. The y-axis error bars indicate standard deviation in the MZW measurements.

Under the above experimental conditions only the α-glycine was crystallized, however, with the habit modified. In contrast, batch crystallization experiments carried out in the presence of aspartic and glutamic acids at the same impurity concentrations have yielded either pure α- and γ-forms, or a mixture of both polymorphs (cf. Table 6-1). The difference in the experimental conditions is that solutions were stirred in the MZW experiments as opposed to unstirred in the crystallization dishes. One possibility for the preferential nucleation of the metastable polymorph in the latter experiments could be unintentional seeding of α-glycine crystals that could induce spontaneous secondary nucleation. Other reason could be heterogeneous primary nucleation of the α-form on the impeller surface. In the interest of verifying the results, additional batch experiments were performed. This time, saturated glycine solution (C_s = 0.33 g of glycine/ g of water at 40 °C (Mullin, 2001)) was prepared at elevated temperatures (50 °C), filtered through 0.2 μm filter, and was fed in a clean (sonicated in an ultrasonic bath) 50 ml jacketed glass crystallizer. After equilibrating the solution at the saturation temperature for 30 min, it was cooled at a rate of 0.5 °C/ min to 10 °C. A clean, Teflon coated magnetic stirrer bar was used to continuously agitate the solution. From these batch experiments, crystals of a mixture of α- and γ-glycine were obtained (Fig. 6-3e).

6.4. Summary

In this chapter, a systematic approach has been proposed based on the principles of stereochemical nucleation control and self-poisoning mechanisms to select amino acid impurities that can affect polymorph formation of glycine crystals. Accordingly, aspartic and glutamic acids that inhibit the development of α-glycine crystals along the fastest growing *c*-axis is predicted to suppress nucleation of the metastable form at the higher

impurity concentrations. Supporting this, metastable zone widths of glycine solutions doped with these impurities indicated an additional supersaturation barrier imposed for nucleation of the metastable α-form. Under these conditions, the crystallizing solution desupersaturates to yield the thermodynamically stable γ-glycine. As a result of this observation, a direct link between solution speciation of the impurities controlled by pH, and the nucleation of crystal polymorphs has been found.

CHAPTER 7

In situ Investigations using Atomic Force Microscopy

In chapter 4, habit modification in α-glycine crystals by added amino acid impurities were explained on the basis of stereospecific interactions of the impurities with the (010) face. In this chapter, atomic force microscopy (AFM) is used toward understanding the physical processes involved in crystal growth inhibition by the impurities. The growth behavior in pure aqueous solution and in the presence of a racemic impurity (D- + L-phenylalanine) is studied by monitoring in situ the nanoscale growth features on the (010) face. The effects of supersaturation and impurity concentration on the molecular step motion are investigated.

7.1. In situ imaging in pure glycine solution

In Fig. 7-1 are shown representative images obtained on scanning the (010) surface of α-glycine crystal in pure aqueous glycine solution. A supersaturation of 0.118 ($\sigma = \ln (C/ C_s)$) was achieved by cooling saturated glycine solution (3.6 M) to room temperature (~23 ºC) (small temperature changes due to possible heating of the electronic system during scanning are neglected). The (010) surface topology shows straight and long [001] step ledges that are parallel to the vertical scan axis (Fig. 7-1a). As reported previously (Carter et al., 1994), these step ledges are oriented along the direction of strong intermolecular (hydrogen) bonding energies in the α-glycine crystal structure. The (010) steps and terraces (Fig. 7-1d) clearly demonstrate the spiral dislocation growth mechanism in α-glycine (Li and Rodríguez-Hornedo, 1992).

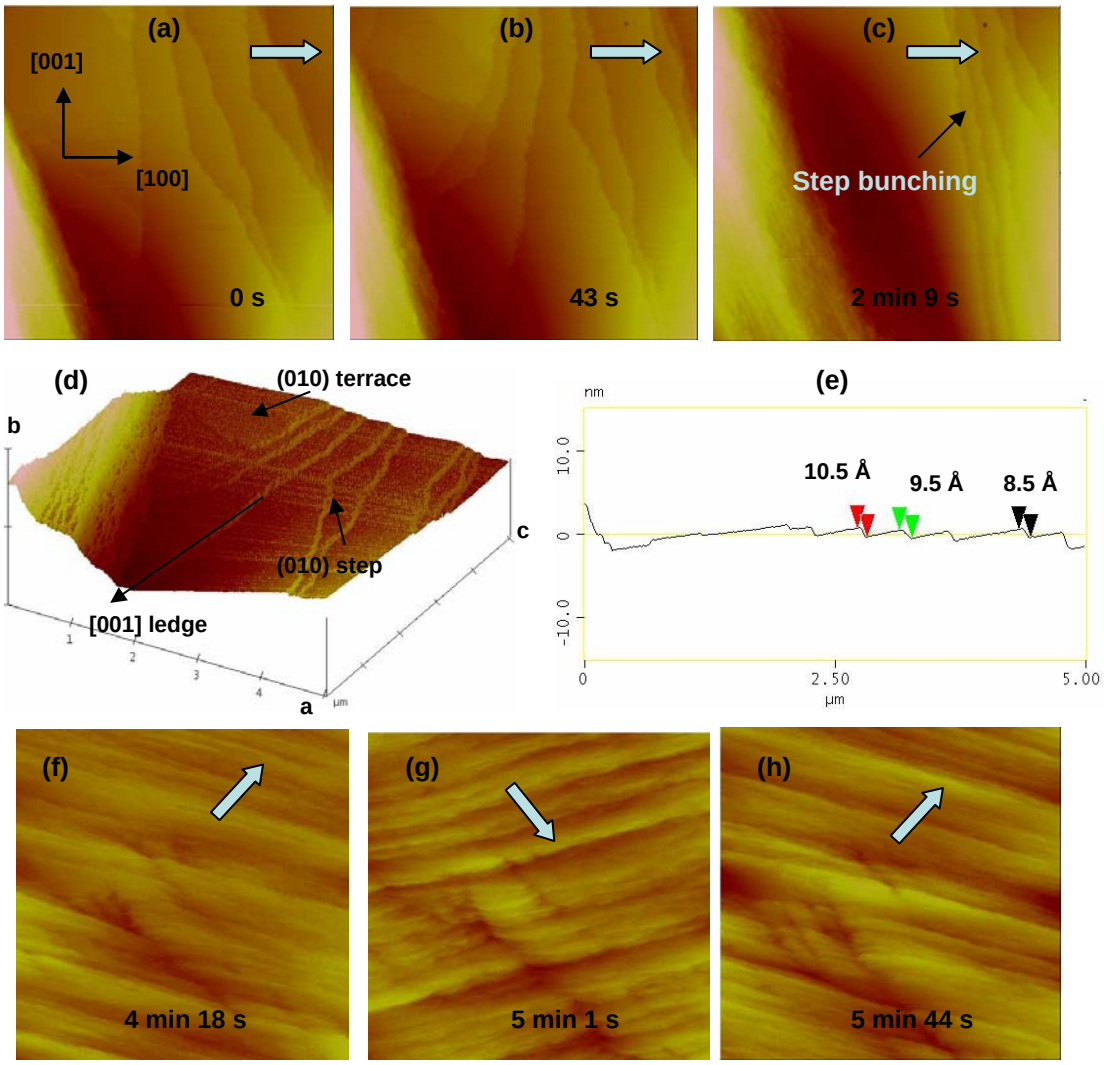

Figure 7- 1 AFM images (5 µm X 5 µm) showing growth on the (010) surface of an α-glycine crystal in aqueous solution: (a)–(c) and (f)–(h) show the advancement of molecular steps with time (along the direction indicated by the block arrows); (d) 3D representation (of image (a)) showing the topographic growth features assigned according to the Kossel model; (e) sectional analysis (of image (a)) showing the heights of molecular steps.

The (010) step planes advanced laterally in the direction of growth at different velocities leading to a phenomenon known as "step bunching" (cf. Fig. 7-1c). As the steps progressed their apparent orientation changed between the consecutive images (Fig. 1f–h). As reported previously (Land et al., 1997), this is due to the fact that during the up-scan the AFM tip is "chasing" the steps, and during the down-scan the steps are moving toward the tip. Consequently, the angle of the step train differs in the images

taken during the down-scan and the up-scan. The step velocity was computed from the "true" step directions by applying the method of angles (Land et al. 1997) and found to be 30 ± 5 nm/s.

From the sectional analysis (cf. Fig. 1e), the heights of (010) steps were measured in the order of 1 nm. This is approximately equal to the minimum lattice spacing (11.96 Å) in the growth direction (i.e. the unit cell length along the *b*-axis). Previous studies (Gidalevitz et al., 1997) have reported the height of an 'elementary step' on the (010) surface ~7 Å, which corresponds to the thickness of a glycine molecule dimer. Combining this information, together with identification of functional groups (using grazing incidence X-ray diffraction) at the (010) crystal–solution interface, and diffusivity measurements in supersaturated glycine solution, it was inferred that the "growth unit" of α-glycine crystal is the zwitterionic cyclic dimer (Ginde and Myerson, 1993; Gidalevitz et al., 1997).

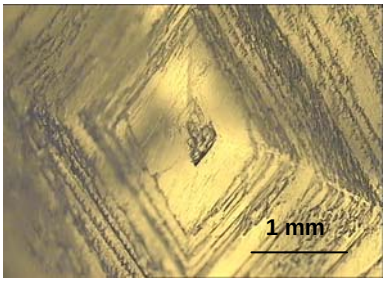

Figure 7- 2 An optical microscope image illustrating spiral dislocation growth on the (010) surface of an α-glycine crystal 'as grown' from aqueous solution.

On imaging the (010) surface of an 'as grown' α-glycine crystal (using an optical polarized light microscope) the appearance of (macro) steps as rectangular spirals with the dislocation source at the centre (Fig. 7-2) was observed. These macrosteps are, presumably, made up of elementary step bunches. Such a spiral dislocation pattern,

however, was not observed using AFM because of the presence of infinitely long steps on the (010) surface.

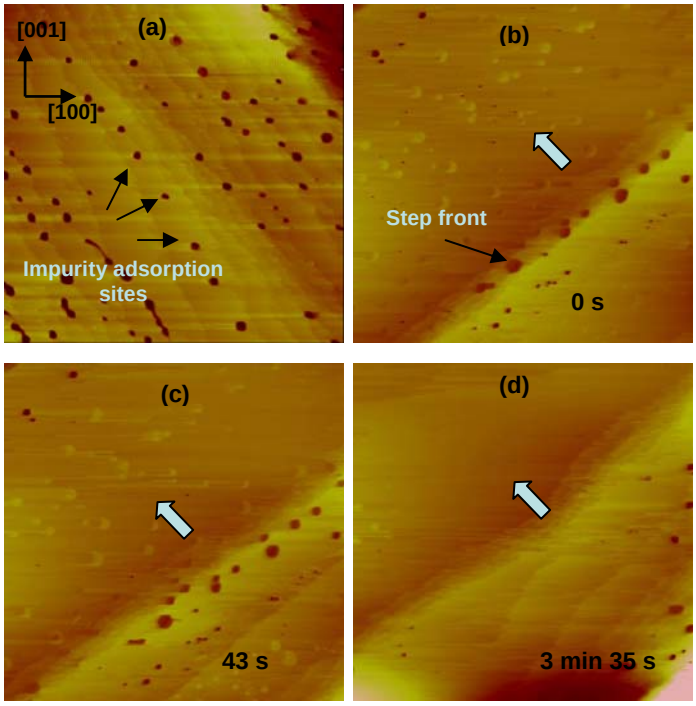

Figure 7- 3 AFM images (5 μm X 5 μm) of the (010) surface of an α-glycine crystal in aqueous solution doped with 0.5 wt % (w/w glycine) of D- + L-Phe (a) Impurity adsorption leading to hollow regions on the (010) terraces and steps; (b)–(d) Advancement of step front across the impurity adsorption sites.

7.2. In situ imaging in impurity doped glycine solution

Following the above observations, step growth dynamics on the (010) surface was monitored in glycine solution ($\sigma = 0.118$) doped with 0.5 wt % (w/w glycine) of D- + L-Phe impurity. In sharp contrast to step growth in pure solution, hollow regions appeared on the steps and terraces between the steps (Fig. 7-3a, b). These were typically 10–20 nm in depth, and corresponded to 10 to 20 times the elementary step heights. The formation of hollow regions could be explained on the basis of impurity adsorption on the crystal surface. As discussed earlier (cf. chapters 4 and 5), the impurity molecule, which mimics the glycine molecule and hence "tailor-made", can dock stereospecifically into the crystal

lattice at a kink site on the (010) step (Fig. 7-4). Subsequently, the imposter segment of the impurity molecule can offer to an incoming solute molecule a modified binding energy which makes incorporation less favorable. This disruption can halt the progress of the kink site, and thus, result in the formation of "voids" as the step moves over the poisoned surface.

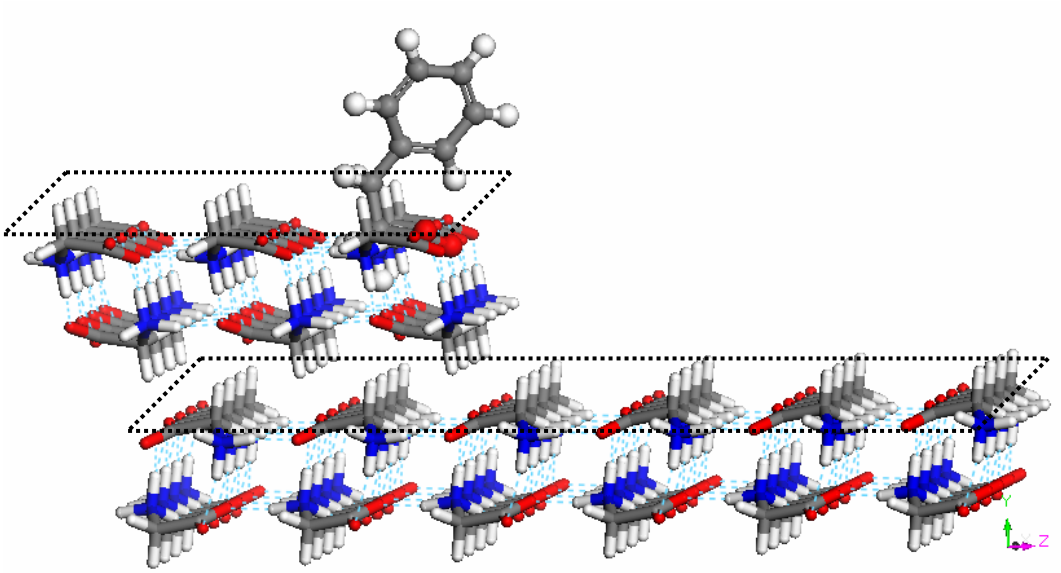

Figure 7- 4 Molecular modeling of the interaction of phenylalanine at the (010) step plane of α-glycine.

As the step front advanced in the direction of growth the hollow regions remained immobile (Fig. 7-3b and c). Subsequently, new growth-layers appeared that gradually sheathed the hollow regions, and advanced with a regular step terrain (Fig. 7-3d). However, unlike in pure solution, the orientation of steps did not change during successive scans indicating that step flow velocity was substantially reduced in the presence of adsorbed impurities.

Following this, crystal growth was monitored in glycine solutions doped with 0.75 wt % of D- + L-Phe. As the steps progressed they jutted out between the "voids", developing a corrugated step terrain (Fig. 7-5a–c). In addition, the step flow velocity

decreased significantly. This growth behavior corroborates with the "impurity pinning" model of Cabrera and Vermilyea (1958). The Cabrera–Vermilyea (C–V) model proposes that impurities adsorb onto terraces between steps, creating a field of "blockers" that pin the step edge as it moves (Fig. 7-5d). For lengths of steps longer than $2\rho_c$ (diameter of a critical two-dimensional nucleus given by the Gibbs–Thomson relationship given in eq. 7-1), the steps can proceed by squeezing through the "impurity fence". For steps shorter than $2\rho_c$, the addition of solute molecules causes an increase in free energy and hence the step is thermodynamically prevented from advancing. With enough impurities adsorbed on the surface, this condition exists for all step segments and the step becomes immobile.

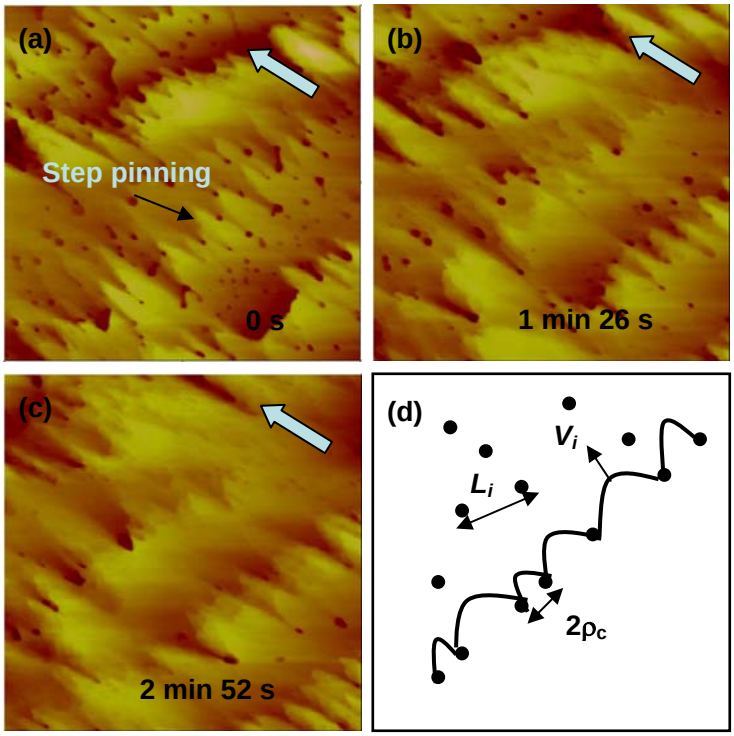

Figure 7- 5 (a)–(c) AFM images (5 μm X 5 μm) of the (010) surface of an α-glycine crystal in aqueous solution doped with 0.75 wt % (w/w glycine) of D- + L-Phe. Images show step pinning due to impurity adsorption; (d) Illustration of Cabrera–Vermilyea model. The step is pinned by impurities adsorbed onto terraces and separated by a average distance L_i. Step segments move with velocity V_i, but cannot exceed curvature $1/2\rho_c$, where ρ_c is given by the Gibbs–Thomson relationship.

In line with the above proposition, on increasing impurity concentration to 1.0 and 2.0 wt % respectively, the measured step flow velocities decreased to values less than 3 nm/s. However, in this case, the appearance of corrugated step front was less evident (Fig. 7-6). This may be explained based on adsorption of impurities giving monolayer coverage at the step, which, in turn, can reduce the number of kink sites available for growth at the step. Consequently, the adsorbed impurities can slow step advancement by poisoning kink sites without pinning the steps (Davey and Mullin, 1974; Weaver et al., 2006).

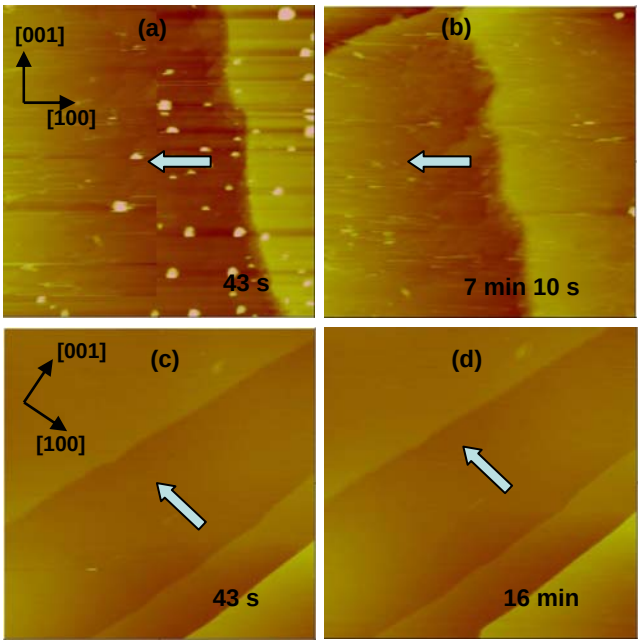

Figure 7- 6 AFM images (5 μm X 5 μm) of the (010) surface of an α-glycine crystal in aqueous solutions doped with 1.0 wt % (a, b) and 2 wt % (c, d) of D- + L-Phe impurity.

7.3. Effect of supersaturation

As the degree of solution supersaturation determines the chemical (potential) driving force for crystal growth, its effect on the step motion dynamics was investigated. To this end, crystal growth was monitored in glycine solution doped with 1.5 wt % D- + L-Phe (an impurity concentration was chosen within the levels at which complete growth

inhibition occurred in the previous set of experiments). An increased supersaturation of σ = 0.256 was achieved by preparing glycine solutions at a higher initial concentration (4.13 M).

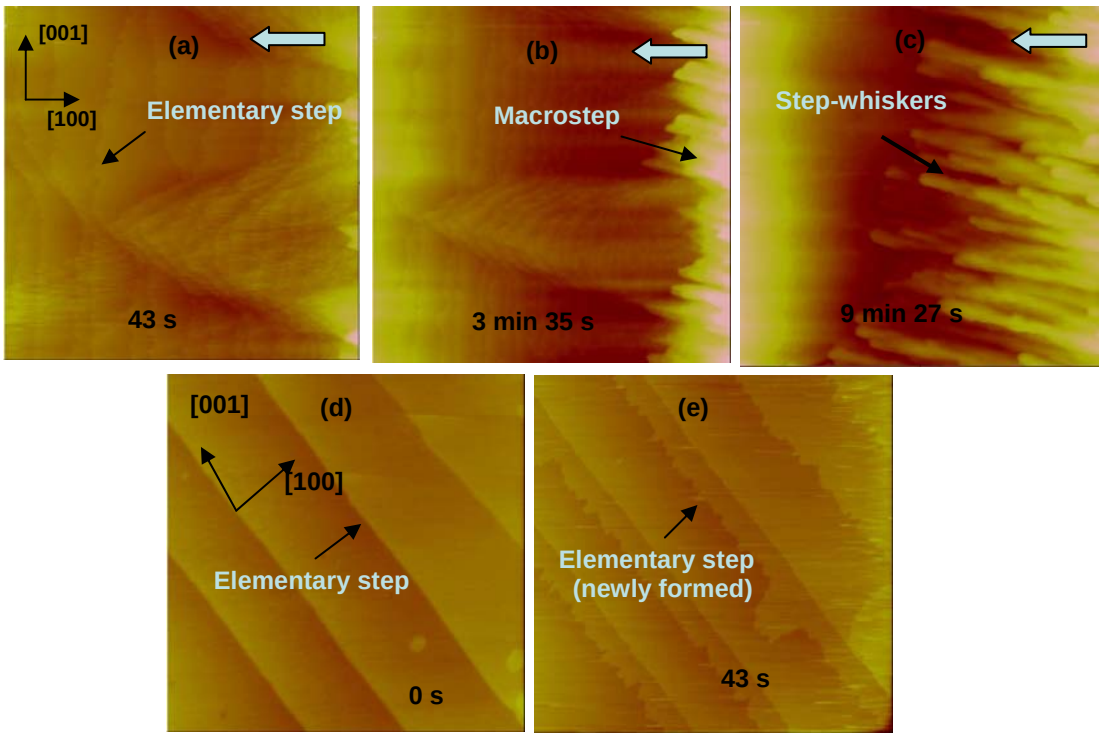

Figure 7- 7 AFM images (5 μm X 5 μm) of the (010) surface of an α-glycine crystal in aqueous solutions (σ = 0.256) doped with D- + L-Phe: (a) – (c) 1.5 wt %; (d), (e) 2.0 wt %. The images show resurrection of crystal growth at a higher supersaturation.

In Fig. 7-7 are shown representative images obtained at different time intervals. Initially, elementary steps advanced in the direction of growth at a reduced step velocity (ca.10 nm/ s). Following these steps, a macrostep comprising 'finger-like' features developed and grew laterally into what could be called as "step-whiskers" (Fig. 7-7b, c). Interestingly, such growth features were neither observed in pure solution, nor in solutions doped with the impurity at the lower supersaturation. Generally, crystal growth leading to step whiskers is characteristic of high interfacial supersaturation at the crystal–solution interface. Furthermore, it is evident from the corrugated terrain of the

evolving macrostep that impurity molecules adsorbed on the steps are pinning down their motion.

During crystal growth in solutions at a higher impurity concentration (2.0 wt %), new elementary steps were observed developing on the ledges of the existing steps (Fig. 7-7d, e). The steps had a 'molecularly roughened' surface and were nearly immobile (until about 30 min of scan time) indicating that supersaturation available was insufficient to resurrect crystal growth from the dead zone. Attempts to carry out growth experiments at a higher supersaturation, however, failed because of spontaneous nucleation.

The observed effects of supersaturation on the step motion could be explained using the Gibbs–Thomson effect, which relates differences in free energy between step and solution to step curvature. This effect predicts a critical curvature $2\rho_c$, above which the excess free energy exceeds the chemical potential difference between crystal and solution. Consequently, steps can not exceed this curvature, which is defined in eq. 7-1.

$$2\rho_c = 2\omega\gamma / kT\sigma \qquad \textbf{7- 1}$$

Here, ω is the molecular volume and γ is the step-edge free energy per unit step height. The supersaturation is defined by $\sigma \equiv \Delta\mu / kT$, where $\Delta\mu$ is the change in the chemical potential per molecule upon crystallization, k is Boltzmann constant, and T is absolute temperature. Because the radius of curvature of step has an inverse relationship with the interfacial supersaturation, therefore, crystal growth can be resurrected from impurity poisoning by increasing σ above a critical value. Then for some step segments, $2\rho_c$ becomes smaller than L_i and the steps begin to squeeze through the "fence" of impurities. This is exactly revealed by the growth behavior observed in Figs. 7-7 c and e.

These arguments are verified quantitatively using the C–V model and discussed further in the ensuing section.

7.4. Linking step growth kinetics to impurity poisoning

In order to be more precise about the nature of the inhibition process it is necessary to consider the kinetic process taking place at the growing surface. Cabrera and Vermilyea (1958) have related the "impurity pinning" model to crystal growth rates by use of the relation

$$V_I = V_0(1 - 2\rho_c / L_i)^{1/2} \qquad \textbf{7- 2}$$

which is the step velocity of an infinite step, $V_{0,}$ compared to that of the impurity affected step (V_I). Here, V_I is taken to be a geometrical average of that for pinned and unpinned step segments. L_i is the average spacing between adsorbed impurity molecules and $2\rho_c$ is given by eq. 7-1.

In order to compare eq. 7-2 with measured data, the distance L_i has to be related to the surface coverage, θ, of adsorption sites (Black et al., 1986). Presuming that the separation of lattice sites available to the impurity is L, for a square array of sites the surface concentration, N, corresponding to complete coverage of sites, would be $1/L^2$. If the actual concentration of impurity molecules is n and these are located on a square array which is a multiple of L in size, then

$$n = 1/(aL)^2 = 1/L_i^2, \theta = n/N = L^2/L_i^2.$$

Consequently, eq. 7-2 can be written as

$$[1 - (V_I/V_0)^2]^2 = (2\rho_c^2/L)\theta. \qquad \textbf{7- 3}$$

The step flow velocity measured at various impurity concentrations is shown in Fig. 7-8. Herein, while calculating the impurity concentration in terms of mole fraction, a

reduction factor of 2 has been used. This is in keeping with the fact that only chirally resolved fraction of the racemic mixture (i.e. L- or D-Phe) can interact with the (010) face of α-glycine (cf. Chapter 4). In this analysis, the reduction in step velocity to zero with impurity concentration is consistent with the C–V model (Black et al., 1986; Weaver et al., 2006).

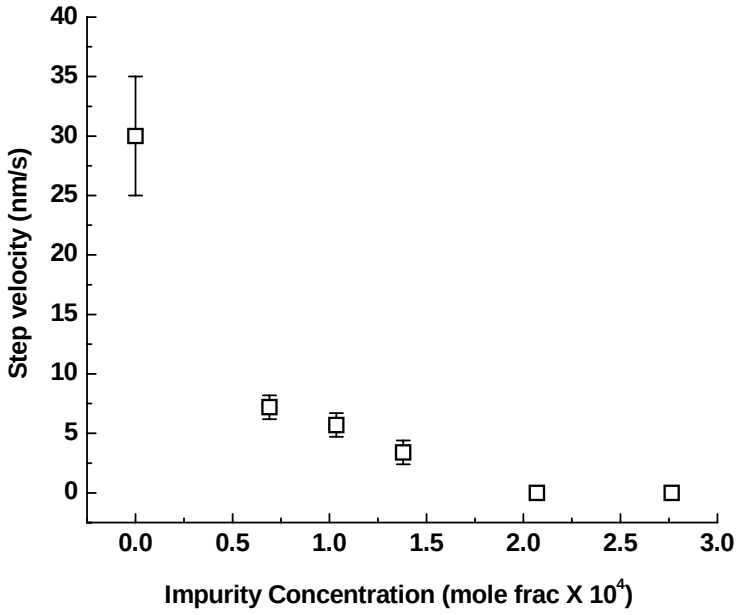

Figure 7- 8 The influence of phenylalanine (impurity) on the step growth rate on the (010) face of α-glycine.

Continuing further, the step velocity versus impurity concentration data is plotted according to eq. 7-3 and shown in Fig. 7-9. The kinetic data can be confronted with the C–V model by assuming some form for the adsorption isotherm. In the original C–V analysis, surface impurity coverage θ was assumed to be proportional to solution impurity concentration C_i. However, the dotted curve in Fig. 7-9, which is fit to the data in accordance to the simple linear adsorption isotherm (i.e. $\theta \propto C_i$), shows that it cannot fully account for the experimental data. The discrepancy can be explained because of the

assumed proportionality between surface impurity coverage and solution impurity concentration which can only hold true for a low surface coverage, and may not reflect on the actual adsorption dynamics (Davey et al., 1974; Black et al., 1986; Weaver et al., 2006).

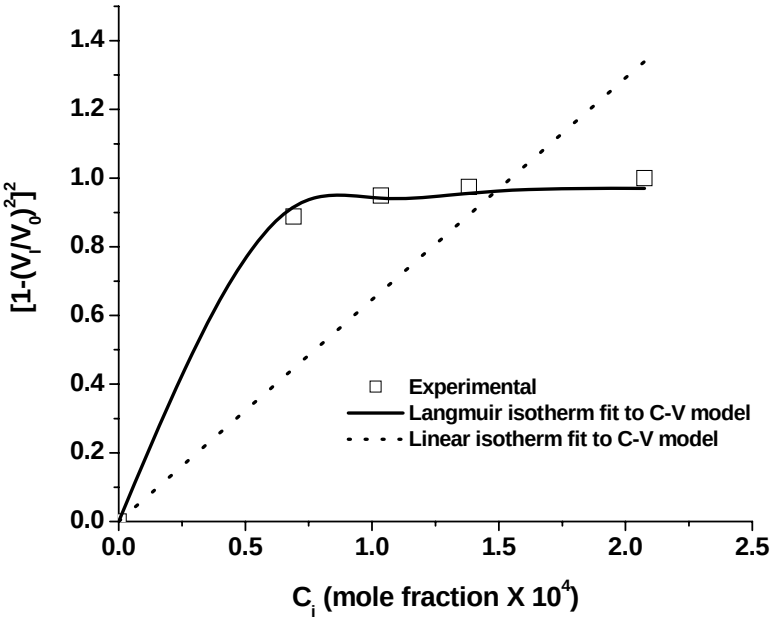

Figure 7- 9 Test of isotherm models for adsorption of phenylalanine (impurity) on the (010) face of α-glycine.

Considering this fact, the more accepted Langmuir model of adsorption dynamics is used to fit the experimental data. By equating the rates of adsorption and desorption of impurities on the surface at equilibrium (i.e. at $V_i = 0$), it can be derived that

$$\theta = KC_i/(1+KC_i), \qquad \textbf{7- 4}$$

where

$$K = (k_{ads}/k_{des}) = \exp(-\Delta G/RT). \qquad \textbf{7- 5}$$

Here, k_{ads} and k_{des} are the adsorption and desorption rate constants, and ΔG is the free energy of adsorption of the impurity species. In deriving these equations, the crystal surface is considered as a matrix of adsorption sites, with no interaction occurring

between adsorbed species on neighboring sites. Further, the rate of adsorption of impurity is linearly dependent on its concentration in solution and the area of free surface (Davey et al., 1974).

As Fig. 7-9 shows, the measured dependency of step velocity on impurity concentration is well fit by the Langmuir-type adsorption isotherm. This shows that over the range of concentrations considered the adsorption isotherm should have reached a higher surface coverage. Building on this analysis, the C–V model can be applied to relate the impurity concentration at which the growth rate is reduced to zero to the critical diameter ($2\rho_c$). Assuming that the ratio of phenylalanine to glycine molecules in the surface follows the Langmuir-type adsorption (cf. eq. 7-4), a mole fraction of 2 X 10^{-4} corresponds to 1 phenylalanine for every 320 glycine molecules. In one dimension this corresponds to 1 phenylalanine for every 18 glycine molecules, and therefore, is equivalent to a step length of ~8 nm along the [001] step ledge. Thus, from eq. 7-1

$$2\rho_c \approx 19\omega \approx 2\omega\gamma / kT\sigma,$$

or

$$\gamma / kT = 2.432 \quad (\sigma = 0.256),$$

which seems in reasonable agreement with other systems reported such as for asparagine (1.15) (Black et al., 1986) and lysozyme (2.7) (Nakada et al., 1999).

Consequently, the free energy of adsorption of phenylalanine on the (010) surface was calculated using equation 7-5 to be –6.86 kJ/ mol. The relatively lower value of ΔG could imply the ease with which the tailor-made impurity molecule can incorporate stereospecifically into the crystal lattice. Thus, the growth inhibition in α-glycine is consistent with the structural model (cf. Fig. 7-4) proposed previously.

7.5. Summary

In situ observations of the (010) surface of α-glycine using AFM provided a molecular scale picture of the physical processes taking place during crystal growth in the impure solution. The interaction of phenylalanine (impurity) with the glycine surface caused "pinning" effect on step motion, as proposed previously. As a result, the adsorbed impurities inhibited the advancement of steps and reduced their velocity. From the morphological changes observed on the growth surface at the various impurity concentrations, it could be surmised that the impurity molecules selectively adsorbed at kink sites on the (010) step, which corroborates with the structural model proposed for impurity interaction. Furthermore, the form of the observed relationships between the step velocity and impurity concentration is consistent with the Cabrera-Vermilyea model when the Langmuir isotherm model is used to describe the impurity adsorption dynamics.

In line with the current observations, in situ monitoring of the effects of amino acid impurities with excess carboxylic acid side chain groups (viz. aspartic and glutamic acids) on the step dynamics can perhaps shed more light on the new experimental observations on habit modification in α-glycine crystals.

CHAPTER 8

Conclusions and Scope for Future Work

Toward a robust crystallization process design, an understanding of the role of impurities on crystal nucleation and growth could enable a better control, and perhaps, provide guidelines to optimize solid-state attributes of crystal products obtained from solutions containing admixtures. With this objective, the effects of structurally–related impurities (amino acids) on the crystallization of glycine were investigated in this work. The main findings are briefly reviewed herein.

8.1. Significant Contributions

8.1.1. Molecular speciation controlling stereoselectivity of impurities

Our study has demonstrated that the impurities interact preferentially with the α-glycine crystal faces in accordance with the "stereoselectivity" mechanism reported previously, i.e., dependent on the absolute configuration (viz. L- or D-amino acids), and subsequently, inhibit growth normal to the crystal facet. Additionally, interactions of diprotic amino acids (aspartic and glutamic acids) with the α-glycine crystal faces is controlled by the dominant molecular species (viz. zwitterions and anions) present at the solution pH conditions. Consequently, these impurities cause habit modification along the *b*-axis and *c*-axis of α-glycine crystals, in comparison with other amino acid impurities that cause habit modification only along the *b*-axis. This observation was explained based on face-specific intermolecular interactions between the impurity species and glycine molecules occurring at the crystal surfaces.

8.1.2. Polymorphic nucleation of glycine crystals

Our study has shown a direct link between solution speciation of the impurities as controlled by pH, and the nucleation of glycine crystal polymorphs. As a result, impurities (viz. aspartic and glutamic acids) could be selected that selectively inhibited the formation of the metastable form (α-glycine), and consequently, resulted in the nucleation of the thermodynamically stable form (γ-glycine). The principles of "stereochemical nucleation control" and "self poisoning" mechanisms were invoked to rationalize nucleation of the glycine polymorphs in the presence of impurities.

8.1.3. In situ monitoring of crystal growth

In situ monitoring of crystal growth using AFM provided direct evidence for the "pinning" effect of adsorbed impurity molecules on the advancement of molecular steps at the crystal–solution interface. The thermodynamic relationship between interfacial supersaturation and step pinning could be established through measurements of step velocities. The effect of impurity concentration on the step kinetics agreed well with the classical Cabrera–Vermilyea model on using the Langmuir isotherm model to describe the impurity adsorption dynamics.

8. 2. Scope for Future work

8.2.1. Additives selection for Morphology Engineering

In several cases, designer additives are intentionally added to modify crystal habits (Wood, 2001; Ballabh et al., 2006; Deij et al., 2007), stabilize a metastable polymorph (Staab et al., 1990; Davey et al, 1997), crystallize the stable polymorph (Weissbuch et al., 1994), or control the solution mediated phase transformation (Makuta et al., 2005). These additives/ impurities are known to interact with the crystalline phase

stereochemically (Weissbuch et al., 2003), and in the process, influence the nucleation and growth kinetics. This type of interaction mechanism has been established through studies on stereoselective habit modification and nucleation control in molecular crystals with 'tailor-made' additives. By utilizing this approach, additives could be selected to achieve the desired crystal morphology and form, and, in turn, improve the efficacy of solid–liquid separation. Nevertheless, in this case, it is also important to maintain the purity of product crystals within the specified limits.

8.2.2. Solvent selection for Morphology Engineering

In the design of a solution crystallization process, solvent selection is important in terms of maximizing product yield, selecting the desired solid form and optimizing downstream separation process. With respect to the latter, different solvents can impact product morphology and hence careful selection is needed to ensure formation of particles which, for example, can give better filtration performance (Parmer et al., 2007). The strong influence of solvent on crystal habit could be rationalized on the basis of face-specific, solute–solvent interactions resulting in different degrees of solvent binding that causes inhibition of crystal growth on specific crystal habit planes (Lahav and Leiserowitz, 2001). Recently, molecular modeling methods for estimating solution binding at crystal habit surfaces has been extended to the prediction of solvent-mediated crystal morphology (Winn and Doherty, 2000; Bisker-Leib and Doherty, 2003; Hammond et al., 2006, 2007). In these, interfacial surface energies for the "probe" solvent molecules were computed and combined with the calculations involving solution-effected attachment energies. Other approaches have been suggested to study the growth of crystals from solution using kinetic Monte Carlo simulations (Cuppen et al., 2004;

Piana and Gale, 2006), and/ or molecular dynamics simulations (Liu et al., 1995; Piana and Gale, 2005). By utilizing these methods, it could be possible to select solvents for crystallization processes from the standpoint of particle engineering and product design.

8.2.3. Prediction of impurity segregation

There has been a continuous effort to develop thermodynamic models for the correlation and prediction of crystal solubility and purity when solid solution formation is the dominant mechanism that leads to impure crystals (Givand et al., 2002; Teja et al., 2002). In this approach, the purity of the crystals (amino acids) obtained from aqueous solutions is related to the relative solubilities of the product and impurity in the solvent. Such models should prove useful in identifying cosolvents and/or additives that, when added to dilute aqueous solutions of two or more isomorphous compounds, would yield product crystals of enhanced purity (Olivera-Toro et al., 2007). Molecular modeling techniques can play a complementary role in this process (Koolman and Rousseau, 1996; Hendriksen et al., 1998); for instance, some quantitative inferences could be drawn from binding energy calculations of impurities towards predicting segregation coefficients in crystals grown from solutions containing admixtures.

8.2.4. High-throughput screening

It is known that impurities, at different concentration levels, can impact crystal growth process to varying degrees. Besides, several other process variables, for examples, supersaturation, cooling rates and crystallization temperature can have a combined influence. Therefore, in an effort to understand the effects of impurities in a more comprehensive manner, imaging methodologies with shape characterization for quick measurement of crystal growth can be useful. For example, Willneff et al. (2006)

have developed a modular medium-throughput microcrystallizer for the preparation and characterization of solid phases. This microcrystallizer (a well plate housing 96 glass vials of 0.5 ml capacity) allowed multiple cooling or evaporative crystallization experiments to be carried out per day. Solids formation was identified with light transmission and visible light microscopy and polymorphic outcome was characterized with Raman microscopy. Microfluidic crystallization platforms, additionally, can provide potential for high-throughput screening for solvents and admixtures under different hydrodynamic flow conditions (Davey et al., 2003; Morissette et al., 2004). Using high-throughput technology several companies, for examples, TransForm Pharmaceuticals Inc. (USA) and Solvias AG (Switzerland) have been successful in tackling some of the problems (polymorphs, solvates) related to solid form discovery of pharmaceutical, crystalline solids (Peterson et al., 2002; Hilfiker et al., 2003).

References

Allen, K., R. J. Davey, E. Ferrari, C. S. Towler, G. J. Tiddy, M. O. Jones, R. G. Pritchard. The crystallization of glycine polymorphs from emulsions, microemulsions, and lamellar phases. *Cryst. Growth. Des*., **2 (6)**, pp. 523-527. 2002.

Anwar, J., P. K. Boateng. Computer simulation of crystallization from solution. *J. Am. Chem. Soc.,* **120**, pp. 9600-9604. 1998.

Ballabh, A., D. R. Trivedi, P. Dastidar, P. K. Ghosh, A. Pramanik, V. G. Kumar. A practical approach to produce near-spherical common salt crystals with better flow characteristics. *Cryst. Growth. Des*., **6 (7)**, pp. 1591-1594. 2006.

Beckmann, W., M. Behrens, R. Lacmann, J. Rolfs, U. Tanneberger. The effect of additives on nucleation: A low cost automated apparatus. *J. Cryst. Growth*, **99**, pp. 1061-1064. 1990.

Becke, A. D. Density-functional exchange-energy approximation with correct asymptotic behavior. *Phys. Rev. A.*, **38**, pp. 3098-3100. 1988.

Bellamy, L. J. The Infrared Spectra of Complex Molecules, 3rd ed. Methuen, London.1980.

Bennema, P. Morphology of crystals: Past and Future. In: J. P. van der Eerden and O. S. L. Bruinsma (eds.). *Science and Technology of Crystal Growth.* pp. 149-164, Kluwer Academic Publishers. 1995.

Berkovitch-Yellin, Z., J. van Mil, L. Addadi, M. Idelson, M. Lahav, L. Leiserowitz. Crystal morphology engineering by "Tailor-made" inhibitors: A new probe to fine intermolecular interactions. *J. Am. Chem. Soc.* **107**, pp. 3111-3122.1985.

Berkovitch-Yellin, Z. Toward an ab initio derivation of crystal morphology. *J. Am. Chem. Soc.*, **107,** pp. 8239-8253. 1985.

Bernstein, J. Polymorphism in Molecular Crystals. Oxford University Press: Oxford, 2002.

Bisker-Leib, V., M. F. Doherty. Modeling the crystal shape of polar organic materials: Prediction of urea crystals grown from polar and nonpolar solvents. *Cryst. Growth. Des.* **1(6)**, pp. 455-461. 2001.

Bisker-Leib, V., M. F. Doherty. Modeling crystal shape of polar organic materials: Application to Amino acids. *Cryst. Growth. Des.* 3**(2)**, pp. 221-237. 2003.

Black, S. N., R. J. Davey, M. Halcrow. The kinetics of crystal growth in the presence of tailor-made additives. *J. Cryst. Growth*, **79**, pp. 765-774. 1986.

Blagden, N., R. J. Davey, R. Rowe, R. Roberts. Disappearing polymorphs and the role of reaction by-products: the case of sulphathiazole. *Int. J. Pharm.* **172**, pp. 169-177. 1998.

Blagden, N., R. J. Davey, H. Lieberman, L. Williams, R. Paynem, R. Roberts, R. Rowe, R. Docherty. Crystal chemistry and solvent effects in polymorphic systems: sulphathiazole. *J. Chem. Soc. Faraday Trans.*, **98**, pp. 1035-45. 1998a.

Blagden, N., R. J. Davey. Polymorph selection: challenges for the future? *Cryst. Growth Des.*, **3(6)**, pp. 873-885. 2003.

Blagden, N., M. Song, R. J. Davey, L. Seton, C. C. Seaton. Ordered aggregation of benzamide crystals induced using a "motif capper" additive. *Cryst. Growth Des.*, **5(2)**, pp. 467-471. 2005.

Bonafede, S. J., M. D. Ward. Selective nucleation and growth of an organic polymorph by ledge-directed epitaxy on a molecular crystal substrate. *J. Am. Chem. Soc.*, **117**, pp. 7853-7861. 1995.

Brunsteiner, M., S. L. Price. Morphologies of organic crystals: Sensitivity of attachment energy predictions to the model intermolecular potential. *Cryst. Growth Des.,* **1(6)**, pp. 447-453. 2001.

C. J. Cramer. Essentials of Computation Chemistry: Theories and Models. pp. 275. John Wiley & Sons, Chichester, England. 2004.

Cabrera, N., D. Vermilyea. The growth of crystals from solution. In. *Growth and Perfection of Crystals*, eds. R. H. Doremus, B. W. Roberts, D. Turnbull, pp. 393-410, John Wiley & Sons. Inc., New York, Chapman & Hall Ltd., London, 1958.

Cardew P. T., R. J. Davey. Kinetic factors in the appearance and transformation of metastable phases. In *Tailoring of Crystal Growth*, Institute of Chemical Engineers (North-Western Branch), 1982.

Carter, P. W., M. D. Ward. Topographically directed nucleation of organic crystals on molecular single-crystal substrates. *J. Am. Chem. Soc.* **115**, pp. 11521-11535. 1993.

Carter, P. W., A. C. Hillier, M. D. Ward. Nanoscale surface topography and growth of molecular crystals: The role of anisotropic intermolecular bonding. *J. Am. Chem. Soc.*, **116**, pp. 944-953. 1994.

Chattopadhyay, S., D. Erdemir, J. M. B. Evans, J. Ilavsky, H. Amenitsch, C. U. Segre, A. S. Myerson. SAXS study of the nucleation of glycine crystals from a supersaturated solution. *Cryst. Growth Des.*, **5 (2)**, pp. 523-527. 2005.

Chemburkar, S. R. et al. Dealing with the impact of ritonavir polymorphs on the late stages of bulk drug process development. *Org. Process Res. Dev.*, **4**, pp. 413-417. 2000.

Chew, J. W., S. N. Black, P. S. Chow, R. B. H. Tan, K. J. Carpenter. Stable polymorphs: difficult to make and difficult to predict. *CrystEnggComm*, **9**, pp. 128. 2007.

Clydesdale, G., K. J. Roberts, R. Docherty. HABIT95 – a program for predicting the morphology of molecular crystals as a function of the growth environment. *J. Cryst. Growth*, 166, pp. 78-83. 1996.

Clydesdale, G., G. B. Thomson, E. M. Walker, K. J. Roberts, P. Meenan, R. Docherty. A molecular modeling Study of the crystal morphology of adipic acid and its habit modification by homologous impurities. *Cryst. Growth. Des.,* **5 (6)**, pp. 2154-2163. 2005.

Clydesdale, G., R. B. Hammond, V. Ramachandran, K. J. Roberts, P. Mougin. Molecular modeling of the morphology of organic crystals in the presence of impurity species: Recent applications to naphthalene, phenanthrene, and caprolactum crystals. *Mol. Cryst. Liq. Cryst.,* **440**, pp. 235-257. 2005a.

Coombes, D. S., C. R. A. Catlow, J. D. Gale, A. L. Rohl, S. L. Price. Calculation of attachment energies and relative volume growth rates as an aid to polymorph prediction. Cryst. Growth. Des., **5(3)**, pp. 879-885. 2005.

Cuppen, H. M., A. R. T. van Eerd, H. Meekes. Needlelike morphology of aspartame. Cryst. Growth. Des. **4(5)**, pp.989-997, 2004.

Dauber-Osguthorpe, P., V. A. Roberts, D. J. Osguthorpe, J. Wolff, M. Genest, A. T. Hagler. Structure and energetics of ligand-binding to proteins – Escherichia-coli Dihydrofolate Reductase Trimethoprim, A Drug-Receptor System. *Proteins: Struct. Function genetics*, **4 (1),** pp. 31-47. 1988.

Davey, R. J., J. W. Mullin. Growth of the {100} facets of ammonium dihydrogen phosphate crystals in the presence of ionic species. *J. Cryst. Growth*, **26**, pp. 45-51. 1974.

Davey, R. J., P. T. Cardew, D. McEwan, D. E. Sadler. Rate controlling processes in solvent-mediated phase transformations. *J. Cryst. Growth*, **79**, pp. 648-653. 1986.

Davey, R. J., W. Fila, J. Garside. The influence of biuret on the growth kinetics of urea crystals from aqueous solutions. *J. Cryst. Growth*. **79**, pp. 607-613. 1986.

Davey, R. J., S. N. Black, D. Logan, S. J. Maginn, J. E. Fairbrother, D. J. W. Grant. Structural and kinetic features of crystal growth inhibition: Adipic acid growing in the presence of *n*-alkanoic acids. *J. Chem. Soc. Faraday Trans*., **88**, pp. 3461-3466. 1992.

Davey, R. J., N. Blagden, G. D. Potts, R. Docherty. Polymorphism in molecular crystals: Stabilization of a metastable form by conformational mimicry. *J. Am. Chem. Soc.*, **119**, pp. 1767-1772. 1997.

Davey, R. J., J. Garside. From Molecules to Crystallizers. pp. 26-32. Oxford Chemistry Primer, 86, Oxford University Press, U. K. 2000.

Davey, R. J., N. Blagden, S. Righini, H. Alison, M. J. Quayle, S. Fuller. Crystal polymorphism as a probe for molecular self-assembly during nucleation from solutions: The case of 2,6-Dihydroxybenzoic acid. *Cryst. Growth. Des.*, **1(1)**, pp. 59-65. 2001.

Davey, R. J., W. Liu, M. J. Quayle, G. J. T. Tiddy. In situ monitoring of crystallization process using synchrotron X-ray diffraction: The search for structural precursors. *Cryst. Growth. Des.,* **2**, pp. 269-272. 2002.

Davey, R. J., N. Blagden, S. Righini, H. Alison, E. S. Ferrari. Nucleation control in solution mediated polymorphic phase transformation: the case of 2,6-Dihydroxybenzoic acid. *J. Phys. Chem. B*, **106**, pp. 1954-1959. 2002a.

Davey, R. J. Pizzas, polymorphs and pills. *Chem Commun*. **13**, pp.1463-1467. 2003.

Davies, K. J., P. M. Dove, J. J. De Yoreo. The role of Mg^{2+} as an impurity in calcite growth. Science, **290 (5494)**, pp. 1134-1137. 2000.

Dawson, A., D. R. Allan, S. A. Belmonte, S. J. Clark, W. I. F. David, P. A. McGregor, S. Parsons, C. R. Pulham, L. Sawyer. Effect of high pressures on the crystal structures of polymorphs of glycine. *Cryst. Growth. Des.,* **5(4)**, pp. 1415-1427. 2005.

Deij, M. A., T. Vissers, H. Meekes, E. Vlieg. Toward rational design of Tailor-made additives using growth site statistics. *Cryst. Growth. Des.,* **7(4)**, pp. 778-786. 2007.

Delley, B. From molecules to solids with the $Dmol^3$ approach. *J. Chem. Phys*., **113**, pp. 7756-7764. 2000.

Devarakonda, S., J. M. B. Evans, A. Y. Lee, A. S. Myerson. Molecular dynamics study of the interactions of ice inhibitors on the ice {001} surface. *Langmuir*, **20**, pp. 5353-5357. 2004.

Docherty, R. The application of computational chemistry to the study of molecular materials. In. A. S. Myerson, D. A. Green, P. Meenan (eds.). *Crystal Growth of Organic Materials.* pp. 2-14, Washington, Dc: American Chemical Society. 1996.

Dressler, D. H., Y. Mastai. Controlling polymorphism by crystallization on self-assembled multilayers. *Cryst. Growth. Des.*, **7 (5)**, pp. 847-850. 2007.

Endo, H., H. Cölfen, D. Schwahn. An analysis of a polymer additive for calcium carbonate crystallization - a small-angle neutron scattering investigation by applying contrast variation. *J. Appl. Cryst*., **36**, pp.568-572. 2003.

Ewald, P. P. *Ann. Phys*., **64,** pp 253. 1921.

Fiebig, A., M. J. Jones, J. Ulrich. Predicting the effect of impurity adsorption on crystal morphology. *Cryst. Growth Des*., **7(9**), pp. 1623-1627. 2007.

Ferrari E. S., R. J. Davey, W. I. Cross, A. L. Gillon, C. S. Towler. Crystallization in polymorphic systems: the solution-mediated transformation of β to α glycine. *Cryst. Growth. Des.*, **3(1)**, pp. 53-60. 2003.

Ferrari, E. S., R. J. Davey. Solution-mediated transformation of α to β L-glutamic acid: Rate enhancement due to secondary nucleation. *Cryst. Growth. Des*. **4(5)**, pp. 1061-1068. 2004.

Fujiwara, M., P. S. Chow, D. L. Ma, R. D. Braatz. Paracetamol crystallization using backscattering and ATR-FTIR spectroscopy: Metastability, agglomeration, and control. *Cryst. Growth Des*., **2**, pp. 363-370. 2002.

Gidalevitz, D., R. Feidenhans'l, S. Matlis, D-M. Smilgies, M. J. Christensen, L. Leiserowitz. Monitoring in situ growth and dissolution of molecular crystals: Towards determination of the growth units. *Angew. Chem. Int. Ed. Engl.*, **36 (9)**, pp. 955-959. 1997.

Ginde, R. M., A. S. Myerson. Cluster size estimation in binary supersaturated solutions. *J. Cryst. Growth*, **116**, pp-41-47. 1992.

Ginde, R. M., A. S. Myerson. Effect of impurities on cluster growth and nucleation. *J. Cryst. Growth*, **126**, pp. 216-222. 1993.

Givand, J., R. W. Rousseau, P. J. Ludovice. Characterization of L-isoleucine crystal morphology from molecular modeling. J. Cryst. Growth, **194**, pp. 228-238. 1998.

Givand, J., B. K. Chang, A. S. Teja, R. W. Rousseau. Distribution of isomorphic amino acids between a crystal phase and an aqueous solution. *Ind. Eng. Chem. Res*., **41(7)**, pp. 1873-1876. 2002.

Gnanasambandam, S., J, Jiang, R. Rajagopalan. Growth morphology of α-glycine crystals in solutions: A computational study. Ph.D Thesis Proposal, National University of Singapore, 2007.

Hammond, R. B., K. Pencheva, K. J. Roberts. Simulation of energetic stability of facetted L-glutamic acid nanocrystalline clusters in relation to their polymorphic phase stability as a function of crystal size. *J. Phys. Chem. B.*, **109**, pp. 19550-19552. 2005.

Hammond, R. B., K. Pencheva, K. J. Roberts. A structural–kinetic approach to model face-specific solution/crystal surface energy associated with the crystallization of acetyl salicylic acid from supersaturated aqueous/ethanol solution. *Cryst. Growth Des.,* **6(6)**, pp. 1324-1334. 2006.

Hammond, R. B., K. Pencheva, V. Ramachandran, K. J. Roberts. Application of grid-based molecular methods for modeling solvent-dependent crystal growth morphology: Aspirin crystallized from aqueous ethanolic solution. *Cryst. Growth Des.,* **7(9)**, pp. 1571-1574. 2007.

Harano, Y., T. Nakata, H. Yamamoto. In: Proc. 8th Symp. on Industrial Crystallization. Jančić and E. J. de Jong (eds.) pp. 3-9, North-Holland Publishing Company. 1982.

Hartman, P., W. G. Perdok. On the relations between structure and morphology of crystals. I. *Acta Cryst.* **8**, pp. 49-52. 1955.

He, G., V. Bhamidi, S. R. Wilson, R. B. H. Tan., P. J. A. Kenis, C. F. Zukoski. Direct growth of γ-glycine from neutral aqueous solutions by slow, evaporation-driven crystallization. *Cryst. Growth. Des.* **6(8)**, pp. 1746-1749. 2006.

Hendriksen, B. A., D. J. W. Grant. The effect of structurally related substances on the nucleation kinetics of paracetamol. *J. Cryst. Growth*, **156**, pp. 252-260. 1995.

Hendriksen, B. A., D. J. W. Grant, P. Meenan, D. A. Green. Crystallization of paracetamol (acetaminophen) in the presence of structurally related substances. *J. Cryst. Growth*, **183**, pp. 629-640.1998.

Hennessy, A., A. Neville, K. J. Roberts. In-situ SAXS/WAXS and turbidity studies of the structure and composition of multihomologous n-alkane waxes crystallized in the absence and presence of flow improving additive species. *Cryst. Growth. Des.,* **4(5)**, pp. 1069-1078. 2004.

Hilfiker, R. et al. Polymorphism – Integrated approach from high-throughput screening to crystallization optimization. *J. Therm. Anal. Cal.*, **73**, pp. 429-440. 2003.

Iitaka, Y. The crystal structure of *β*-glycine. *Acta Cryst.* **13**, pp. 35-45. 1960.

Jones, H. P., R. J. Davey, B. G. Cox. Crystallization of a salt of a weak organic acid and base: Solubility relations, supersaturation control and polymorphic behavior. *J. Phys. Chem. B*, **109**, pp. 5273-5278. 2005.

Jönsson, P. -G., Å. Kvick. Precision neutron diffraction structure determination of protein and nucleic acid components. III. The crystal and molecular structure of the amino

acid α-glycine. *Acta Crystallogr. Sect B: Struct. Crystallogr. Cryst. Chem.* **28**, pp. 1827-1833. 1972.

Kang, J. F., J. Zaccaro, A. Ulman, A. S. Myerson. Nucleation and growth of glycine crystals on self-assembled monolayers on gold. *Langmuir*, **16**, pp. 3791-3796. 2000.

Kashchiev, D. Nucleation – Basic Theory with Applications, pp. 431, Butterworth-Heinemann, Oxford, 2000.

Keel, T. R., C. Thomson, M. C. Davies, S. J. B.Tendler, C. J. Roberts. AFM studies of the crystallization and habit modification of an excipient material, adipic acid. *Int. J. Pharm.* **280**, pp.185-198. 2004.

Kemp, W. Organic Spectroscopy. 2nd Ed. pp. 12-81, English Language Book Society Macmillan. 1987.

Kirwan, D. J., C. J. Orella. Crystallization in the pharmaceutical and bioprocessing industries. In *Handbook of Industrial Crystallization* (2nd Ed), Ed by A. S. Myerson, pp. 249-251. Butterworth-Heinemann, 2002.

Kitamura, M., K Onuma. In situ observation of growth process of α-L-Glutamic acid with Atomic Force Microscopy. *J. Colloid Int. Sci*., **224**, pp. 311-316. 2000.

Kitamura, M. Controlling factors and mechanism of polymorphic crystallization. *Cryst. Growth. Des.*, **4(6)**, pp. 1153-1159. 2004.

Knight, C. A. Adding to the antifreeze agenda. *Nature*, **406**, pp. 249-251. 2000.

Koolman, H. C., R. W. Rousseau. Effects of isomorphic compounds on the purity and morphology of L-isoleucine crystals. *AIChE J*., **42**, pp.147-153. 1996.

Kuznetsov, Y. G., A. J. Malkin, A. McPherson. AFM studies of the nucleation and growth mechanisms of macromolecular crystals. *J. Cryst. Growth.* **196**, pp. 489-502. 1999.

Kvick, A., W. M. Canning, T. F. Koetzle, G. J. B. Williams. *Acta Crystallogr. Sect B: Struct. Crystallogr. Cryst. Chem.*, **36**, pp. 115. 1980.

Lahav, M., L. Leiserowitz. The effect of solvent on crystal growth and morphology. *Chem. Eng. Sci.*, **56**, pp. 2245-2253. 2001.

Land, T. A., J. J. De Yoreo, J. D. Lee. An in-situ AFM investigation of canavalin crystallization kinetics. *Surf. Sci*. **384**, pp. 136-155. 1997.

Land, T. A., T. L. Martin, S. Potapenko, G. T. Palmore, J. J. De Yoreo. Recovery of surfaces from impurity poisoning during crystal growth. *Nature*, **399**, pp. 442-445. 1999.

Leach, A. R. Molecular Modeling Principles and Applications. pp. 202-203, 334-339. Pearson Prentice Hall. 2001.

Lee, A. Y., A. Ulman, A. S. Myerson. Crystallization of amino acids on self-assembled monolayers of rigid thiols on gold. *Langmuir*, **18**, pp. 5886-5898. 2002.

Lee, A. Y., I. S. Lee, S. S. Dette, J. Boerner, A. S. Myerson. Crystallization on confined engineered surfaces: A method to control crystal size and generate different polymorphs. *J. Am. Chem. Soc.*, **127**, pp. 14982-14983. 2005.

Lee, C., W. Yang, R. G. Parr. Development of the Colle-Salvetti correlation-energy formula into a functional of the electron density. *Phys. Rev. B.*, **37**, pp. 785-789. 1998.

Leunge, K., S. B. Rempe. *Ab initio* molecular dynamics study of glycine intramolecular proton transfer in water. *J. Chem. Phys.*, **122**, pp. 184506. 2005.

Li, L., N. Rodríguez-Hornedo. Growth kinetics and mechanism of glycine crystals. *J. Cryst. Growth*, **121**, pp. 33-38. 1992.

Li, P., Zhao, L. Developing early formulations: Practice and perspective. *Int. J. Pharm*. **341**, pp. 1-19. 2007.

Lide, D. R (ed). CRC Handbook of Chemistry and Physics. 85th ed. pp. 7-1, CRC Press: Boca Raton, FL. 2004.

Liu, X. Y., E. S. Boek, W. J. Briels, P. Bennema. Prediction of crystal growth morphology based on structural analysis of the solid-fluid interface. *Nature*, **374**, pp. 342-345. 1995.

Lo, P. Y., A. S. Myerson. Cluster formation and diffusion in supersaturated binary and ternary amino acid solutions. *J. Cryst. Growth*, **110**, pp. 26-33. 1991.

Malkin, A. J., R. E. Thorne. Growth and disorder of macromolecular crystals: insights from atomic force microscopy and X-ray diffraction studies. *Methods*, **34,** pp. 273-299. 2004.

Materials Studio Modeling, Accelrys Software Inc. USA, *Version 4.0.* 2005.

Mayo, S. L., B. D. Olafson, W. A. Goddard III. DREIDING: A generic force field for molecular simulations. *J. Phys. Chem.*, **94**, pp. 8897-8909. 1990.

McPherson, A., A. J. Malkin, Y.G. Kuznetsov, S. Koszelak. Incorporation of impurities into macromolecular crystals. *J. Cryst. Growth*, **168,** pp. 74-92.1996.

Mercury Ver.1.4.2. Cambridge Crystallographic Data Centre, U.K. http://www.ccdc.cam.ac.uk/products/mercury/

Mersmann, A., K. Bartosch. How to predict the metastable zone width? *J. Cryst.Growth.* **183**, pp. 240-250.1998.

Morissette, S. L., O. Almarsson, M. L. Peterson, J. F. Remenar, M. J. Read, A. V. Lemmo, S. Ellis, M. J. Cima, C. R. Garder. High-throughput crystallization: polymorphs, salts, co-crystals and solvates of pharmaceutical solids. *Adv. Drug. Delivery Reviews*, **56**, pp. 275-300. 2004.

Moscosa-santillán, M., O. Bals, H. Fauduet, C. Porte, A. Delacroix. Study of batch crystallization and determination of an alternate temperature –time profile by on-line turbidity analysis – application to glycine crystallization. *Chem. Eng. Sci.*, **55**, pp. 3759-3770. 2000.

Mughal, R. K., R. J. Davey, N. Blagden. Application of crystallization inhibitors to chiral separations. 1. Design of additives to discriminate between the racemic compound and the pure enantiomer of mandelic acid. *Cryst. Growth. Des.*, **7(2)**, pp. 218-224. 2007.

Mukuta, T., A. Y. Lee, T. Kawakami, A. S. Myerson. Influence of impurities on the solution-mediated phase transformation of an active pharmaceutical ingredient. *Cryst. Growth Des.*, **5(4)**, pp. 1429-1436. 2005.

Mullin, J. W. Crystallization. 4th ed. Butterworth-Heinemann, 2001.

Myerson, A. S., P. Y. Lo. Cluster formation and diffusion in supersaturated binary and Ternary amino acid solutions. *J. Cryst. Growth*, **110,** pp. 26-33.1991.

Myerson, A. S., S. M. Jang. A comparison of binding energy and metastable zone width for adipic acid with various additives. *J. Cryst. Growth*, **156**, pp.459-466. 1995.

Myerson, A. S., R. Ginde. Crystals, crystal growth, and nucleation. In *Handbook of Industrial Crystallization* (2nd Ed), Ed by A. S. Myerson, pp. 33-57. Butterworth-Heinemann, 2002.

Nakada, T., G. Sazaki, S. Miyashita, S. D. Durbin, H. Komatsu. Direst AFM observations of impurity effects on a lysozyme crystal. *J. Cryst. Growth.* **196**, pp. 503-510. 1999.

No, K. T., J. A. Grant, M. S. Jhon, H. A. Scheraga. Determination of net atomic charges using a modified partial equalization of orbital electronegativity method. Application

to ionic and aromatic molecules as models for polypeptides. *J. Phys. Chem.*, **94**, pp. 4740-4796. 1990.

Nývlt, J., O. Söhnel, M.Matuchová, M. Broul. The Kinetics of Industrial Crystallization. Elsevier Science Publishers, 1985.

Olivera-Toro, A., R. W. Rousseau, A. S. Teja. Thermodynamic models for the solubility and purity of amino acid crystals in multi-component systems. *AIChE Annual Meeting*, Salt Lake City. 2007.

Parmer, M. M. O. Khan, L. Seton, J. L. Ford. Polymorph selection with morphology control using solvents. *Cryst. Growth. Des.*, **7(9)**, pp. 1635-1642. 2007.

Parveen, S., R. J. Davey, G. Dent, R. G. Pritchard. Linking solution chemistry to crystal nucleation: the case of tetrolic acid. *Chem. Commun.* **12**, pp. 1531-1533. 2005.

Pearson, J. F., M. A. Slifkin. The infrared spectra of amino acids and dipeptides. *Spectrochimica Acta*, **28A**, pp. 2403-2417. 1972.

Perlovich, G. L., L. K. Hansen, A. Bauer-Brandl. The polymorphism of glycine Thermochemical and structural aspects. *J. Therm. Anal. Cal.*, **66**, pp. 699-715. 2001.

Peterson, M. L. et al. Iterative high-throughput polymorphism studies on acetaminophen and an experimentally derived structure for Form III. *J. Am. Chem. Soc.*, **124**, pp. 10958-10959. 2002.

Piana, S., J. D. Gale. Understanding the barriers to crystal growth: Dynamical simulation of the dissolution and growth of urea from aqueous solution. *J. Am. Chem. Soc.*, **127**, pp. 1975-1982. 2005.

Piana, S., J. D. Gale. Three-dimensional kinetic Monte Carlo simulation of crystal growth from solution. *J. Cryst. Growth.* **294**, pp. 46-52. 2006.

Pino-García, O., A. C. Rasmuson. Influence of additives on nucleation of vanillin: Experiments and introductory molecular simulations. *Cryst. Growth Des.*, **4(5)**, pp.1025-1037. 2004.

Price, S. L. The computational prediction of pharmaceutical crystal structures and polymorphism. *Adv. Drug. Delivery Reviews*, **56**, pp. 301-319. 2004.

Profio, G. D., Tuccci, E. Curcio, E. Drioli. Selective glycine polymorph crystallization by using microporous membranes. *Cryst. Growth Des.,* **7(3)**, pp. 526-530. 2007.

Profir, V. M., E. Furusju, Lars-Göran Danielsson, A. C. Rasmuson, A. C. Study of the crystallization of Mandelic acid in water using in situ ATR-IR spectroscopy. *Cryst. Growth. Des.*, **2**, pp. 273-279. 2002.

Qiu, S. R., A. Wierzbicki, E. A. Salter, S. Zepeda, C. A. Orme, J. R. Hoyer, G. H. Nancollas, A. M. Cody, J. J. De Yoreo. Modulation of calcium oxalate monohydrate crystallization by citrate through selective binding to atomic steps. *J. Am. Chem. Soc*., **127**, pp. 9036-9044. 2005.

Quate, C. F. The AFM as a tool for surface imaging. *Surf. Sci.* **299/300,** pp. 980-995. 1994.

Rappé, A. K., C. J. Casewit, K. S. Colwell, W. A. Goddard, W. M. Skiff. UFF, A full periodic-table force field for molecular mechanics and molecular dynamics simulations. *J. Am. Chem. Soc.*, **114,** pp. 10024-10035. 1992.

Roberts, K. J., J. N. Sherwood, C. S. Yoon, R. Docherty. Understanding the solvent-induced habit modification of benzophenone in terms of molecular recognition at the crystal/ solution interface. *Chem. Mater.* **6**, pp. 1099-1102. 1994.

Rodríguez-Hornedo, N., D. Murphy. Significance of controlling crystallization mechanisms and kinetics in pharmaceutical systems. *J. Pharm. Sci.* **88 (7)**, pp. 651-660. 1999.

Sakai, H., H. Hosogai, T. Kawakita, K. Onuma, K. Tsukamoto. Transformation of α-glycine to γ-glycine. *J. Cryst. Growth*, **116**, pp 421-426. 1992.

Sangwal, K., E. Mielniczek-Brzóska. Effect of impurities on metastable zone width for the growth of ammonium oxalate monohydrate crystals from aqueous solutions. *J. Cryst. Growth,* **267**, pp. 662-675. 2004.

Scott, C., S. Black. In-line analysis of impurity effects on crystallization. *Org. Process Res. Dev.*, **9**, pp. 890-893. 2005.

Shekunov, B. Yu., P. York. Crystallization processes in pharmaceutical technology and drug delivery design. *J. Cryst. Growth*, **211**, pp. 122-136. 2000.

Sonoda, Y., F. Hirayama, H. Arima, Y. Yamaguchi, W. Saenger, K. Uekama. Selective crystallization of the metastable Form IV polymorph of tolbutamide in the presence of 2,6-Di-*O*-methyl-β-cyclodextrin in aqueous solution. *Cryst. Growth. Des.*, **6(5)**, pp. 1181-1185. 2006.

Spruijtenburg, R. Examples of the selective preparation of a desired crystal modification by an appropriate choice of operating parameters. *Org. Process Res. Dev.*, **4(5)**, pp. 403-406. 2000.

Staab, E., L. Addadi, L. Leiserowitz, M. Lahav. Control of polymorphism by 'tailor-made' polymeric crystallization auxiliaries. Preferential precipitation of a metastable polar form for second harmonic generation. *Adv. Mater.* **2(1)**, pp. 40-43. 1990.

Sun, H. COMPASS: An ab initio force-field optimized for condensed-phase applications – Overview with details on alkane and benzene compounds. *J. Phys. Chem. B*, **102,** pp. 7338-7364, 1998.

Svec, H. J., D. D. Clyde. Vapor Pressures of some α-Amino acids. *J. Chem. Eng. Data*, **10**, pp. 151-152. 1965.

Teja, A. S., J. C. Givand, R. W. Rousseau. Correlation and prediction of crystal solubility and purity. *AIChE J*. **48(11)**, pp. 2629-2634. 2002.

ter Horst, J. H., H. J. M. Kramer, P. J. Jansens. A new molecular modeling approach to predict concomitant nucleation of polymorphs. *Cryst. Growth. Des*., **2(5)**, pp. 351-356. 2002.

Thompson, C., M. C. Davies, C. J. Roberts, S. J. B. Tendler, M. J. Wilkinson. The effects of additives on the growth and morphology of paracetamol (acetaminophen) crystals. *Int. J. Pharm*., **280**, pp.137-150. 2004.

Threlfall, T. Crystallization of polymorphs: Thermodynamic insight into the role of solvent. *Org. Process Res. Dev*., **4**, pp. 384-390. 2000.

Togkalidou, T., H-H Tung, Y. Sun, A. Andrews, R. D. Braatz. Solution concentration prediction for pharmaceutical crystallization process using robust chemometrics and ATR FTIR spectroscopy. *Org. Process Res. Dev.,* **6**, pp. 317-322. 2002.

Torbeev, V. Y., E. Shavit, I. Weissbuch, L. Leiserowitz, M. Lahav. Control of crystal polymorphism by tuning the structure of auxiliary molecules as nucleation inhibitors. The β-polymoph of glycine grown in aqueous solutions. *Cryst. Growth. Des.* **5(6)**, pp. 2190-2196. 2005.

Towler, C. S., R. J. Davey, R. W. Lancaster, C. J. Price. Impact of molecular speciation on crystal nucleation in polymorphic systems: The conundrum of γ glycine and molecular 'self poisoning'. *J. Am. Chem. Soc*., **126**, pp.13347-13353. 2004.

Ulrich, J., C. Strege. Some aspects of the importance of metastable zone width and nucleation in industrial crystallizers. *J. Cryst. Growth*, **237-239**, pp. 2130-2135. 2002.

Ulrich, J, M. J. Jones. Industrial crystallization – Developments in research and technology. *Chemical Engineering Research and Design*, **82(A12)**, pp. 1567-1570. 2004.

Voogd, J., J. L. Derissen, F. B. van Duijneveldt. Calculation of proton-transfer energies and electrostatic lattice energies of various amino acids and peptides using CNDO/2 and ab initio SCF methods. *J. Am. Chem. Soc*., **103(26)**, pp. 7701-7706. 1981.

Weaver, M. L., S. R. Qiu, J. R. Hoyer, W. H. Casey, G. H. Nancollas, J. J. De Yoreo. Improved model for inhibition of pathological mineralization based on citrate-calcium oxalate monohydrate interaction. *ChemPhysChem*, **7**, pp. 2081-2084. 2006.

Weissbuch, I., L. Addadi, Z. Berkovitch-Yellin, E. Gati, S. Weinstein, M. Lahav, L. Leiserowitz. Centrosymmetric crystals for the direct assignment of the absolute configuration of chiral molecules. Application to the α-amino acids by their effect on glycine crystals. *J. Am. Chem. Soc*., **105**, pp. 6615-6621. 1983.

Weissbuch, I., M. Lahav, L. Leiserowitz, G. R. Meredith, H. Vanherzeele. Centrosymmetric crystals as host matrices for second-order optical nonlinear effects. *Chem. Mater.*, **1**, pp.114-118. 1989.

Weissbuch, I., L. Addadi, M. Lahav, L. Leiserowitz. Molecular recognition at crystal interfaces. *Science*, **253**, pp. 637-645. 1991.

Weissbuch, I., L. Leiserowitz, M. Lahav. "Tailor-made" and charge-transfer auxiliaries for the control of the crystal polymorphism of glycine. *Adv. Mater.*, **6(12)**, pp. 952-956. 1994.

Weissbuch, I., R. Popovitz-biro, M. Lahav, L. Leiserowitz. Understanding and control of nucleation, growth, habit, dissolution and structure of two- and three-dimensional crystals using 'tailor-made' auxiliaries. *Act. Cryst.* **B51**, pp. 115-148. 1995.

Weissbuch, I., M. Lahav, L. Leiserowitz. Toward stereochemical control, monitoring and understanding of crystal nucleation. *Cryst. Growth Des*., **3(2)**, pp.125-150. 2003.

Weissbuch, I., V. Y. Torbeev, L. Leiserowitz, M. Lahav. Solvent effect on crystal polymorphism: Why addition of methanol or ethanol to aqueous solutions induces the precipitation of the least stable β form of glycine. *Angew. Chem. Int. Ed.,* **44**, pp. 3226-3229. 2005.

Weissbuch, I., L. Leiserowitz, M. Lahav. Self-poisoning at {011} faces of α-resorcinol crystals may explain its unidirectional growth in the vapor phase: A molecular modeling study. *Cryst. Growth. Des.,* **6 (3)**, pp 625-628. 2006.

Willneff, E. A., R. J. Davey, C. L. Richards, R. C. Burton, J. J. Cilliers. Development and applications of an inexpensive modular medium-throughput microcrystallizer for the preparation and characterization of solid phases. *J. Cryst. Growth*, **294**, pp. 29-34. 2006.

Williams-Seton, L., R. J. Davey, H. F. Lieberman. Solution chemistry and twinning in saccharin crystals: A combined probe for the structure and functionality of the crystal–fluid interface. *J. Am. Chem. Soc*., **121**, pp. 4563-4567. 1999.

Winn, D., Doherty, M. F. Modeling crystal shapes of organic materials grown from solution. *AIChE J*. 46(7), pp. 1348-1367. 2000.

Windmill Software Ltd., Manchester, U. K. http://www.windmill.co.uk/windmill.html

Wood, W. M. L. A bad (crystal) habit–and how it was overcome. *Powder Tech.*, **121**, pp.53-59. 2001.

Yu, Z. Particle Engineering in Anti-solvent Crystallization. Ph.D. Thesis. National University of Singapore. 2006.

List of Publications

International refereed journals:

[1] Poornachary, S. K., Chow, P. S., Tan, R. B. H. and Davey R. J. **Molecular speciation controlling stereoselectivity of additives: Impact on the habit modification in α-glycine crystals**. *Crystal Growth & Design*, 7(2), pp. 254–261, **2007**. *(Featured as a cover article)*

[2] Poornachary, S. K., Chow, P. S. and Tan, R. B. H. **Influence of solution speciation of impurities on polymorphic nucleation in glycine.** *Crystal Growth & Design*, 8(1), pp. 179–185, **2008**.

[3] Poornachary, S. K., Chow, P. S. and Tan, R. B. H. **Effect of solution speciation of impurities on α-glycine crystal habit: A molecular modeling study.** *J. Crystal Growth*, 310, pp. 3034–3041, **2008.**

[4] Poornachary, S. K., Chow, P. S. and Tan, R. B. H. **Impurity effects on the growth of molecular crystals: Experiments and modeling.** Invited article**,** *Adv. Powder Technol.* Vol. 19 No.5 (**Oct 2008**).

International conference contributions:

[1] Poornachary, S. K., Chow, P. S. and Tan, R. B. H. **Effects of impurities on glycine nucleation and crystal habit**. In Proceedings of the *7th World Congress of Chemical Engineering*. Glasgow, Scotland. **2005**.

[2] Poornachary, S. K., Chow, P. S. and Tan, R. B. H. **Effect of molecular speciation of impurities on amino acid crystallization**. Oral presentation at the American *Institute of Chemical Engineers (AIChE) Annual Meeting*. Cincinnati, USA. **2005**.

[3] Poornachary, S. K., Chow, P. S. Tan, R. B. H., and Davey, R. J. **Stereoselective habit modification and crystal polymorphism in glycine: Impact of molecular speciation of impurities.** Poster presentation at the *7th International Workshop on the Crystal Growth of Organic Materials (CGOM-7)*, Rouen, France. **2006**.

[4] Poornachary, S. K., Chow, P. S. and Tan, R. B. H. **Nucleation in polymorphic systems: Effects of pH, supersaturation and molecular speciation of impurities.** Oral presentation at the *AIChE Annual Meeting*. San Francisco, USA. **2006**.

[5] Poornachary, S. K., Chow, P. S. and Tan, R. B. H. **Solution speciation of impurities: A force field simulation of its impact on α-glycine crystal habit.** Oral presentation at the *AIChE Annual Meeting*. Salt Lake City, USA. **2007**.